NASA Technical Memorandum 2000–206892, Volume 11

SeaWiFS Postlaunch Technical Report Series

Stanford B. Hooker, Editor
NASA Goddard Space Flight Center
Greenbelt, Maryland

Elaine R. Firestone, Senior Technical Editor
SAIC General Sciences Corporation
Beltsville, Maryland

Volume 11, SeaWiFS Postlaunch Calibration and Validation Analyses, Part 3

John E. O'Reilly
NOAA, National Marine Fisheries Service, Narragansett, Rhode Island

Stéphane Maritorena, Margaret C. O'Brien, David A. Siegel, Dierdre Toole, David Menzies, and Raymond C. Smith
University of California at Santa Barbara, Santa Barbara, California

James L. Mueller
CHORS/San Diego State University, San Diego, California

B. Greg Mitchell and Mati Kahru
Scripps Institution of Oceanography, San Diego, California

Francisco P. Chavez and P. Strutton
Monterey Bay Aquarium Research Institute, Moss Landing, California

Glenn F. Cota
Old Dominion University, Norfolk, Virginia

Stanford B. Hooker and Charles R. McClain
NASA Goddard Space Flight Center, Greenbelt, Maryland

Kendall L. Carder and Frank Müller-Karger
University of South Florida, St. Petersburg, Florida

Larry Harding and Andrea Magnuson
Horn Point Laboratory, Cambridge, Maryland

David Phinney
Bigelow Laboratory for Ocean Sciences, West Boothbay Harbor, Maine

Gerald F. Moore and James Aiken
Plymouth Marine Laboratory, Plymouth, United Kingdom

Kevin R. Arrigo
Stanford University, Stanford, California

Ricardo Letelier
Oregon State University, Corvallis, Oregon

Mary Culver
NOAA, Coastal Services Center, Charleston, South Carolina

Table of Contents

Prologue **1**
1. OC2v2: Update on the Initial Operational SeaWiFS Chlorophyll *a* Algorithm **3**
1.1 Introduction **3**
1.2 The SeaBAM Data Set **3**
1.3 OC2v2 Algorithm **7**
1.4 Conclusions **8**
2. Ocean Color Chlorophyll *a* Algorithms for SeaWiFS, OC2, and OC4: Version 4 ..... **9**
2.1 Introduction **10**
2.2 The *In Situ* Data Set **10**
2.3 OC2 and OC4 ..... **15**
2.4 Conclusions **19**
3. SeaWiFS Algorithm for the Diffuse Attenuation Coefficient, $K(490)$, Using Water-Leaving Radiances at 490 and 555 nm **24**
3.1 Introduction **24**
3.2 Data and Methods **25**
3.3 Results **25**
3.4 Discussion **25**
4. Long-Term Calibration History of Several Marine Environmental Radiometers (MERs) **28**
4.1 Introduction **28**
4.2 ICESS Facility and Methods **28**
4.3 Results **33**
4.4 Long-Term Averages **41**
4.5 Other Issues **43**
4.6 Conclusions **45**
Glossary **46**
Symbols **46**
References **47**
The SeaWiFS Postlaunch Technical Report Series **48**

Abstract

Volume 11 continues the sequential presentation of postlaunch data analysis and algorithm descriptions begun in Volume 9. Chapters 1 and 2 present the OC2 (version 2) and OC4 (version 4) chlorophyll *a* algorithms used in the SeaWiFS data second and third reprocessings, August 1998 and May 2000, respectively. Chapter 3 describes a revision of the $K(490)$ algorithm designed to use water-leaving radiances at 490 nm which was implemented for the third reprocessing. Finally, Chapter 4 is an analysis of *in situ* radiometer calibration data over several years at the University of California, Santa Barbara (UCSB) to establish the temporal consistency of their in-water optical measurements.

PROLOGUE

The SeaWiFS Project Calibration and Validation Team (CVT) is responsible for the overall quality of the data products and for verifying the processing code. The prelaunch quality control strategy was outlined in Volume 38 of the *SeaWiFS Technical Report Series* (Prelaunch). Since SeaWiFS began routine data processing in September 1997, the CVT has constantly worked to resolve data quality issues and improve on the initial data evaluation methodologies. These evaluations resulted in three major reprocessings of the entire data set (February 1998, August 1998, and May 2000). Each reprocessing addressed the data quality issues that could be identified up to the time of each reprocessing.

The number of chapters (21) needed to document this extensive work in the *SeaWiFS Postlaunch Technical Report Series* requires three volumes: Volumes 9, 10, and 11. Volume 11 continues the sequential presentation of postlaunch data analysis and algorithm descriptions, begun in Volume 9, by describing the algorithm improvements to two versions of the chlorophyll *a* algorithm and the revised diffuse attenuation coefficient algorithm at 490 nm, $K(490)$, developed for the third reprocessing. In addition, an analysis of radiometer calibration data at the University of California Santa Barbara (UCSB) is described, which establishes the temporal consistency of their in-water optical measurements.

It is expected that other improvements, including new geophysical data products, and updated algorithms will be developed in the future which will require additional reprocessings. The SeaWiFS Project Office will remain dedicated to providing better products and to the documentation of future analysis and algorithm improvement studies.

A short synopsis of each chapter in this volume is given below.

1. *OC2v2: Update on the Initial Operational SeaWiFS Chlorophyll a Algorithm*

The original at-launch SeaWiFS algorithm (OC2 for Ocean Chlorophyll 2-band algorithm) was derived from the SeaWiFS Bio-optical Algorithm Mini-workshop (SeaBAM) data set (the number of data sets, $N = 919$) which contains coincident *in situ* remote sensing reflectance, $\tilde{R}_{\rm rs}$, and *in situ* chlorophyll *a*, $\tilde{C}_a$, measurements from a variety of oceanic provinces. Following the SeaWiFS launch, the accuracy of SeaWiFS chlorophyll *a* estimates using the OC2 algorithm was evaluated against new *in situ* measurements. These new data indicated that OC2 was performing generally well in Case-1 waters with $\tilde{C}_a$ concentration, between 0.03–1 mg m^{-3}, but tended to overestimate $\tilde{C}_a$ at higher concentrations. To strengthen the SeaBAM data set at $\tilde{C}_a > 1$ mg m^{-3}, 255 new stations were added to the original data set. These new data generally showed lower $R_{\rm rs}(490)/R_{\rm rs}(555)$ band ratios at $\tilde{C}_a > 4$ mg m^{-3} than in the original SeaBAM data set, which would explain some of the overestimations observed with OC2. The new SeaBAM data set was used to refine the coefficients for the OC2 modified cubic polynomial (MCP) function. The updated algorithm (OC2v2) is presented along with its statistical performance and a comparison with the original version of the algorithm.

2. *Ocean Color Chlorophyll a Algorithms for SeaWiFS, OC2, and OC4: Version 4*

This chapter describes the revisions (version 4) to the ocean chlorophyll two- and four-band algorithms as well as the very large *in situ* data set used to update these algorithms for use in the third reprocessing of SeaWiFS data. The *in situ* data set is substantially larger (N = 2,853) than was used to develop earlier versions of OC2 and OC4. The data set includes samples from a greater variety of bio-optical provinces, and better represents oligotrophic and eutrophic waters. The correlation between chlorophyll *a* concentration, C_a, estimated using OC4 and *in situ* C_a ($\tilde{C}_a$) estimated from fluorometric and high performance liquid chromatography (HPLC) analyses was slightly higher than that for OC2. OC4 would be expected to perform better than OC2, when applied to satellite-derived, water-leaving radiances retrieved from oligotrophic and eutrophic areas. Variations of the OC4 algorithm are provided for other ocean color sensors to facilitate comparisons with SeaWiFS.

3. *SeaWiFS Algorithm for the Diffuse Attenuation Coefficient, $K(490)$, Using Water-Leaving Radiances at 490 and 555 nm*

A new algorithm has been developed using the ratio of water-leaving radiances at 490 and 555 nm to estimate $K(490)$, the diffuse attenuation coefficient of seawater at 490 nm. The standard uncertainty of prediction for the new algorithm is statistically identical to that of the SeaWiFS prelaunch $K(490)$ algorithm, which uses the ratio of water-leaving radiances at 443 and 490 nm. The new algorithm should be used whenever the uncertainty of the SeaWiFS determination of water-leaving radiance at 443 is larger than that at 490 nm.

4. *Long-Term Calibration History of Several Marine Environmental Radiometers (MERs)*

The accuracy of upper ocean apparent optical properties (AOPs) for the vicarious calibration of ocean color satellites ultimately depends on accurate and consistent *in situ* radiometric data. The Sensor Intercomparison and Merger for Biological and Interdisciplinary Oceanic Studies (SIMBIOS) project is charged with providing estimates of normalized water-leaving radiance for the SeaWiFS instrument to within 5%. This, in turn, demands that the radiometric stability of *in situ* instruments be within 1% with an absolute accuracy of 3%. This chapter is a report on the analysis and reconciliation of the laboratory calibration history for several Biospherical Instruments (BSI) marine environmental radiometers (MERs), models MER-2040 and -2041, three of which participate in the SeaWiFS Calibration and Validation Program. This analysis includes data using four different FEL calibration lamps, as well as calibrations performed at three SeaWiFS Intercalibration Round-Robin Experiments (SIRREXs). Barring a few spectral detectors with known deteriorating responses, the radiometers used by the University of California, Santa Barbara (UCSB) during the Bermuda Bio-Optics Project (BBOP) have been remarkably stable during more than five years of intense data collection. Coefficients of variation for long-term averages of calibration slopes, for most detectors in the profiling instrument, were less than 1%. Long-term averages can be applied to most channels, with deviations only after major instrument upgrades. The methods used here to examine stability accommodate the addition of new calibration data as they become available. This enables researchers to closely track any changes in the performance of these instruments and to adjust the calibration coefficients accordingly. This analysis may serve as a template for radiometer histories which will be cataloged by the SIMBIOS Project.

Chapter 1

OC2v2: Update on the Initial Operational SeaWiFS Chlorophyll *a* Algorithm

Stéphane Maritorena
ICESS/University of California at Santa Barbara
Santa Barbara, California

John E. O'Reilly
NOAA National Marine Fisheries Service
Narragansett, Rhode Island

Abstract

The original at-launch SeaWiFS algorithm (OC2 for Ocean Chlorophyll 2-band algorithm) was derived from the SeaBAM data set ($N = 919$) which contains coincident remote sensing reflectance, $\tilde{R}_{\rm rs}$, and *in situ* chlorophyll *a*, $\tilde{C}_a$, measurements from a variety of oceanic provinces. Following the SeaWiFS launch, the accuracy of SeaWiFS chlorophyll *a* estimates using the OC2 algorithm was evaluated against new *in situ* measurements. These new data indicated that OC2 was performing generally well in Case-1 waters with $\tilde{C}_a$ concentration, between 0.03–1 mg m^{-3}, but tended to overestimate $\tilde{C}_a$ at higher concentrations. To strengthen the SeaBAM data set at $\tilde{C}_a > 1\,{\rm mg\,m^{-3}}$, 255 new stations were added to the original data set. These new data generally showed lower $R_{\rm rs}(490)/R_{\rm rs}(555)$ band ratios at $\tilde{C}_a > 4\,{\rm mg\,m^{-3}}$ than in the original SeaBAM data set, which would explain some of the overestimations observed with OC2. The new SeaBAM data set was used to refine the coefficients for the OC2 MCP function. The updated algorithm (OC2v2) is presented along with its statistical performance and a comparison with the original version of the algorithm.

1.1 INTRODUCTION

The at-launch SeaWiFS chlorophyll *a* algorithm, named OC2 for Ocean Chlorophyll 2-band algorithm, is an empirical equation relating remote sensing reflectances, $R_{\rm rs}$, in the 490 and 555 nm bands to chlorophyll *a* concentration, C_a (O'Reilly et al. 1998). OC2 was derived from a large data set ($N = 919$) of coincident *in situ* remote sensing reflectance and chlorophyll *a* concentration measurements, $\tilde{R}_{\rm rs}(\lambda)$ and $\tilde{C}_a$, respectively. This large data set covered a $\tilde{C}_a$ range of 0.02–32 mg m^{-3} from a variety of oceanic provinces, and was assembled during SeaBAM. The main SeaBAM objective was to evaluate a variety of bio-optical algorithms and produce an at-launch operational algorithm suitable for producing chlorophyll *a* images at global scales from SeaWiFS data (Firestone and Hooker 1998). The OC2 algorithm was chosen by the SeaBAM participants, because it represented a good compromise between simplicity and performance over a wide range of C_a.

The formulation of the OC2 algorithm is an MCP:

$$C_a = 10^{(a_0 + a_1 R_2 + a_2 R_2^2 + a_3 R_2^3)} + a_4, \quad (1)$$

where $R_2 = \log_{10}\left(R_{555}^{490}\right)$ and $R_{\lambda_j}^{\lambda_i}$ is a compact notation for the $R_{\rm rs}(\lambda_i)/R_{\rm rs}(\lambda_j)$ band ratio.

1.2 The SeaBAM DATA SET

While the SeaBAM data set (Fig. 1) is a large, quality-controlled data set, it has several known limitations:

1. It is mostly representative of Case-1, nonpolar waters;
2. Data from very oligotrophic ($\tilde{C}_a < 0.05\,{\rm mg\,m^{-3}}$) and eutrophic ($\tilde{C}_a > 3\,{\rm mg\,m^{-3}}$) areas are underrepresented;
3. The chlorophyll *a* concentration data are determined from both fluorometric and HPLC techniques; and
4. Because some of the $\tilde{R}_{\rm rs}(\lambda)$ measurements were not exactly centered on the SeaWiFS wavelengths, radiometric adjustments were necessary (O'Reilly et al. 1998).

Additionally, even though the SeaBAM data were quality controlled, there was still significant variability in the radiometric data (i.e., variations perpendicular to the x-axis in Fig. 1). This variability is partly natural, caused

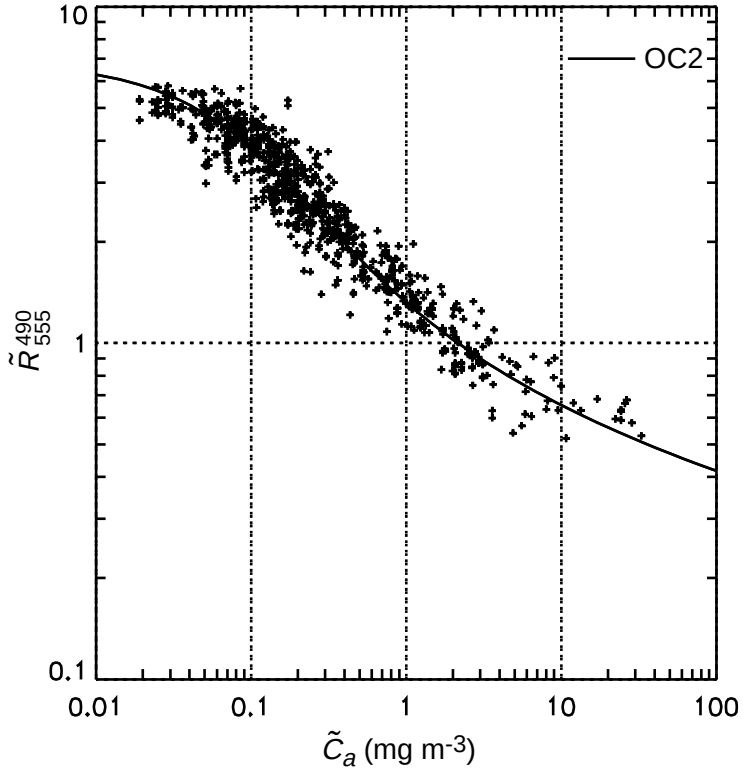

Fig. 1. A scatterplot of $\tilde{R}^{490}_{555}$ versus $\tilde{C}_a$ for the original SeaBAM data set ($N = 919$). The curve represents the OC2 algorithm.

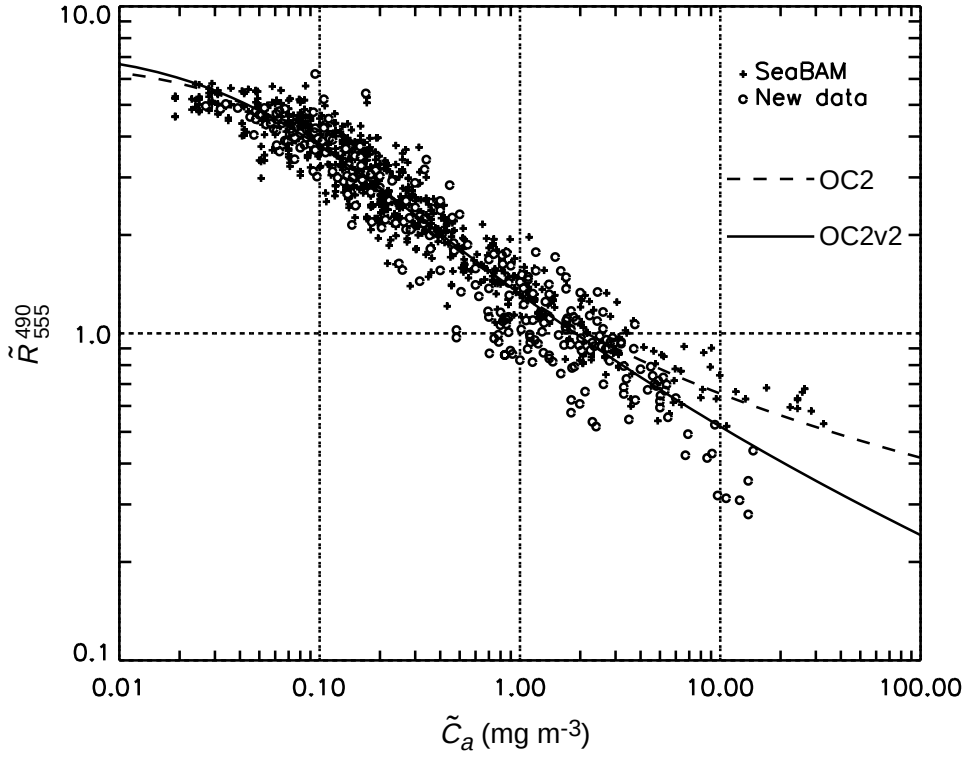

Fig. 2. A scatterplot of $\tilde{R}^{490}_{555}$ versus $\tilde{C}_a$ for the original SeaBAM (crosses) and the new data (circles). The dotted curve represents the original OC2 algorithm; the solid curve represents OC2v2, the new algorithm.

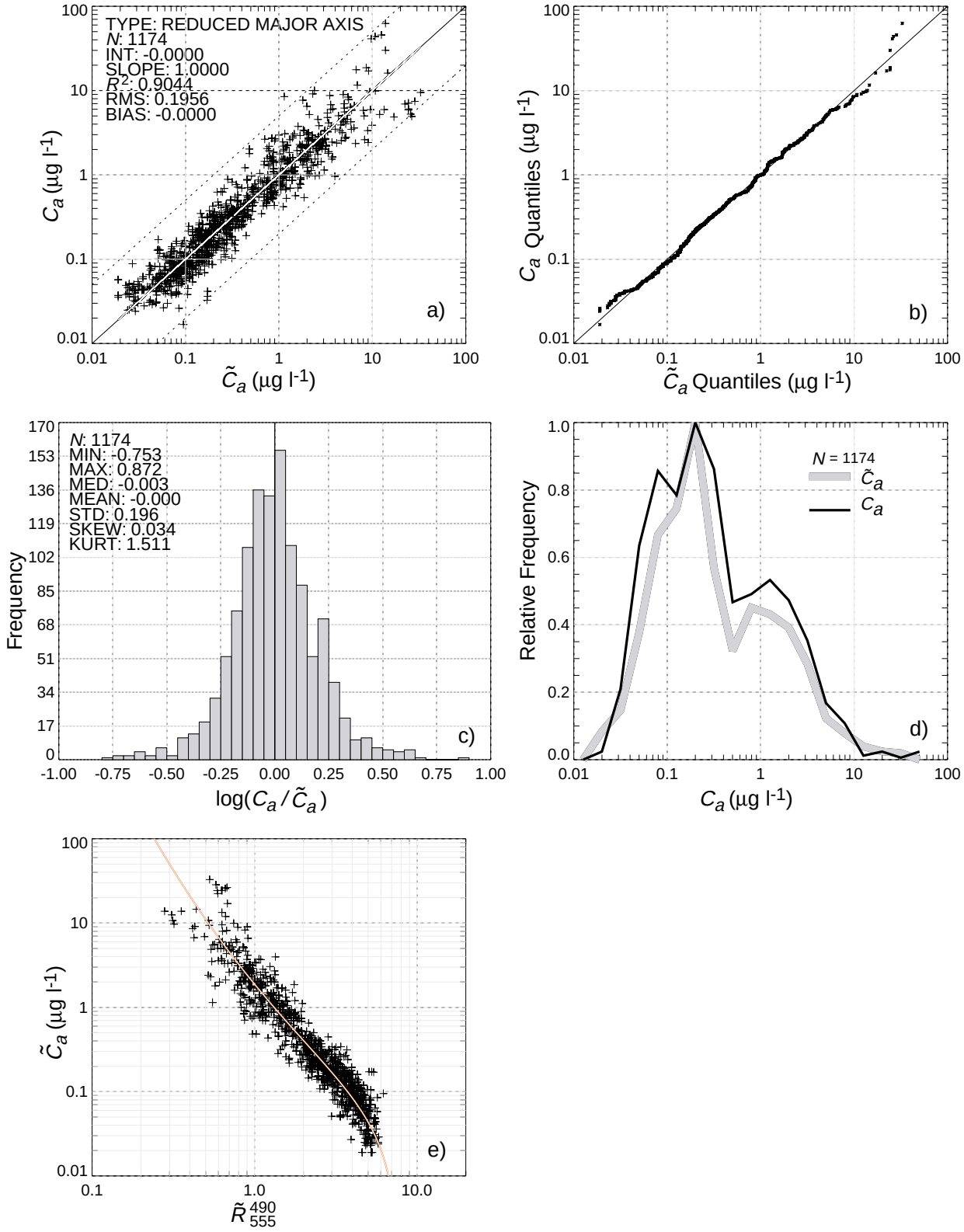

Fig. 3. Comparisons between OC2v2 (modeled) C_a values and (*in situ*) $\tilde{C}_a$ data: **a)** scatterplot of C_a versus $\tilde{C}_a$; **b)** quantile–quantile plot of C_a versus $\tilde{C}_a$; **c)** frequency distribution of $\log(C_a/\tilde{C}_a)$; **d)** relative frequency of C_a (thin solid curve) and $\tilde{C}_a$ (thick gray curve); **e)** R_{555}^{490} versus C_a. Also shown is the OC2v2 model (solid curve).

Table 1. Data sources and characteristics of the combined SeaBAM data set. The BBOP data sets were taken monthly, and the California Cooperative Fisheries Institute (CalCOFI) data sets were taken quarterly. N_F is the number fluorometric chlorophyll *a* sets, and N_H is the number of HPLC chlorophyll *a* sets. The last six subsets are the new data that were added to the original SeaBAM data.

Data Set	*Provider*	*Location*	*Date(s)*	*N*	N_F	N_H	*Wavelengths*
BBOP92-93	D. Siegel	Sargasso Sea	1992–1993	72	72	72	410 441 488 520 565 665
BBOP94-95	D. Siegel	Sargasso Sea	1994–1995	67	61	67	410 441 488 510 555 665
WOCE	J. Marra	50°S–13°N, 88–91°W	Mar93	70	70		410 441 488 520 565 665
		10°S–30°N, 18–37°W	Apr94				
EqPac	C. Davis	0°, 140°W	Mar92, Sept92	126		126	410 441 488 520 550 683
NABE	C. Trees	46–59°N, 17–20°W	May89	72		72	412 441 488 521 550
NABE	C. Davis	46°N, 19°W	Apr89	40		40	410 441 488 520 550 683
Carder	K. Carder	N. Atlantic	Aug91	87	87		412 443 490 510 555 670
		Pacific	Jul92				
		Gulf of Mexico	Apr93				
		Arabian Sea	Nov94, Jun95				
CalCOFI	G. Mitchell	Calif. Current	Aug93–Sept96	303	303		412 443 490 510 555 665
MOCE-1	D. Clark	Monterey Bay	Sept92	8	8	8	412 443 490 510 555
MOCE-2	D. Clark	Gulf of Calif.	Apr93	5	5	5	412 443 490 510 555
North Sea	R. Doerffer	55–52°N, 0–8°E	Jul94	10		10	412 443 490 510 555 670
Chesapeake Bay	L. Harding	37°N, 75°W	Apr95 and Jul95	9		9	412 443 490 510 555 671
Canadian Arctic	G. Cota	74.38°N, 95°W	Aug96	8	8		412 443 490 509 555 665
AMT-1	S. Hooker	50°N–50°S, 0–60°W	Sept95 and Apr96	42	42	33	412 443 490 510 555
AMT-2	G. Moore						
MBARI	F. Chavez	9°N–9°S, 120–180°W	Oct97–Dec97	34		34	412 443 490 510 555 670
CoASTS	G. Zibordi	45.3°N, 12.5°E	Sept97–Jan98	35		35	412 443 490 510 555 670
CARIACO	F. Müller-Karger	10.3°N, 64.4°W	May96–Aug97	14	14	5	412 443 490 510 555 670
AMT-5	S. Hooker	50°N–50°S, 20°E–60°W	Sept97–Jun98	82		82	412 443 490 510 555 670
AMT-6	S. Hooker						
ROAVERRS 96–97	K. Arrigo	Ross Sea	Dec97–Jan98	67	67		412 443 490 510 555 670
CSC	M. Culver	30–35°N, 76–82°W	May97–Nov97	23	22	15	412 443 490 510 555
			Total	1174	759	613	

1. BBOP: Bermuda Bio-Optical Prfiler
2. WOCE: World Ocean Circulation Experiment
3. EqPac: Equatorial Pacific (Process Study)
4. NABE: North Atlantic Bloom Experiment
5. CalCOFI: California Cooperative Fisheries Institute
6. MOCE: Marine Optical Characterization Experiment
7. AMT: Atlantic Meridional Transect
8. MBARI: Monterey Bay Aquarium Research Institute
9. CoASTS: Coastal Atmosphere and Sea Time Series
10. ROAVERRS: Research on Ocean–Atmosphere Variability and Ecosystem Response in the Ross Sea
11. CSC: Coastal Services Center (NOAA)

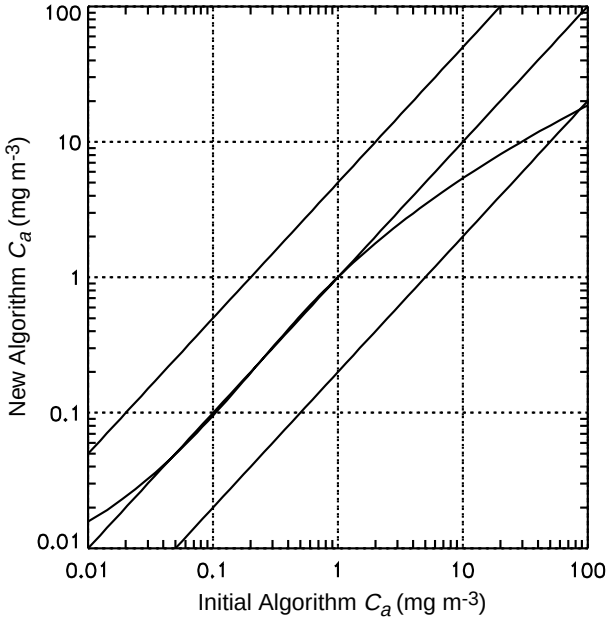

Fig. 4. Statistical and graphical comparisons of the OC2 and OC2v2 algorithms. The thick solid curve illustrates how both algorithms compare in the 0.01–100 mg m^{-3} C_a concentration range (when the same R_{555}^{490} ratios are used for both equations). The 1:1 (center), 1:5 (bottom), and 5:1 (top) lines are also plotted.

by the bio-optical variability among the different oceanic provinces sampled (e.g., variation in phytoplankton species, relative concentration, and the influence of accessory pigments or the physiological state of phytoplanktonic cells, etc.), but some of this radiometric variability results from differences in methodologies, instrument designs, calibrations, data processing, and environmental conditions (sea and sky state).

1.3 OC2v2 ALGORITHM

Since the SeaBAM workshop, new *in situ* measurements have become available and were used to test the accuracy of the OC2 algorithm. These new data indicated that OC2 was performing generally well (within the ±35% accuracy) in Case-1 waters with $\tilde{C}_a$ between 0.03–1 mg m^{-3}, but at chlorophyll *a* concentrations exceeding 2–3 mg m^{-3}, OC2 tended to overestimate $\tilde{C}_a$. This tendency was also apparent in SeaWiFS chlorophyll retrievals from some offshore, chlorophyll-rich waters, where ample historical sea-truth data suggest that the frequency of these high SeaWiFS chlorophyll retrievals are improbable.

As indicated above, the SeaBAM data set contains relatively few chlorophyll *a* measurements above 2 mg m^{-3}. Moreover, those above 2 mg m^{-3} are from a limited number of regions and may not adequately represent the full range of bio-optical variability expected in chlorophyll-rich waters. To strengthen the SeaBAM data set at $\tilde{C}_a >$ 1 mg m^{-3}, 255 new measurements of $\tilde{R}_{555}^{490}$ and $\tilde{C}_a$ were added to the original SeaBAM data set. Characteristics of the combined data (original SeaBAM data and new data) are illustrated in Table 1 and Fig. 2. Note that not all new data are from chlorophyll-rich waters. Nevertheless, all available new data were used to form the combined set, because these new sources increase the bio-optical diversity of the data set. Among these new data, the highest chlorophyll concentrations come from the ROAVERRS 96–97 and AMT-6 surveys. It is important to note the $\tilde{R}_{555}^{490}$ band ratios measured during these two surveys, at $\tilde{C}_a > 4$ mg m^{-3}, are substantially lower than the lowest band ratios present in the original SeaBAM data (Fig. 2).

The dispersion of the combined data is greater than in the original SeaBAM data set, particularly at chlorophyll values exceeding 2 mg m^{-3}. This increased dispersion is expected at high $\tilde{C}_a$ values, because some of these data come from near-shore coastal locations and may be influenced by various optically active components other than phytoplankton [colored dissolved organic matter (CDOM), sediments, nonbiogenous detrital substances, etc].

It is clear from Fig. 2 that the original SeaBAM data set did not adequately encompass the range of variability in $\tilde{R}_{555}^{490}$ band ratios present in chlorophyll-rich waters, and that OC2 derived from SeaBAM would overestimate chlorophyll *a* for many of the new observations with $\tilde{C}_a >$ 2 mg m^{-3}. Assuming the combined data shown in Fig. 2 are an improved representation of the natural variability present in productive oceanic and coastal zones, the combined data set was used to refine the OC2 functional coefficients. Because the underlying assumptions and appropriateness for using the MCP function remain valid (O'Reilly et al. 1998), other formulations were not explored. The

updated algorithm (OC2v2) is as follows:

$$C_a = 10^{(0.2974 - 2.2429R_2 + 0.8358R_2^2 - 0.0077R_2^3)} - 0.0929 \quad (2)$$

where R_2 is defined as in (1).

Statistical and graphical comparisons between chlorophyll a concentrations derived from OC2v2 versus $\tilde{C}_a$ are presented in Fig. 3. A comparison of the output from OC2 and OC2v2 is illustrated in Fig. 4. OC2 and OC2v2 yield very similar results for C_a ranging between 0.03–1.5 mg m^{-3}. At chlorophyll a values exceeding 3 mg m^{-3}, OC2v2 estimates are substantially lower than OC2. At very low chlorophyll a concentrations, 0.01–0.02 mg m^{-3}, OC2v2 produces slightly higher concentrations than OC2.

1.4 CONCLUSIONS

While, on average, OC2v2, should result in an improvement over OC2 in chlorophyll-rich areas, the uncertainties remain large for $\tilde{C}_a > 3$–4 mg m^{-3}. It must be emphasized that because the variability of the data increases at high concentrations, the precision of the SeaWiFS retrievals is inevitably degraded. It must also be kept in mind that the limitations of the original SeaBAM data set remain valid for the new combined data. More good quality $\tilde{R}_{\rm rs}(\lambda)$ and $\tilde{C}_a$ data are needed from regions with chlorophyll a concentrations above 3.0 and below 0.04 mg m^{-3} to better characterize the bio-optical variability of these waters and, thus, to identify potential strategies to achieve reasonable satellite chlorophyll a retrievals.

Acknowledgments

The authors wish to thank all the participants of the SeaBAM workshop for their help and contribution to the data set: K.L. Carder, S.A. Garver, S.K. Hawes, M. Kahru, C.R. McClain, B.G. Mitchell, G.F. Moore, J.L. Mueller, B.D. Schieber, and D.A. Siegel. We also would like to acknowledge J. Aiken, K.R. Arrigo, F.P. Chavez, D.K. Clark, G.F. Cota, M.E. Culver, C.O. Davis, R. Doerffer, L.W. Harding, S.B. Hooker, J. Marra, F.E. Müller-Karger, A. Subramaniam, C.C. Trees, and G. Zibordi who kindly provided some of their data.

Chapter 2

Ocean Color Chlorophyll *a* Algorithms for SeaWiFS, OC2, and OC4: Version 4

John E. O'Reilly
NOAA, National Marine Fisheries Service, Narragansett, Rhode Island

Stéphane Maritorena, David A. Siegel, Margaret C. O'Brien, and Dierdre Toole
ICESS/University of California Santa Barbara, Santa Barbara, California

B. Greg Mitchell and Mati Kahru
Scripps Institution of Oceanography, University of California, San Diego, California

Francisco P. Chavez and P. Strutton
Monterey Bay Aquarium Research Institute, Moss Landing, California

Glenn F. Cota
Old Dominion University, Norfolk, Virginia

Stanford B. Hooker and Charles R. McClain
NASA Goddard Space Flight Center, Greenbelt, Maryland

Kendall L. Carder and Frank Müller-Karger
University of South Florida, St. Petersburg, Florida

Larry Harding and Andrea Magnuson
Horn Point Laboratory, University of Maryland, Cambridge, Maryland

David Phinney
Bigelow Laboratory for Ocean Sciences, West Boothbay Harbor, Maine

Gerald F. Moore and James Aiken
Plymouth Marine Laboratory, Plymouth, United Kingdom

Kevin R. Arrigo
Department of Geophysics, Stanford University, Stanford, California

Ricardo Letelier
College of Oceanic and Atmospheric Sciences, Oregon State University

Mary Culver
NOAA, Coastal Services Center, Charleston, South Carolina

Abstract

This chapter describes the revisions (version 4) to the ocean chlorophyll two- and four-band algorithms, as well as the very large *in situ* data set used to update these algorithms for use in the third reprocessing of SeaWiFS data. The *in situ* data set is substantially larger ($N = 2{,}853$) than was used to develop earlier versions of OC2 and OC4. The data set includes samples from a greater variety of bio-optical provinces, and better represents oligotrophic and eutrophic waters. The correlation between chlorophyll *a* concentration, C_a, estimated using OC4 and *in situ* C_a ($\tilde{C}_a$) estimated from fluorometric and HPLC analyses was slightly higher than that for OC2. OC4 would be expected to perform better than OC2, when applied to satellite-derived, water-leaving radiances retrieved from oligotrophic and eutrophic areas. Variations of the OC4 algorithm are provided for other ocean color sensors to facilitate comparisons with SeaWiFS.

2.1 INTRODUCTION

The accuracy, precision, and utility of an empirical ocean color algorithm for estimating global chlorophyll *a* distributions depends on the characteristics of the algorithm and the *in situ* observations used to develop it. The empirical pigment and chlorophyll algorithm widely used in the processing of the global Coastal Zone Color Scanner (CZCS) data set was developed using fewer than 60 *in situ* radiance and chlorophyll *a* pigment observations (Evans and Gordon 1994). Since the CZCS period, a number of investigators have measured *in situ* remote sensing reflectance, $\tilde{R}_{\rm rs}(\lambda)$, and *in situ* chlorophyll *a* concentration, $\tilde{C}_a$, from a variety of oceanic provinces. In 1997, the SeaBAM group (Firestone and Hooker 1998) assembled a large $\tilde{R}_{\rm rs}(\lambda)$ and $\tilde{C}_a$ data set containing 919 observations. This data set was used to evaluate the statistical performance of chlorophyll *a* algorithms and to develop the ocean chlorophyll 2-band (OC2) and ocean chlorophyll 4-band (OC4) algorithms (O'Reilly et al. 1998).

OC2 predicts C_a from the $R_{\rm rs}(490)/R_{\rm rs}(555)$ band ratio using an MCP formulation. Hereafter, the $R_{\rm rs}$ ratio constructed from band A divided by band B is indicated by R_B^A, i.e., the $R_{\rm rs}(490)/R_{\rm rs}(555)$ band ratio is represented by R_{555}^{490}. OC4 also relates band ratios to chlorophyll *a* with a single polynomial function, but it uses the maximum band ratio (MBR) determined as the greater of the R_{555}^{443}, R_{555}^{490}, or R_{555}^{510} values. OC2 was employed as the standard chlorophyll *a* algorithm by the SeaWiFS Project following the launch of SeaWiFS in September 1997. Although the statistical characteristics of OC4 were superior to those of OC2, the SeaBAM group recommended using the simpler 2-band OC2 at launch.

With the goal of improving estimates in chlorophyll-rich waters, OC2 was revised (version 2) based on an expanded data set of 1,174 *in situ* observations (Maritorena and O'Reilly 2000) and applied by the SeaWiFS Project in the second data reprocessing (McClain 2000). Additional *in situ* data have become available as the result of new programs (e.g., SIMBIOS) and the continuation and expansion of ongoing field campaigns. These new data increase the variety of bio-optical provinces represented in the original data set and fill in regions of the $R_{\rm rs}(\lambda)$ and C_a domain which were not previously well represented. Also, results from over 2.5 years of SeaWiFS data are now available to assess the overall performance of the SeaWiFS instrument and identify areas where improvements are needed in the processing of satellite ocean color data (McClain 2000).

An update to the OC2 and OC4 chlorophyll algorithms for SeaWiFS are presented in this chapter, along with a description of the major features of the very large *in situ* data set used to refine these models, and a comparison of the updated algorithms with earlier versions. MBR chlorophyll algorithms for several other satellite ocean color sensors are also provided to facilitate intercomparisons with SeaWiFS.

2.2 THE *IN SITU* DATA SET

A very large data set of $\tilde{R}_{\rm rs}(\lambda)$ and $\tilde{C}_a$ measurements were assembled for the purpose of updating ocean color chlorophyll algorithms for SeaWiFS calibration and validation activities. The data sets and the principal investigators responsible for collecting the data are provided in Table 2. Table 3 gives the location and acquisition time periods of the data, along with an indication of the number of observations, how the chlorophyll *a* concentration was determined (fluorometry or HPLC), and how the radiometric observations were made (above- or in-water). The wavelengths of the latter are presented in Table 4.

The data set has a total of 2,853 *in situ* observations. It is the largest ever assembled for algorithm refinement, and represents a large diversity of bio-optical provinces. The C_a data are derived from a mixture of HPLC and fluorometric measurements from surface samples: 28% and 72% of the data, respectively (Table 3). The C_a values range from 0.008–90 mg m^{-3}. The relative frequency distribution of C_a has a primary and secondary peak at 0.2 mg m^{-3} and approximately 1 mg m^{-3}, respectively (Fig. 5). Oceanic regions with C_a between 0.08–3 mg m^{-3} are relatively well represented. There are 238 observations of C_a exceeding 5 mg m^{-3} and 116 observations with C_a less than 0.05 mg m^{-3}. A comparison of the C_a frequency distribution with those from previous versions (O'Reilly et al. 1998 and Maritorena and O'Reilly 2000) shows that oligotrophic and eutrophic waters are relatively better represented in the current data set. The present data set also has a more equitable distribution over a broader range of C_a (i.e., 0.08–3 mg m^{-3}).

Measurements of $R_{\rm rs}(\lambda)$ were made using both above- and in-water radiometers: 88% and 12% of the data, respectively (Table 3). In several subsets, multiple $R_{\rm rs}$ measurements were taken at stations where only a single C_a measurement was made. For these subsets (BBOP9293, WOCE, EqPac, NABE, GoA97, Ber96, Ber95, Lab97, Lab96, Res96, Res95–2, Res94), the median $R_{\rm rs}$ value was paired with the solitary C_a observation and added to the data set.

Except in a limited number of circumstances, band ratios determined from the median $R_{\rm rs}$ values agreed well with the individual band ratios. Several subsets, however, required adjustments to the $\tilde{R}_{\rm rs}(\lambda)$ values to conform with the SeaWiFS band set. The $\tilde{R}_{\rm rs}(555)$ value was estimated from the $\tilde{R}_{\rm rs}(565)$ measurement for the BBOP9293 and WOCE data using an equation derived from concurrent measurements of $\tilde{R}_{\rm rs}(555)$ and $\tilde{R}_{\rm rs}(565)$ from 1994–1995 BBOP surveys (equation 2 from O'Reilly et al. 1998). The $\tilde{R}_{\rm rs}(555)$ value for the CB-MAB subset was computed by averaging the $\tilde{R}_{\rm rs}(550)$ and $\tilde{R}_{\rm rs}(560)$ values. The $\tilde{R}_{\rm rs}(510)$ value was estimated from the $\tilde{R}_{\rm rs}(520)$ values for the EqPac, WOCE, NABE, and BBOP9293 data sets using the following conversion equation based on Morel and Maritor-

Table 2. The data sets and the investigators responsible for the data collection activity.

No.	*Data Set*	*Investigators*
1	ROAVERRS 96–97	Arrigo, K.
2	CARDER	Carder, K.
3	CARDER	Carder, K.
4	CARDER	Carder, K.
5	CARDER	Carder, K.
6	MF0796	Carder, K.
7	TOTO	Carder, K.
8	CoBOP	Carder, K., J. Patch
9	EcoHAB	Carder, K., J. Patch
10	Global	Chavez, F.
11	MBARI EqPac	Chavez, F., P. Strutton
12	MOCE-1	Clark, D.
13	MOCE-2	Clark, D.
14	MOCE-4	Clark, D., C. Trees
15	GoA97	Cota, G.
16	Ber95	Cota, G., S. Saitoh
17	Ber96	Cota, G., S. Saitoh
18	Lab96	Cota, G., G. Harrison
19	Lab97	Cota, G., G. Harrison
20	Res94	Cota, G.
21	Res95-2	Cota, G.
22	Res96	Cota, G.
23	Res98	Cota, G.
24	CSC	Culver, M., A. Subramaniam
25	CSC	Culver, M., A. Subramaniam
26	CSC	Culver, M., A. Subramaniam
27	EqPac	Davis, C.
28	NABE	Davis, C.
29	CB-MAB	Harding, L., A. Magnuson
30	AMT-1	Hooker, S., G. Moore
31	AMT-2	Moore, G., S. Hooker
32	AMT-3	Hooker, S., J. Aiken, S. Maritorena
33	AMT-4	Hooker, S., S. Maritorena
34	AMT-5	Hooker, S., S. Maritorena
35	AMT-6B	Moore, G., S. Hooker, S. Maritorena
36	AMT-6	Hooker, S., S. Maritorena
37	AMT-7	Hooker, S., S. Maritorena
38	AMT-8	Hooker, S., S. Maritorena
39	HOT	Letelier, R., R. Bidigare, D. Karl
40	WOCE	Marra, J.
41	WOCE	Marra, J.
42	CalCOFI	Mitchell, G., M. Kahru
43	CalCOFI	Mitchell, G., M. Kahru
44	RED9503	Mitchell, G., M. Kahru
45	AI9901	Mitchell, G., M. Kahru
46	JES9906	Mitchell, G., M. Kahru
47	CARIACO	Müller-Karger, F., R. Varela, J. Akl, A. Rondon, G. Arias
48	NEGOM	Müller-Karger, F., C. Hu, D. Biggs, B. Nababan, D. Nadeau, J. Vanderbloemen
49	ORINOCO	Müller-Karger, F., R. Varela, J. Akl, A. Rondon, G. Arias
50	GOM	Phinney, D., C. Yentch
51	Arabian Sea	Phinney, D., C. Yentch
52	FL-Cuba	Phinney, D., C. Yentch

Table 2. (cont.) The data sets and the investigators responsible for the data collection activity.

No.	*Data Set*	*Investigators*
53	BBOP 9293	Siegel, D., M. O'Brien, N. Nelson, T. Michaels
54	BBOP 9499	Siegel, D., M. O'Brien, N. Nelson, T. Michaels
55	Plumes & Blooms	Siegel, D., D. Toole, L. Mertes, R. Smith, L. Washburn, M. Brzezinski
56	NABE	Trees, C.
57	CoASTS	Zibordi, G.

Table 3. Data sources, locations, and acquisition dates (summarized by the three-letter month abbreviation and the two-digit year) of the global data set. N is the number of samples, the C_a column indicates the method(s) used for chlorophyll a determination (F for fluorometry and H for HPLC), and the $R_{\rm rs}$ column indicates the type of radiometric used for measuring remote sensing reflectance (A for above water and B for below water).

No.	*Data Set*	*Location*	*Dates*	N	C_a	$R_{\rm rs}$
1	ROAVERRS 96–97	Ross Sea	Dec97–Jan98	73	H	B
2	CARDER	North Atlantic	Aug91	87	F	A
3	CARDER	Pacific	Jul92		F	A
4	CARDER	Gulf of Mexico	Apr93		F	A
5	CARDER	Arabian Sea	Nov94, Jun95		F	A
6	MF0796	Bering Sea	Apr96	22	F	A
7	TOTO	Bahamas	Apr98, Apr99	26	F	A
8	CoBOP	Bahamas	May98, May–Jun99	43	F	A
9	EcoHAB	W. Florida Shelf	Mar99–Mar00 (6 Surveys)	57	F	A
10	Global	Global	Nov93–Jul98 (18 Surveys)	284	F	B
11	MBARI EqPac	Equatorial Pacific	Oct97–Nov99 (6 Surveys)	89	F	B
12	MOCE-1	Monterey Bay	Sep92	8	H	B
13	MOCE-2	Gulf of California	Apr93	5	H	B
14	MOCE-4	Hawaii	Jan–Feb98	20	F	B
15	GoA97	Gulf of Alaska	Oct97	10	F	B
16	Ber95	Bering Sea	Jul95	17	F	B
17	Ber96	Bering Sea	Jul96	16	F	B
18	Lab96	Labrador Sea	Oct–Nov96	68	F	B
19	Lab97	Labrador Sea	May–Jun97	71	F	B
20	Res94	Resolute	Aug94	9	F	B
21	Res95-2	Resolute	Aug95	14	F	B
22	Res96	Resolute	Aug96	11	F	B
23	Res98	Resolute	Aug98	91	F	B
24	CSC	Onslow Bay and S. MAB	May97	12	F	B
25	CSC	S. Mid-Atlantic Bight	Sep97, Nov97, Apr98, Feb99	45	F	B
26	CSC	Gulf of Mexico	Apr99	6	F	B
27	EqPac	0°N,140°W	Mar92, Sep92	36	H	B
28	NABE	46°N,19°W	Apr89	6	H	B
29	CB-MAB	Chesapeake Bay and MAB	Apr96–Oct98 (9 Surveys)	197	H	B
30	AMT-1	E. North Atlantic and W. South Atlantic	Sep–Oct95	23	F	B
31	AMT-2	E. North Atlantic and W. South Atlantic	Apr–May96	19	F	B
32	AMT-3	E. North Atlantic and W. South Atlantic	Sep–Oct96	20	H	B
33	AMT-4	E. North Atlantic and W. South Atlantic	Apr–May97	21	H	B
34	AMT-5	E. North Atlantic and W. South Atlantic	Sep–Oct97	45	H	B
35	AMT-6B	E. North Atlantic and W. South Atlantic	Apr–May98	62	H	B
36	AMT-6	E. North Atlantic and E. South Atlantic	May–Jun98	35	H	B
37	AMT-7	E. North Atlantic and W. South Atlantic	Sep–Oct98	52	H	B
38	AMT-8	E. North Atlantic and W. South Atlantic	May–Jun99	46	H	B
39	HOT	N. Pacific Subtropical Gyre (ALOHA)	Feb98–May99	50	H,F	B
40	WOCE	50°S–13°N,88–91°W	Mar–Apr93	15	F	B

Table 3. (cont.) The data sources, locations, and acquisition dates of the global data set.

No.	*Data Set*	*Location*	*Dates*	*N*	C_a	R_{rs}
41	WOCE	10°S–30°N,18–37°W	Apr–May94	27	F	B
42	CalCOFI	California Coast	93–97 (16 Surveys)	299	F	B
43	CalCOFI	California Coast	97–99 (6 Surveys)	100	F	B
44	RED9503	California Coast (Red Tide)	Mar95	9	F	B
45	AI9901	Subtrop. Atlantic, Indian Ocean	Jan–Mar99	36	F	B
46	JES9906	E. Japan Sea	Jun–Jul99	37	F	B
47	CARIACO	Cariaco Basin	May96–Aug99	35	F	A
48	NEGOM	NE Gulf of Mexico	Jul–Aug98	13	F	A
49	ORINOCO	Orinoco Delta, Paria Gulf, Orinoco Plume	Jun98, Oct98, Feb99, Oct99	48	F	A
50	GOM	Gulf of Maine	Mar95–Apr99 (11 Surveys)	92	F	C
51	Arabian Sea	Arabian Sea	Jul95, Sep95, Oct95	15	F	C
52	FL-Cuba	Florida–Cuba	Mar99	13	F	C
53	BBOP 9293	Sargasso Sea (BATS)	92–93	30	H	B
54	BBOP 9499	Sargasso Sea (BATS)	Jan94–Aug99	83	H	B
55	Plumes & Blooms	Santa Barbara Channel	Aug96–June99	251	F	B
56	NABE	46–59°N,17–20°W	May89	19	H	B
57	CoASTS	N. Adriatic Sea	Sep97–Jan98	35	H	B

Table 4. The wavelengths of the radiometer data.

No.	*Data Set*	*Nominal Center Wavelengths* [nm]
1	ROAVERRS 96–97	412 443 490 510 555 655
2	CARDER	412 443 490 510 555 670
3	CARDER	412 443 490 510 555 670
4	CARDER	412 443 490 510 555 670
5	CARDER	412 443 490 510 555 670
6	MF0796	412 443 490 510 555 670
7	TOTO	412 443 490 510 555 670
8	CoBOP	412 443 490 510 555 670
9	EcoHAB	412 443 490 510 555 670
10	Global	412 443 490 510 555 656 665
11	MBARI EqPac	412 443 490 510 555 670
12	MOCE-1	412 443 490 510 555
13	MOCE-2	412 443 490 510 555
14	MOCE-4	412 443 490 510 555 670
15	GoA97	405 412 443 490 510 520 532 555 565 619 665 683 700
16	Ber95	412 443 490 510 555 665 683
17	Ber96	405 412 443 490 510 520 532 555 565 619 665 683 700
18	Lab96	405 412 443 490 510 520 532 555 565 619 665 683 700
19	Lab97	405 412 443 490 510 520 532 555 565 619 665 683 700
20	Res94	412 443 490 510 555 665 683
21	Res95-2	412 443 490 510 555 665 683
22	Res96	405 412 443 490 510 520 532 555 565 619 665 683 700
23	Res98	405 412 443 490 510 520 532 555 565 619 665 683 700
24	CSC	380 412 443 490 510 555 683
25	CSC	380 412 443 490 510 555 683
26	CSC	380 412 443 490 510 555 683
27	EqPac	410 441 488 520 550 683
28	NABE	410 441 488 520 550 683
29	CB-MAB	412 443 455 490 510 532 550 560 589 625 671 683 700
30	AMT-1	412 443 490 510 555 665
31	AMT-2	412 443 490 510 555 665

Table 4. (cont.) The wavelengths of the radiometer data.

No.	*Data Set*	*Nominal Center Wavelengths* [nm]
32	AMT-3	412 443 490 510 555 665
33	AMT-4	412 443 490 510 555 665
34	AMT-5	412 443 490 510 555 665
35	AMT-6B	412 443 490 510 555 665
36	AMT-6	412 443 490 510 555 665
37	AMT-7	412 443 490 510 555 665
38	AMT-8	412 443 490 510 555 665
39	HOT	412 443 490 510 555 670
40	WOCE	410 441 488 520 565 665
41	WOCE	410 441 488 520 565 665
42	CalCOFI	340 380 395 412 443 455 490 510 532 555 570 665
43	CalCOFI	412 443 490 510 555 665
44	RED9503	340 380 395 412 443 455 490 510 532 555 570 665
45	AI9901	412 443 490 510 555 665
46	JES9906	412 443 490 510 555 665
47	CARIACO	412 443 490 510 555 656
48	NEGOM	412 443 490 510 555 670
49	ORINOCO	410 443 490 510 555 670
50	GOM	412 443 490 510 555 665
51	Arabian Sea	412 443 490 510 555 665
52	FL-Cuba	412 443 490 510 555 665
53	BBOP 9293	410 441 488 520 565 665
54	BBOP 9499	410 441 465 488 510 520 555 565 589 625 665 683
55	Plumes & Blooms	412 443 490 510 555 656
56	NABE	412 441 488 521 550
57	CoASTS	412 443 490 510 555 655 683

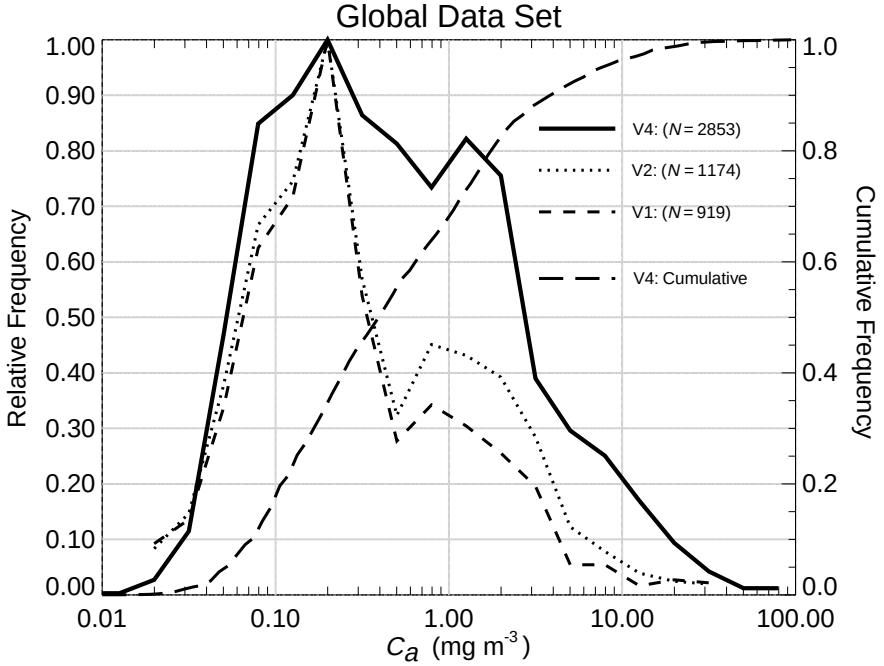

Fig. 5. The relative frequency distribution of C_a concentration in the *in situ* data used to develop versions 4 and earlier versions of the ocean chlorophyll algorithms (V1 is version 1, V2 is version 2, and V4 is version 4). The version 3 data set, an intermediate test set, is not described here). Relative frequency is the observed frequency normalized to the maximum frequency.

ena (2000):

$$R_{\rm rs}(510) \;=\; R_{\rm rs}(520)\Big[1.0605321 \;-\; 0.1721619\,\gamma_a \;+\; 0.0295192\,\gamma_a^2 \;+\; 0.0150622\,\gamma_a^3 \;-\; 0.004133924\,\gamma_a^4\Big] \qquad (3)$$

where $\gamma_a = \log(C_a)$.

The Chesapeake Bay and Mid-Atlantic Bight (CBMAB) $\tilde{R}_{\rm rs}(\lambda)$ measurements were corrected for the influence of radiometer self-shading (Gordon and Ding 1992, and Zibordi and Ferrari 1995) using equations provided by G. Zibordi. Corrections for radiometer shading by the *Acqua Alta* Oceanographic Tower were also applied to the CoASTS $\tilde{R}_{\rm rs}(\lambda)$ data (Zibordi et al. 1999). The CalCOFI, RED9503, and AI9901 data sets were also corrected for radiometer self-shading (Kahru and Mitchell 1998a and 1998b.)

Interpolated estimates of $R_{\rm rs}$ were also generated for non-SeaWiFS wavelengths, which were not consistently present in the global data set, to develop chlorophyll algorithms similar to OC4 for use by other ocean color sensors. The interpolation–extrapolation method consisted of two steps. A cubic spline interpolation method [using the Interactive Data Language (IDL)†, version 5.3] and four measured adjacent $R_{\rm rs}$ values were used to derive the interpolated $R_{\rm rs}$ estimate ($\hat{R}_{\rm rs}$). The interpolated values were then regressed against those measured $R_{\rm rs}$ values present in the global data set; the resulting regresssion equation (Table 5) was applied in the second step to remove bias in the interpolated values. This scheme resulted in good agreement between interpolated and measured $R_{\rm rs}$ over a wide range of chlorophyll concentration (Fig. 6).

The characteristics of the $R_{\rm rs}$ data most relevant to bio-optical algorithms are illustrated in Fig. 7. An important feature revealed by these plots is the dispersion of the data (variability is orthogonal to the major axis of the data). A pattern common to these plots is the progressive increase in dispersion with increasing chlorophyll concentration and decreasing band ratio. This is most evident in the plots of R_{555}^{412} and R_{555}^{443} versus C_a. In addition to bio-optical variability, some of the scatter is caused by a variety of methodological errors (for example, surface effects, ship shadow, and lower radiometric precision and extrapolation errors associated with measurements made in turbid waters).

Considering only the degree of scatter evident in these plots, the R_{555}^{443} provide the most precise (lowest dispersion) C_a estimates at concentrations approximately less than $0.4\,{\rm mg\,m^{-3}}$, whereas, the R_{555}^{510} and R_{555}^{490} band ratios would provide relatively more precise estimates of C_a in chlorophyll-rich waters. Over the entire data domain, R_{555}^{490} yields the highest correlation with C_a, $R^2 = 0.862$ (Fig. 7), followed by R_{555}^{443}, $R^2 = 0.847$. It must be kept in mind, however, that R^2 is an index of the degree of linear association and a simple linear model is generally not the best model to describe the band ratio C_a relationships over the entire range of the data.

2.3 OC2 AND OC4

The $R_{\rm rs}$ and C_a data (N=2,853) were used to revise the OC2 and OC4 C_a algorithms. Four observations, with $\tilde{C}_a$ greater than $64\,{\rm mg\,m^{-3}}$, were widely scattered in plots of band ratios versus C_a and were not used. A test version of the OC4 MBR model revealed 45 observations had $\log(C_a)/\log(\tilde{C}_a)$ values exceeding three standard deviations, so these data were also discarded. The final model coefficients were derived using the remaining 2,804 $R_{\rm rs}$ and $\tilde{C}_a$ combinations. Algorithm refinement involved the determination of model coefficients using iterative minimization routines (using IDL) to achieve a slope of 1.000, an intercept of 0.000, minimum root mean square (RMS) error, and maximum R^2 between model and measured $\tilde{C}_a$ concentration. The first version of OC4 (O'Reilly et al. 1998) was formulated as a modified cubic polynomial (i.e., a third order polynomial plus an extra coefficient), however, the current version of OC4 uses a fourth order polynomial (five coefficients), because this yielded better statistical agreement between model (C_a) and $\tilde{C}_a$ than an MCP formulation. An MCP equation was used to refine OC2 to the same set of values (N=2,804) used to update OC4.

The fourth order polynomial equation for OC4 version 4 (OC4v4), is:

$$C_a \;=\; 10.0^{\big(0.366 \;-\; 3.067R_{\rm 4S} \;+\; 1.930R_{\rm 4S}^2 \;+\; 0.649R_{\rm 4S}^3 \;-\; 1.532R_{\rm 4S}^4\big)} \qquad (4)$$

where $R_{\rm 4S} = \log_{10}\left(R_{555}^{443} > R_{555}^{490} > R_{555}^{510}\right)$, where the argument of the logarithm is a shorthand representation for the maximum of the three values. Hereafter, in an expression such a $R_{\rm 4S}$, the numerical part of the subscript refers to the number of bands used, and the letter denotes a code for the specific satellite sensors [S is SeaWiFS, M is the Moderate Resolution Imaging Spectroradiometer (MODIS), O is the Ocean Color and Temperature Scanner (OCTS), E is the Medium Resolution Imaging Spectrometer (MERIS), and C is CZCS]. The modified cubic polynomial equation for OC2 version 4, hereafter referred to as OC2v4, is:

$$C_a \;=\; 10.0^{\big(0.319 \;-\; 2.336R_{\rm 2S} \;+\; 0.879R_{\rm 2S}^2 \;-\; 0.135R_{\rm 2S}^3\big)} \;-\; 0.071 \qquad (5)$$

where $R_{\rm 2S} = \log_{10}\left(R_{555}^{490}\right)$.

The statistical and graphical characteristics of these two algorithms are illustrated in Figs. 8 and 9. The R^2

† IDL is a software product of Research Systems, Inc., Boulder, Colorado.

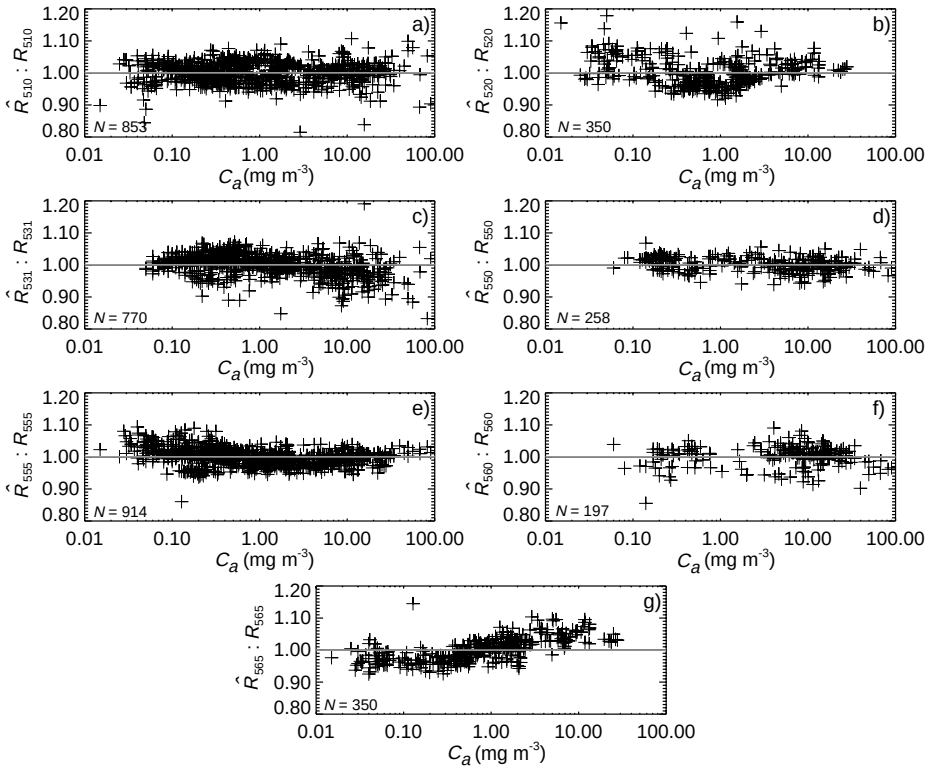

Fig. 6. The ratio of $R_{\rm rs}$ based on interpolated $R_{\rm rs}$ ($\hat{R}$) to measured $R_{\rm rs}$ (R) versus chlorophyll concentration (C_a): a) $\hat{R}_{510}$:R_{510}; b) $\hat{R}_{520}$:R_{520}; c) $\hat{R}_{531}$:R_{531}; d) $\hat{R}_{550}$:R_{550}; e) $\hat{R}_{555}$:R_{555}; f) $\hat{R}_{560}$:R_{560}; and g) $\hat{R}_{565}$:R_{565}.

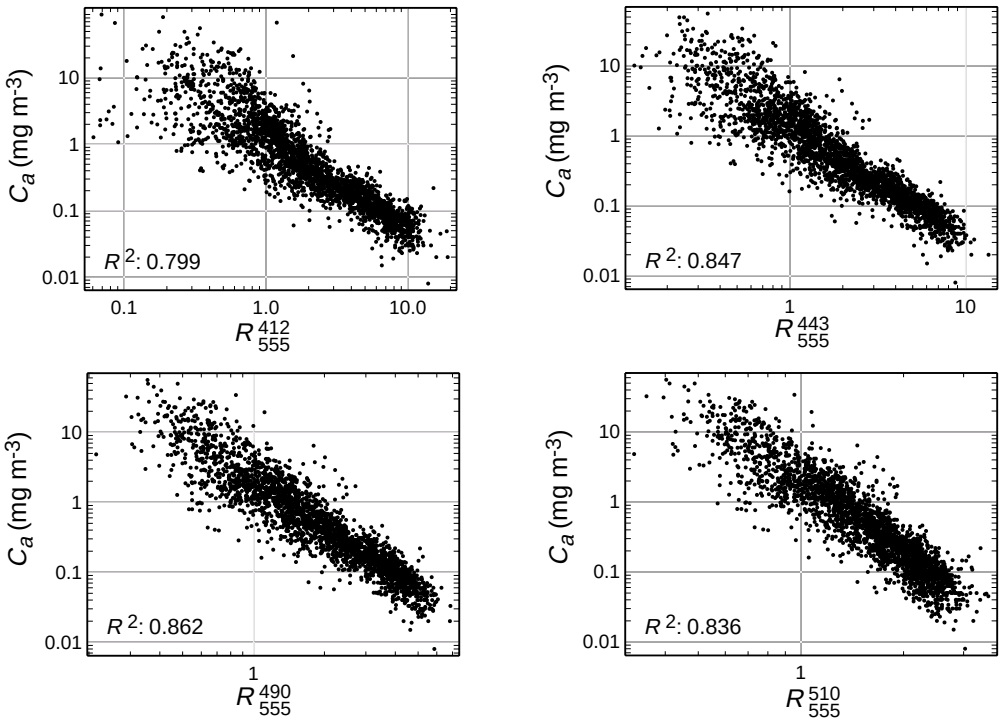

Fig. 7. The relationship between R^{412}_{555}, R^{443}_{555}, R^{490}_{555}, and R^{510}_{555} band ratios and chlorophyll concentrations less than 64 mg m^{-3} (N = 2,849, except for R^{412}_{555} where N = 2,813).

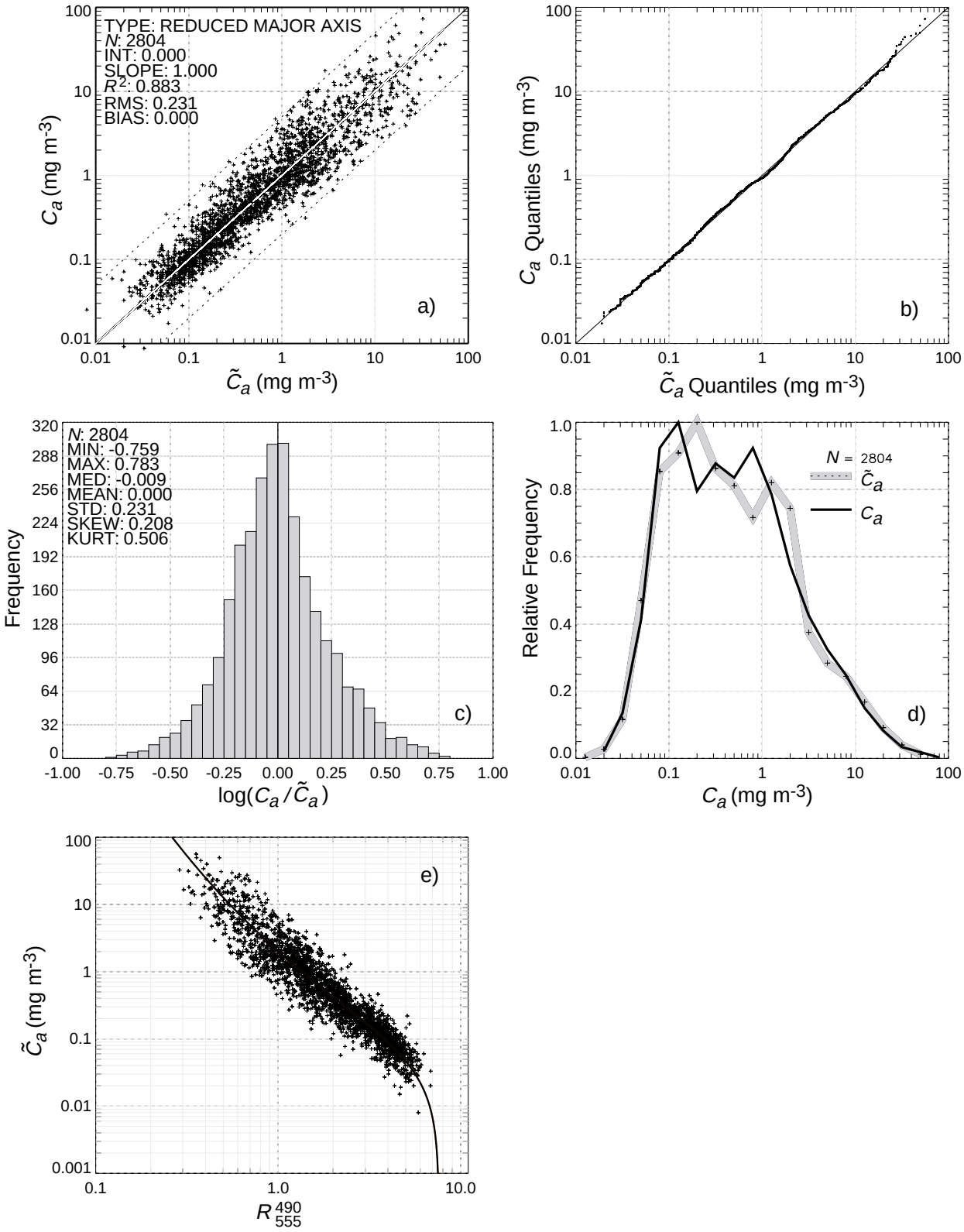

Fig. 8. Comparisons between OC2v4 modeled values (C_a) and *in situ* data ($\tilde{C}_a$): **a)** Scatterplot of C_a versus $\tilde{C}_a$; **b)** Quantile–quantile plot of C_a versus $\tilde{C}_a$; **c)** Frequency distribution of $\log(C_a/\tilde{C}_a)$; **d)** Relative frequency of C_a (thin solid curve) and $\tilde{C}_a$; **e)** R^{490}_{555} versus $\tilde{C}_a$. Also shown is the OC2v4 model (solid curve).

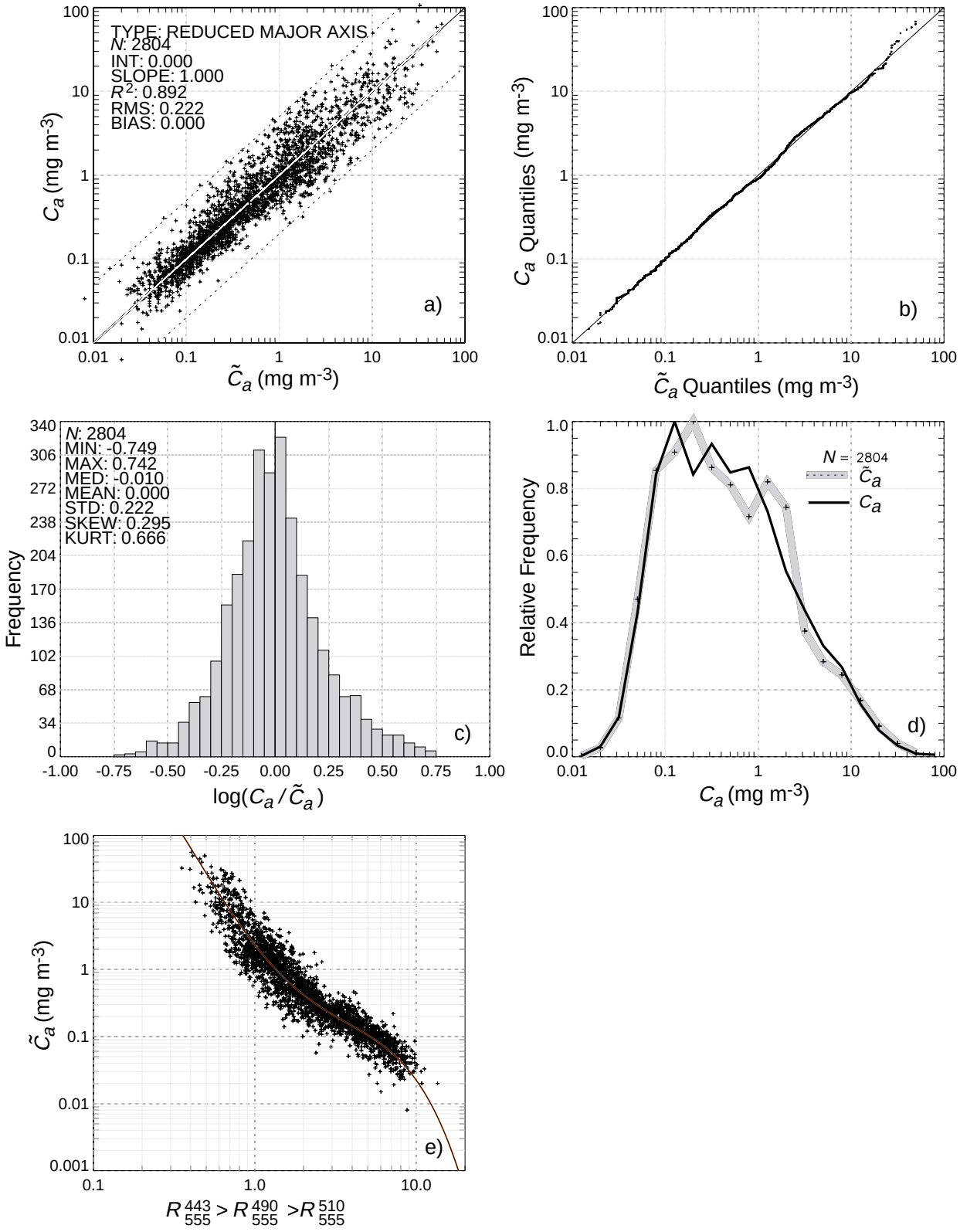

Fig. 9. Comparisons between OC4v4 modeled values (C_a) and *in situ* data ($\tilde{C}_a$): **a)** Scatterplot of C_a versus $\tilde{C}_a$; **b)** Quantile–quantile plot of C_a versus $\tilde{C}_a$; **c)** Frequency distribution of $\log(C_a/\tilde{C}_a)$; **d)** Relative frequency of C_a (thin solid curve) and $\tilde{C}_a$; **e)** R^{490}_{555} versus $\tilde{C}_a$. Also shown is the OC4v4 model (solid curve).

value between $\tilde{C}_a$ and (model) C_a is slightly higher with OC4 (0.892) than OC2 (0.883). Both models yield a relative frequency distribution that is approximately congruent with the $\tilde{C}_a$ distribution. The OC2 and OC4 models are extrapolated to a C_a value of 0.001, well below the lowest concentration ($0.008\,\mathrm{mg\,m^{-3}}$) present in the *in situ* data (Figs. 8e and 9e). If clear (clearest) water is operationally defined as $C_a = 0.001\,\mathrm{mg\,m^{-3}}$, then the clear water reflectance ratio (R^{443}_{555}) predicted by OC4 is within the theoretical range given in Table 6, whereas the extrapolated clear water R^{490}_{555} reflectance ratio for OC2 is greater than the theoretical clear water estimates.

Because the OC2v4 and OC4v4 algorithms were tuned to the same data set, their C_a estimates should be very highly correlated and internally consistent, with a slope of 1 and an intercept of 0. This is illustrated in Fig. 10. The reduced scatter (orthogonal to the 1:1 line), centered at about $1\,\mathrm{mg\,m^{-3}}$, indicates the region where both algorithms use the 490 nm band.

Additional noteworthy characteristics of OC4 are illustrated in Figs. 11 and 12. The R^{443}_{555} ratio dominates (50%) at MBRs above approximately 2.2, R^{490}_{555} between 2.2 and 1.1, and R^{510}_{555} at MBRs below 1.1 (Fig. 11). With respect to chlorophyll concentration, the R^{443}_{555} ratio dominates (50%) when C_a is below approximately $0.33\,\mathrm{mg\,m^{-3}}$, R^{490}_{555} for C_a between 0.33–$1.4\,\mathrm{mg\,m^{-3}}$, and R^{510}_{555} when C_a exceeds approximately $1.4\,\mathrm{mg\,m^{-3}}$ (Fig. 12).

Relative to OC2v2, OC2v4 predicts slightly higher C_a above concentrations of $3\,\mathrm{mg\,m^{-3}}$ (Fig. 13), while OC4v4 generates slightly lower C_a estimates at very high concentrations (Fig. 14). At C_a below $0.03\,\mathrm{mg\,m^{-3}}$, OC2v4 estimates are very similar to OC2v2, while OC4v4 estimates are slightly higher than those from OC4v2, particularly so when C_a is below $0.01\,\mathrm{mg\,m^{-3}}$. (Version 3 equations were preliminary and provided to the SeaWiFS Project for testing and evaluation and are not described here.)

There is considerable interest and benefit from comparing and merging data from various ocean color sensors (Gregg and Woodward 1998). This is one of the major objectives of SIMBIOS (McClain and Fargion 1999). In the particular case of ocean color data merging, one methodological issue to be resolved is how data from satellite sensors having different center band wavelengths can be merged to generate seamless maps of chlorophyll *a* distribution. Among several possible approaches, one is to develop internally consistent, sensor-specific variations of empirical chlorophyll *a* algorithms tuned to the same data set. This implies a comprehensive suite of *in situ* measurements at wavelengths matching the various satellite spectrometers or perhaps hyperspectral *in situ* data. To facilitate comparisons with SeaWiFS chlorophyll *a*, MBR algorithms for several ocean color sensors are presented in Table 7. These algorithms must be considered as an approximation, because the *in situ* data set is biased to SeaWiFS channels and a number of radiometric adjustments were made to the $R_{\mathrm{rs}}(\lambda)$ data to compensate for wavelength differences among the sensors (Table 4).

2.4 CONCLUSIONS

A large data set of $\tilde{R}_{\mathrm{rs}}$ and $\tilde{C}_a$ measurements was compiled and used to update the OC2 and OC4 bio-optical chlorophyll *a* algorithms. The present data set, which is substantially larger (N=2,853) than that used to develop the version 2 algorithms (N=1,174), includes samples from a greater variety of bio-optical provinces, and better represents oligotrophic and eutrophic waters.

Over the four-decade range in chlorophyll *a* concentration encompassed in the data set (0.008–$90\,\mathrm{mg\,m^{-3}}$), the R^{490}_{555} band ratio is the best overall single band ratio index of chlorophyll *a* concentration. In oligotrophic waters, however, the R^{443}_{555} ratio yields the best correlation with C_a and lowest RMS error, while in waters with chlorophyll concentrations exceeding approximately $3\,\mathrm{mg\,m^{-3}}$, the R^{510}_{555} ratio is the best-correlated index. OC4 takes advantage of this band-related shift in precision, and the well-known shift of the maximum of $R_{\mathrm{rs}}(\lambda)$ spectra towards higher wavelengths with increasing C_a. Dispersion between the OC2 model and $\tilde{C}_a$ tended to increase with increasing chlorophyll concentrations above $1\,\mathrm{mg\,m^{-3}}$, whereas dispersion using OC4 remained relatively low and uniform throughout the range of *in situ* data. Consequently, OC4 yields a slightly higher R^2 and lower RMS error than OC2.

Statistical comparisons of algorithm performance with respect to *in situ* data, however, provide only partial information about their performance when applied to satellite-derived water-leaving radiances. Operationally, OC4 would be expected to generate more accurate C_a estimates than OC2 for several reasons. In oligotrophic water, OC4 would be expected to provide more accurate C_a estimates than OC2, because the signal-to-noise ratio (SNR) is greater in the 443 nm band than the 490 nm band. In eutrophic waters, strong absorption in the blue region of the spectrum results in lower SNR for water-leaving radiances retrieved in the 412 nm and 443 nm bands relative to the 490 nm and 510 nm bands. Furthermore, the influence of the atmospheric correction scheme on the accuracy of derived water-leaving radiances used in band-ratio algorithms must be considered. The SeaWiFS atmospheric correction algorithm (Gordon and Wang 1994 and Wang 2000) uses the near infrared bands (765 and 865 nm) to characterize aerosol optical properties and estimates aerosol contribution to total radiance in the visible spectrum by extrapolation. The 510 nm band, being closer to the near infrared bands, is less prone to extrapolation errors than the 490 nm and 443 nm bands. In chlorophyll-rich water, therefore, OC4 would be expected to provide more accurate estimates of C_a than OC2.

The present version of the $\tilde{R}_{\mathrm{rs}}(\lambda)$ and $\tilde{C}_a$ data set represents a significant improvement in size, quality, and bio-optical diversity when compared with earlier versions, but

Table 5. Regression statistics (reduced major axis) for the linear relationship between log (measured $R_{\rm rs}$) and log (interpolated $R_{\rm rs}$), where m is the slope and b is the intercept.

$R_{\rm rs}$	N	R^2	m	b
510	853	0.995	0.9948	0.00299
520	350	0.990	1.0328	0.06280
531	770	0.995	0.9614	−0.1005
550	258	0.999	0.9827	−0.0425
555	914	0.998	1.0032	0.01141
560	197	0.998	1.0178	0.02361
565	350	0.989	1.0487	0.11512

Table 6. Comparison between theoretical and extrapolated clear water reflectance ratios using OC2 and OC4 algorithms, where a is the absorption per meter, b_b is the backward scattering coefficient per meter, and f is the function (unspecified). The theoretical reflectance ratios are based on the absorption and backscattering values from Pope and Fry (1997) and Morel (1974).

$R_{\rm rs}$ *Band Ratio*	$R_{\rm rs} = f\frac{b_b}{a+b_b}$	$R_{\rm rs} = f\frac{b_b}{a}$	*Algorithm*
443:555	16.53	21.78	18.21 (OC4)
490:555	6.13	6.66	7.502 (OC2)

Table 7. The maximum band ratio algorithms for the SeaWiFS, CZCS, OCTS, MODIS, and MERIS sensors. As with the OC4, OC4O, and OC4E algorithms, the argument of the logarithms for OC3M and OC3C is a shorthand representation for the maximum of the indicated values.

Sensor	*Name*	*Equation*
SeaWiFS	OC4	$C_a = 10.0^{\left(0.366 - 3.067R_{\rm 4S} + 1.930R_{\rm 4S}^2 + 0.649R_{\rm 4S}^3 - 1.532R_{\rm 4S}^4\right)}$ where $R_{\rm 4S} = \log_{10}\left(R_{555}^{443} > R_{555}^{490} > R_{555}^{510}\right)$
MODIS	OC3M	$C_a = 10.0^{\left(0.2830 - 2.753R_{\rm 3M} + 1.457R_{\rm 3M}^2 + 0.659R_{\rm 3M}^3 - 1.403R_{\rm 3M}^4\right)}$ where $R_{\rm 3M} = \log_{10}\left(R_{550}^{443} > R_{550}^{490}\right)$
OCTS	OC4O	$C_a = 10.0^{\left(0.405 - 2.900R_{\rm 4O} + 1.690R_{\rm 4O}^2 + 0.530R_{\rm 4O}^3 - 1.144R_{\rm 4O}^4\right)}$ where $R_{\rm 4O} = \log_{10}\left(R_{565}^{443} > R_{565}^{490} > R_{565}^{520}\right)$
CZCS	OC3C	$C_a = 10.0^{\left(0.362 - 4.066R_{\rm 3C} + 5.125R_{\rm 3C}^2 - 2.645R_{\rm 3C}^3 - 0.597R_{\rm 3C}^4\right)}$ where $R_{\rm 3C} = \log_{10}\left(R_{550}^{443} > R_{550}^{520}\right)$
MERIS	OC4E	$C_a = 10.0^{\left(0.368 - 2.814R_{\rm 4E} + 1.456R_{\rm 4E}^2 + 0.768R_{\rm 4E}^3 - 1.292R_{\rm 4E}^4\right)}$ where $R_{\rm 4E} = \log_{10}\left(R_{560}^{443} > R_{560}^{490} > R_{560}^{510}\right)$

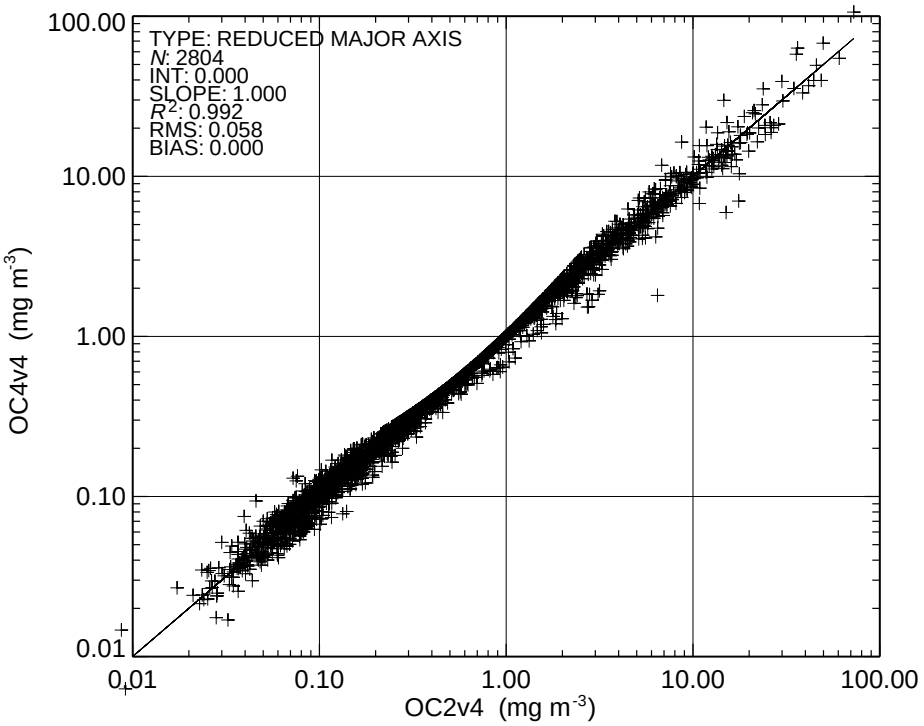

Fig. 10. Comparisons of C_a from OC2 and OC4 when using $\tilde{R}_{\mathrm{rs}}$ from the *in situ* data set.

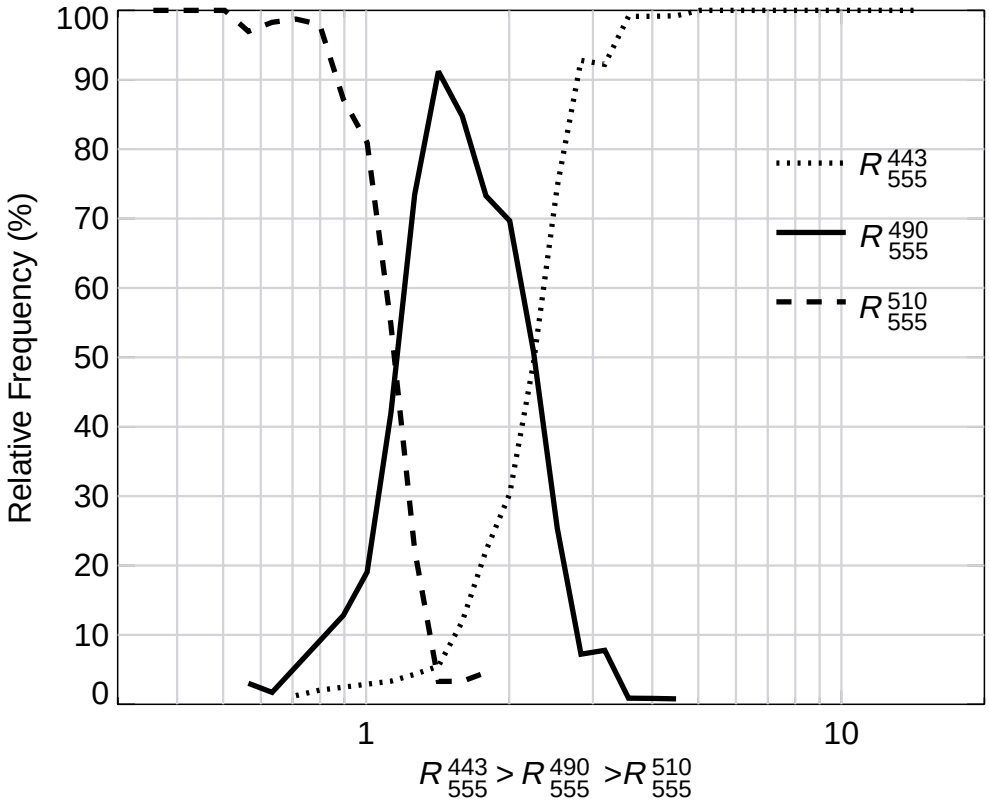

Fig. 11. The relative frequency of band ratios used in the OC4 model versus the maximum band ratio.

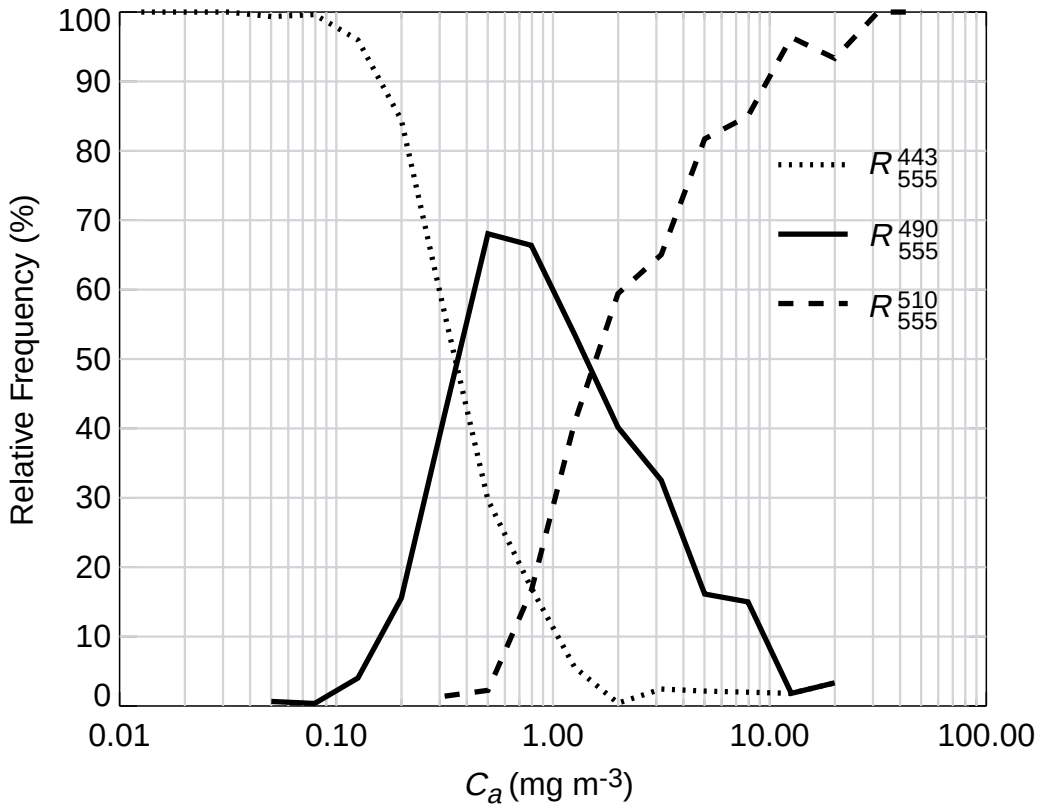

Fig. 12. The relative frequency of band ratios used in the OC4 model versus chlorophyll concentration.

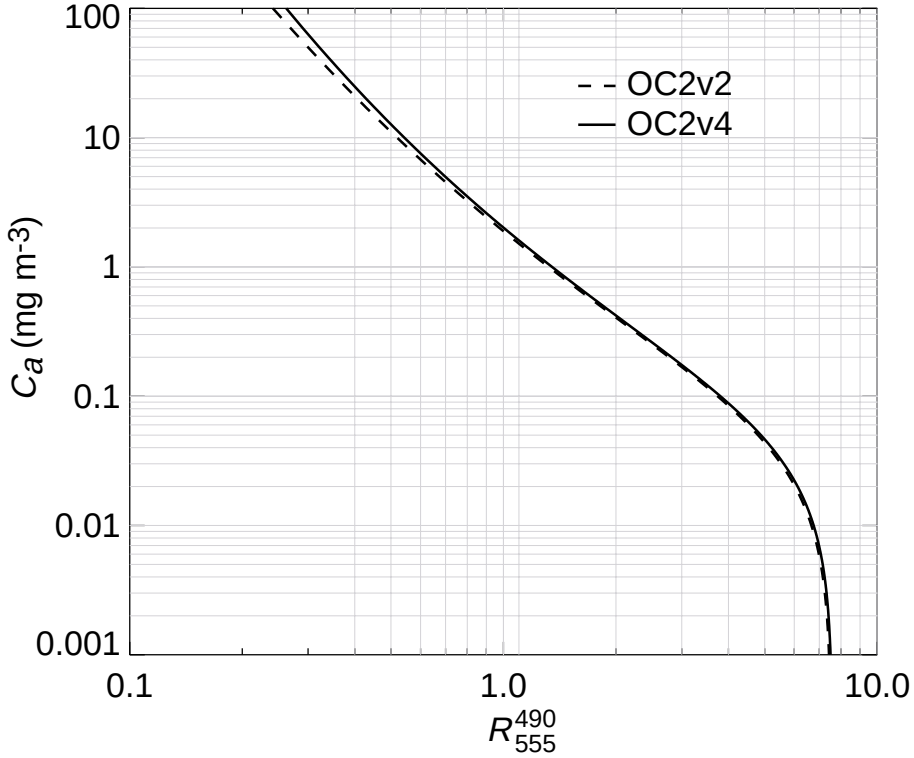

Fig. 13. The comparison of C_a estimates from OC2v4 with OC2v2.

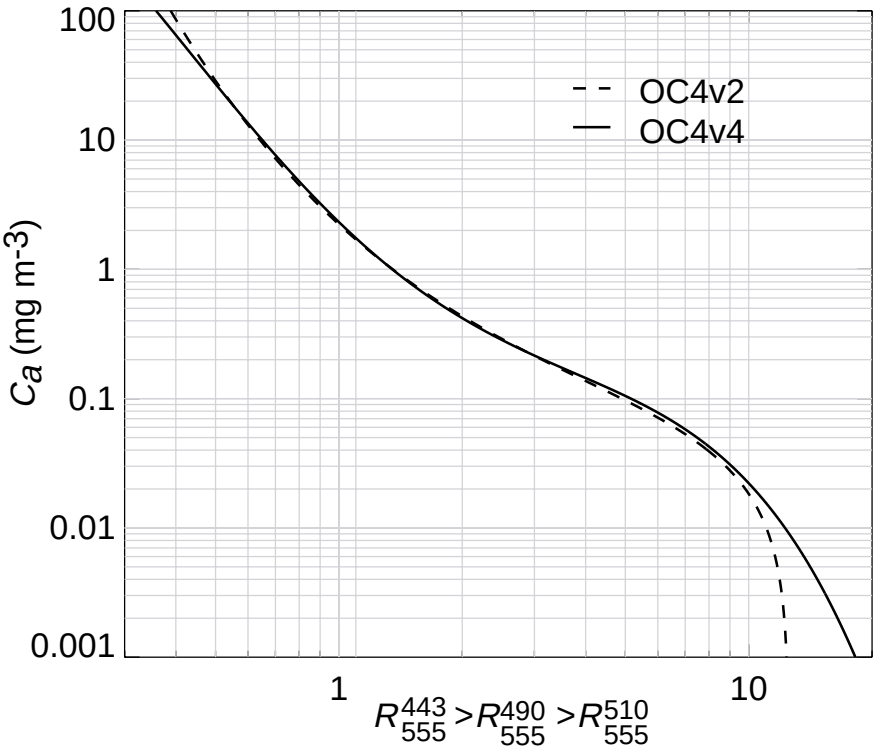

Fig. 14. The comparison of C_a estimates from OC4v4 and OC4v2 models.

it still lacks observations from the clearest oceanic waters. These observations are required to resolve the asymptotic relationship expected between $R_{\rm rs}(\lambda)$ and C_a as chlorophyll a concentration diminishes below $0.01\,{\rm mg\,m^{-3}}$, and reflectance band ratios approach the theoretical values for pure sea water. They are also needed to determine if the OC2 and OC4 extrapolations beyond the lowest $\tilde{C}_a$ are accurate. Given the spatially and temporally comprehensive time series achieved by the SeaWiFS mission, these clearest water regions and optimal sampling times may now be easily identified and targeted for special shipboard surveys. Although clearest waters encompass a relatively small fraction of the global ocean, these and highly eutrophic areas represent bio-optical and ecological extremes and changes in their magnitude or areal distribution may provide very sensitive indicators of global change.

Acknowledgments

The authors would like to acknowledge the following individuals for their significant contribution of *in situ* data and ideas: J. Marra, C Davis, D. Clark, G. Zibordi, C. Trees, R. Bidigare, D. Karl, J. Patch, R. Varela, J. Akl, C. Hu, A. Subramaniam, N. Nelson, T. Michaels, R. Smith, and A. Morel.

Chapter 3

SeaWiFS Algorithm for the Diffuse Attenuation Coefficient, $K(490)$, Using Water-Leaving Radiances at 490 and 555 nm

James L. Mueller
CHORS/San Diego State University
San Diego, California

Abstract

A new algorithm has been developed using the ratio of water-leaving radiances at 490 and 555 nm to estimate $K(490)$, the diffuse attenuation coefficient of seawater at 490 nm. The standard uncertainty of prediction for the new algorithm is statistically identical to that of the SeaWiFS prelaunch $K(490)$ algorithm, which uses the ratio of water-leaving radiances at 443 and 490 nm. The new algorithm should be used whenever the uncertainty of the SeaWiFS determination of water-leaving radiance at 443 is larger than that at 490 nm.

3.1 INTRODUCTION

The attenuation over depth z (in meters), of the spectral downwelling irradiance, $E_d(\lambda, z)$ (in units of mW cm^{-2} nm^{-1} at wavelength λ), is governed by the Beer–Lambert Law:

$$E_d(\lambda, z) \;=\; E_d(\lambda, 0^-)\, e^{-K(\lambda,z)z}, \tag{6}$$

where $K(\lambda, z)$ is the diffuse attenuation coefficient in per unit meters, averaged over the depth range from just beneath the sea surface ($z = 0^-$) to depth z in meters. Gordon and McCluney (1975) showed that 90% of the remotely sensed ocean color radiance is reflected from the upper layer, of depth z_{90}, corresponding to the first irradiance attenuation length, thus satisfying the condition

$$\frac{E_d(\lambda, z_{90})}{E_d(\lambda, 0^-)} \;=\; e^{-1}. \tag{7}$$

The depth z_{90} is found from an irradiance profile, by inspection, as the depth where condition (7) is satisfied. From (6), the remote sensing diffuse attenuation coefficient at wavelength λ can be found as $K(\lambda) = z_{90}^{-1}\,\mathrm{m}^{-1}$.

Austin and Petzold (1981) applied simple linear regression to a sample of spectral irradiance and radiance profiles to derive a $K(490)$ algorithm of the form

$$K(490) \;= K_w(490) \;+\; A\left[\frac{L_W(\lambda_1)}{L_W(\lambda_2)}\right]^B, \tag{8}$$

where $K_w(490)$ is the diffuse attenuation coefficient for pure water, $L_W(\lambda_1)$ and $L_W(\lambda_2)$ are water-leaving radiances at the respective wavelengths of λ_1 and λ_2, and A and B are coefficients derived from linear regression analysis of the data expressed as $\ln[K(490) - K_w(490)]$ and $\ln[L_W(\lambda_1)/L_W(\lambda_2)]$. In Austin and Petzold (1981), $K_w(490) = 0.022\,\mathrm{m}^{-1}$ was taken from Smith and Baker (1981), and because the algorithm was derived for CZCS, $\lambda_1 = 443$ nm and $\lambda_2 = 550$ nm.

The SeaWiFS ocean color instrument has channels at 443 and 555 nm. Mueller and Trees (1997) found a different set of coefficients for (8) using wavelengths $\lambda_1 = 443$ nm and $\lambda_2 = 555$ nm, and also used the ratio of normalized water-leaving radiances. The substitution of normalized water-leaving radiances in (8) had no significant effect, but the change in λ_2 yielded small, but statistically significant different coefficients A and B. Following Austin and Petzold (1981), Mueller and Trees (1997) also assumed $K_w(490) = 0.022\,\mathrm{m}^{-1}$ (Smith and Baker 1981). The Mueller and Trees (1997) result was adopted for the SeaWiFS prelaunch $K(490)$ algorithm.

SeaWiFS determinations of $L_W(443)$ are persistently lower than water-leaving radiances that are determined from matched *in situ* validation measurements. The serious underestimates of SeaWiFS $L_W(443)$ yield correspondingly poor agreement between SeaWiFS and *in situ* $K(490)$ determinations. On the other hand, SeaWiFS determinations of $L_W(490)$ and $L_W(555)$ agree much more closely with validation measurements.

This chapter is the report of an algorithm based on (8) using 490 and 555 nm, which should yield improved uncertainty in SeaWiFS $K(490)$ estimates. The algorithm also adopts a reduced value of $K_w(490)$ based on recently published values of pure water absorption (Pope and Fry 1997).

3.2 DATA AND METHODS

Two samples of $K(490)$ and normalized water-leaving radiances are used in the present analysis. Sample 1 is used for a regression analysis to derive coefficients A and B for (8) with $\lambda_1 = 490\,\mathrm{nm}$ and $\lambda_2 = 555\,\mathrm{nm}$. The data in Sample 2 are entirely independent from Sample 1 and are used to determine standard uncertainties of prediction in $K(490)$ calculated using the algorithm derived here from Sample 1, and using the prelaunch $K(490)$ algorithm (Mueller and Trees 1997).

The data comprising Sample 1 were drawn from spectral irradiance and radiance profiles locally archived at the San Diego State University (SDSU) Center for Hydro-Optics and Remote Sensing (CHORS). Each Sample 1 profile was analyzed to determine $K(490)$ and water-leaving radiance using the integral method of Mueller (1995a). Sample 1 includes the data analyzed by Mueller and Trees (1997), but excludes two cruises for which reliable upwelled spectral radiance profile $[L_u(490, z)]$ measurements were not available. Data from two additional cruises in the Gulf of California were added to Sample 1, bringing the total sample size to 319 data pairs.

Sample 2 was provided from the SeaBASS archives by the SIMBIOS Project Office at GSFC, and consists of 293 sets of $K(490)$, water-leaving radiances and incident surface irradiances (443, 490, and 555 nm) which are independent of Sample 1. Water-leaving radiances in Sample 1 were determined by the SIMBIOS Project using the standard methods employed at GSFC for SeaWiFS match-up validation analysis.

$K(490)$ and normalized water-leaving radiance ratio pairs were determined for each sample using the methods described in Mueller and Trees (1997). A linear regression analysis was performed on the Sample 1 data pairs to determine the values of coefficients A and B in (8), with $\lambda_1 = 490\,\mathrm{nm}$ and $\lambda_2 = 555\,\mathrm{nm}$. Based on Pope and Fry's (1997) recent determination of absorption for pure water $a_w(490) = 0.015\,\mathrm{m}^{-1}$, and the pure water backscattering coefficient $b_w(490) = 0.008\,\mathrm{m}^{-1}$ reported by Smith and Baker (1981), the backscattering fraction is heuristically assumed to be less than 0.5 and performed three regressions assuming values of 0.018, 0.017, and $0.016\,\mathrm{m}^{-1}$ for $K_w(490)$. Finally, standard uncertainties of prediction were calculated, both for the present (490 and 555 nm) and the prelaunch (443 and 555 nm) algorithms, as the RMS differences between the measured and predicted $K(490)$ in Sample 2.

3.3 RESULTS

Three regression analyses were performed on Sample 1 using successive values of 0.018, 0.017, and $0.016\,\mathrm{m}^{-1}$ for $K_w(490)$. The scatter between $\ln[K(490) - 0.016]$ and $\ln[L_W(490)/L_W(555)]$, in per unit meters is illustrated in Fig. 15a, together with the logarithmic regression line corresponding to the algorithm

$$K(490) = 0.016 + 0.15645\left[\frac{L_{WN}(490)}{L_{WN}(555)}\right]^{-1.5401}. \quad (9)$$

In log space, the squared correlation coefficient R^2 increased monotonically from 0.931–0.937, and the standard error decreased from 0.186–0.167, as $K_w(490)$ decreased from 0.018–$0.016\,\mathrm{m}^{-1}$. On this basis, the appropriate algorithm selected for use with SeaWiFS was the $K_w(490) = 0.016\,\mathrm{m}^{-1}$ case.

In linear space, the standard uncertainty of the estimate, calculated as the RMS discrepancy between predicted and measured $K(490)$ for Sample 1, is $0.012\,\mathrm{m}^{-1}$. The scatter between predicted and measured $K(490)$, relative to the one-to-one line, is illustrated in Fig. 15b.

Figures 16a and 16b illustrate the scatter about the one-to-one line when $K(490)$ predictions using (9) are compared to measurements from Sample 2. The standard uncertainty of prediction in $K(490)$ using (9) is estimated from these data to be $0.018\,\mathrm{m}^{-1}$ in the range of $K(490) < 0.25\,\mathrm{m}^{-1}$ (which is the range fit with Sample 1) and corresponds to 26% of the mean for this subsample of 249 pairs. When the algorithm of (9) is extrapolated into the range $K(490) > 0.25\,\mathrm{m}^{-1}$, the standard uncertainty of prediction increases to $0.193\,\mathrm{m}^{-1}$ (48% of the mean for this subsample of 31 pairs). The mean biases in predictions are $-0.002\,\mathrm{m}^{-1}$ for measured $K(490) < 0.25\,\mathrm{m}^{-1}$, and $-0.130\,\mathrm{m}^{-1}$ for measured $K(490) > 0.25\,\mathrm{m}^{-1}$.

The standard uncertainties and mean biases of prediction for $K(490)$ calculated with the SeaWiFS prelaunch algorithm (Mueller and Trees 1997) are 0.020 and $0.000\,\mathrm{m}^{-1}$, respectively, for the subsample of Sample 2 with measured $K(490) < 0.25^{-1}$, and 0.196 and $-0.085\,\mathrm{m}^{-1}$ for the subsample with measured $K(490) > 0.25\,\mathrm{m}^{-1}$.

3.4 DISCUSSION

There is little to choose between the *in situ* performances and uncertainties of the (9) $K(490)$ algorithm, using the ratio of water-leaving radiances at 490 and 555 nm, and the SeaWiFS prelaunch algorithm (Mueller and Trees 1997), using the ratio of water-leaving radiances at 443 and 555 nm. When used with SeaWiFS data, however, (9) may be expected to yield more accurate $K(490)$ estimates as long as the uncertainties in estimated $L_{WN}(490)$ are much lower than those for $L_{WN}(443)$. It is recommended, therefore, that (9) be substituted for the Mueller and Trees (1997) $K(490)$ algorithm for processing SeaWiFS data, at least until future improvements in atmospheric corrections may produce equivalent uncertainties in water-leaving radiances at 490 and 443 nm.

Neither algorithm performs well in water masses where $K(490) > 0.25\,\mathrm{m}^{-1}$. In part, this may be due to extrapolating a regression equation beyond the range of the data

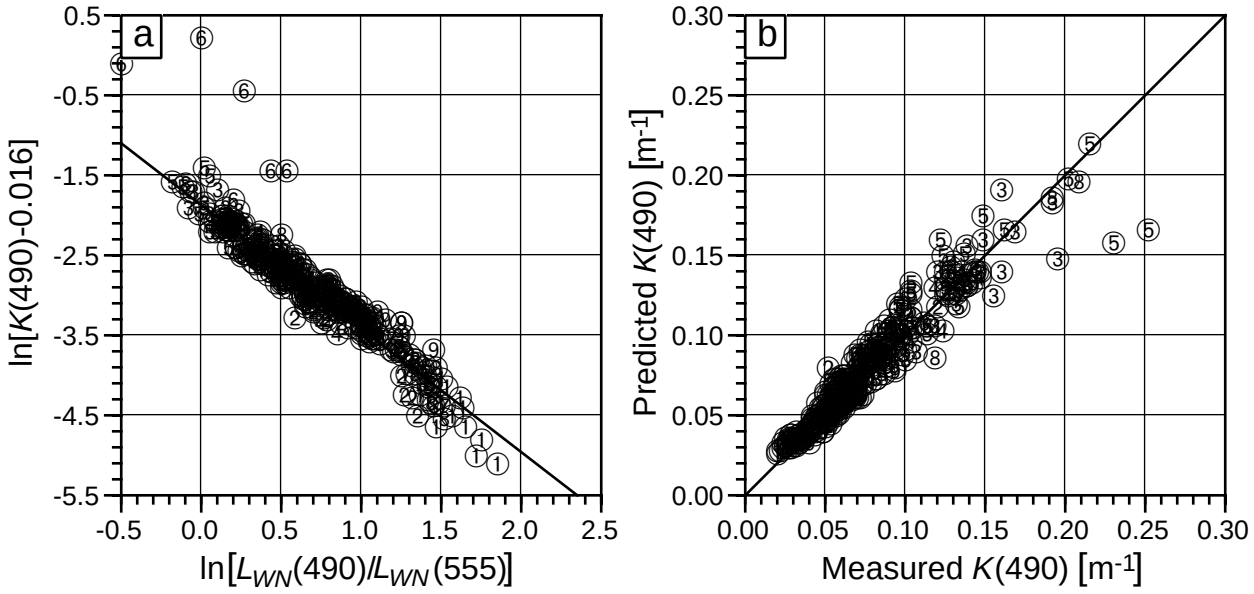

Fig. 15. Scatter comparisons of $K(490)$. **a)** Logarithmic scatter comparison of $K(490)$ versus the ratio of water-leaving radiances at 490 and 555 nm. The solid line is the least squares regression fit to the data (excluding the GoCal98A red tide data) given by (9). **b)** Linear scatter in measured $K(490)$ compared with predictions using (9) with the ratio of water-leaving radiances at 490 and 555 nm. The data are from panel **a)**. The key for these panels are: 1. Siegel: Sargasso Sea 1994; 2. Mitchell: CalCOFI 1994; 3. GoCal 1995; 4. GoCal 1997; 5. GoCal 1998A (with Red Tide Station); 6. GoCal 1998A Red Tide Data; 7. Trees, Arabian Sea, JGOFS Proc. 2; 8. Trees, Arabian Sea, JGOFS Proc. 6; 9. Trees, Arabian Sea, JGOFS Proc. 7.

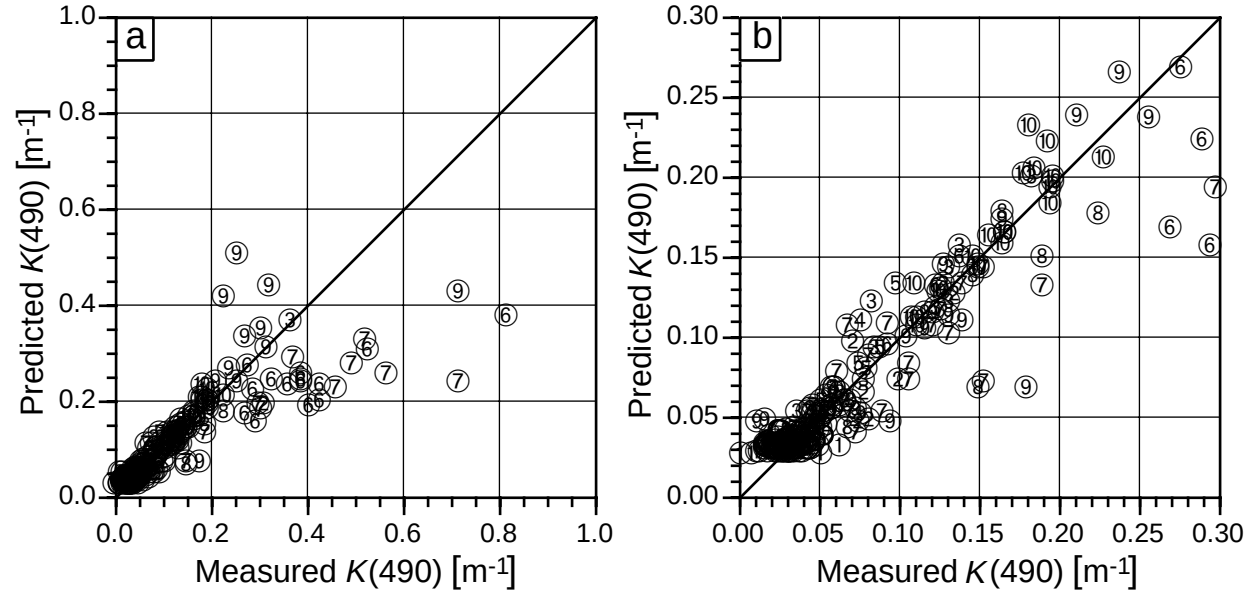

Fig. 16. Scatter comparisons of $K(490)$. **a)** Same as Fig. 15b, but for an independent sample of $K(490)$ and water-leaving radiances at 490 and 555 nm. The solid line corresponds to a one-to-one agreement. **b)** A subset of panel **a)**, where the area of greatest concentration of data points is enlarged for better viewing. The key for these panels are: 1. BATS 1998; 2–5. CalCOFI-9802, -9804, -9807, and -9809, respectively; 6. April 1998 SMAB; 7. November 1998 SMAB; 8. Feb 1999 SMAB; 9. CARIACO 1998; 10. GoA97; and ◯ HOTS 1998.

used to fit its coefficients. In the present circumstances, however, it is at least equally likely that the poor predictions result from extremely large uncertainties in both $K(490)$ and water-leaving radiances derived from radiometric measurements near the sea surface in extremely turbid water masses. In such cases, instrument self shading, wave focusing, uncertainty in instrument depth determination, and uncertainty in extrapolating $L_u(\lambda, z)$ to the sea surface (especially when the linear slope estimation method of analysis is employed) contribute large and poorly understood uncertainties to measured $K(490)$ and water-leaving radiances alike. For the near term, the best policy is to regard SeaWiFS $K(490)$ data with values of greater than $0.25\,\mathrm{m}^{-1}$ with caution and skepticism.

Chapter 4

Long-Term Calibration History of Several Marine Environmental Radiometers (MERs)

Margaret C. O'Brien, David W. Menzies,
David A. Siegel, and Raymond C. Smith
ICESS, University of California, Santa Barbara
Santa Barbara, California

Abstract

The accuracy of upper ocean AOPs for the vicarious calibration of ocean color satellites ultimately depends on accurate and consistent *in situ* radiometric data. The SIMBIOS Project is charged with providing estimates of normalized water-leaving radiance for the SeaWiFS instrument to within 5%. This, in turn, demands that the radiometric stability of *in situ* instruments be within 1% with an absolute accuracy of 3%. This chapter reports on the analysis and reconciliation of the laboratory calibration history for several BSI MERs, models MER-2040 and -2041, three of which participate in the SeaWiFS Calibration and Validation Program. This analysis includes data using four different FEL calibration lamps, as well as calibrations performed at three SIRREXs. Barring a few spectral detectors with known deteriorating responses, the radiometers used by UCSB during the BBOP have been remarkably stable during more than five years of intense data collection. Coefficients of variation for long-term averages of calibration slopes, for most detectors in the profiling instrument, were less than 1%. Long-term averages can be applied to most channels, with deviations only after major instrument upgrades. The methods used here to examine stability accommodate the addition of new calibration data as they become available; this enables researchers to closely track any changes in the performance of these instruments and to adjust the calibration coefficients accordingly. This analysis may serve as a template for radiometer histories which will be cataloged by the SIMBIOS Project.

4.1 INTRODUCTION

The accuracy of upper ocean AOPs, which are needed for the vicarious calibration of ocean color satellites, ultimately depends on accurate and consistent *in situ* radiometric data. Accurate validation of SeaWiFS demands an in-water radiometric stability within 1%, with an accuracy of 3% (Mueller and Austin 1995). Considerable energy has been spent refining calibration protocols for profiling radiometers. The SeaWiFS Project Office has sponsored several workshops through its Calibration and Validation Program, which have yielded significant improvements in the research community's ability to provide accurate AOP estimates. These include the SIRREXs, conducted annually since 1992 (Mueller 1993, Mueller et al. 1994, Mueller et al. 1996, and Johnson et al. 1996), as well as the Data Analysis Round-Robin (DARR) workshop in 1994 (Siegel et al. 1995).

At the Institute for Computational Earth System Science (ICESS) at UCSB, several research projects provide validation data for ocean color satellites. These include BBOP in the Sargasso Sea, the Plumes and Blooms Project in the Santa Barbara Channel, and the Palmer Area Long Term Ecological Research (LTER) site on the Antarctic Peninsula. The ICESS Calibration Laboratory and BBOP have participated in all of the workshops held by the Calibration and Validation Program.

This report presents an analysis of the multiyear laboratory calibration history for several BSI MERs, models MER-2040 and -2041. This analysis includes data using four different FEL calibration lamps, as well as calibrations performed at three SIRREX exercises. This report will show that, barring a few sensors with known deteriorating responses, the radiometers used by UCSB during BBOP have been remarkably stable during six years of intense data collection.

4.2 ICESS FACILITY AND METHODS

The ICESS optical calibration facility is housed in a climate-controlled room. A 1.2×1.8 m (4×6 ft) optical table, with threaded holes arranged in a 2.5 cm (1 in) grid, supports one end of a 2.4 m (8 ft) long optical rail. A black, wooden baffle with a 25.4 cm (10 in) diameter hole strad-

dles the rail 61.0 cm (2 ft) from the illumination end of the bench and extends the full 1.2 m (4 ft) width by a height of 1.5 m (5 ft). A 30.5 cm (12 in) square plate can be bolted over the baffle hole to hold a 7.6 cm (3 in) adjustable iris if necessary. An alignment beam, consisting of a helium–neon (He:Ne) laser with two adjustable mirrors, is centered on the hole, parallel to the rail, and is mounted on a platform at the distal end of the optical rail. The table and rail assembly are surrounded by a black, pleated curtain suspended from a track mounted on the ceiling. When the room lights are off and the curtains drawn, no detectable light reaches the instrument except through the hole in the baffle. Shadow forms can be inserted between the lamp and instrument to block direct light during the measurement of stray light.

The lamp holder array consists of a sliding platform on the optical rail supporting two horizontal vernier stages at right angles, a rotary stage, a vertically adjustable post, and an FEL lamp holder. An alignment jig replaces the lamp in the holder to properly position the lamp holder to the alignment laser beam. The lamp holder array can be easily slid along the rail to provide calibration distances from 50 cm to over 2 m. The standard lamps are purchased from, and calibrated by, Optronic Laboratories, Inc.† (Orlando, Florida) and calibrations are traceable to the National Institute of Standards and Technology (NIST). An 83-DS power supply with a 0.02 Ω shunt provides power for the FEL lamp. A 4.5 digit voltmeter is used to monitor the current and voltage during calibrations. The lamp is allowed to warm up for 10 min before each calibration. The current is maintained at 8 A (±1 mA) and is reproducible to 0.03%.

The mounting platform for radiometers consists of a large scissor jack, which can support instruments up to 22.7 kg (50 lbs.) and 20.3 cm (8 in) in diameter. The jack has independent height and crossbeam adjustments to center the instrument on the optical axis. It is attached to a 45.7 cm (18 in), square platform which in turn, can be fastened to the optical bench at any location with 15.2 cm (6 in) tall aluminum posts which are 43.2 cm (17 in) apart. Because the hypotenuse of a 30.5 cm (12 in) right triangle is 43.1 cm (17 in), the platform can be easily positioned at the 45° angle desired for radiance calibrations with a reflective plaque.

During irradiance calibrations, the test instrument is positioned so that its cosine collector is centered on the alignment beam and normal to it. Calibrations are usually performed at a distance of 50 cm, which is measured through the baffle iris using a 50 cm measuring rod. The lamp holder's vernier stage is used to make the final distance adjustment.

Beginning in July 1992, radiance calibrations were performed using a 50.8 cm (20 in) diameter Labsphere, Inc., integrating sphere with a variable (2.54–10 cm, 1–4 in diameter) entrance aperture and 15.2 cm (6 in) diameter exit aperture located 90° from the entrance. It is illuminated externally by the same FEL lamp used for irradiance calibrations. The sphere is positioned on the bench at the end of the optical rail and the lamp is positioned 50 cm from the sphere's 5 cm (2 in) diameter entrance aperture. The raised platform with the scissor jack is positioned to hold the test instrument a few centimeters from the exit aperture and the wooden baffle; black felt is used to block all stray light.

Beginning in August 1994, radiance calibrations were also performed using a 60.1 cm (24 in) Spectralon®‡ reflectance plaque. At the extreme end of the optical bench, a vertical bracket at the plaque's center supports it at a position normal to the laser alignment beam. The lamp holder is positioned at a distance of 200 cm from the plaque, and a baffle with a 25.4 cm (10 in) diameter hole between the lamp and the plaque allows the lamp to illuminate only the plaque. The scissor jack and its platform are moved to align the radiance collector at 45° to, and 33 cm (13 in) from, the plaque. From 1994–1996, radiance calibrations were performed routinely using both the sphere and the plaque.

4.2.1 Calibration Lamp History

Three NIST-traceable FEL lamps were used for calibrating the ICESS radiometers—F219, F303, and F304—all of which were purchased from Optronic Laboratories. There are manufacturer's calibrations for all three lamps. At UCSB, lamp F219 was used for all calibrations from 1989–1991 (Fig. 17). Since that time, it has been used only during lamp intercalibration experiments, so there should have been no further significant aging of this lamp. Lamp F303 was purchased in June 1992 and was used for all routine calibrations at UCSB from July 1992–July 1995. Lamp F303 was recalibrated by Optronic Laboratories in July 1995 after approximately 50 h of service. Lamp F304 was a seasoned, uncalibrated FEL lamp, purchased in June 1992, and used only a few hours until July 1995 when it was calibrated by Optronic Laboratories and put into use for routine calibrations at UCSB. A fourth lamp, F305, was not calibrated by the manufacturer, but has been used for comparisons between other lamps.

All four lamps were intercalibrated during at least two of the three SIRREX calibration workshops in July 1992, June 1993, and September 1994. F219 was examined at SIRREX-1 and again at SIRREX-2 in June 1993. Lamp

† Certain commercial equipment, instruments, or materials are identified in this technical memorandum to foster understanding. Such identification does not imply recommendation or endorsement by NASA, NIST, or ICESS, nor does it imply that the materials or equipment identified are necessarily the best available for the purpose.

‡ Spectralon is a registered trademark of Labsphere, Inc., in North Sutton, New Hampshire.

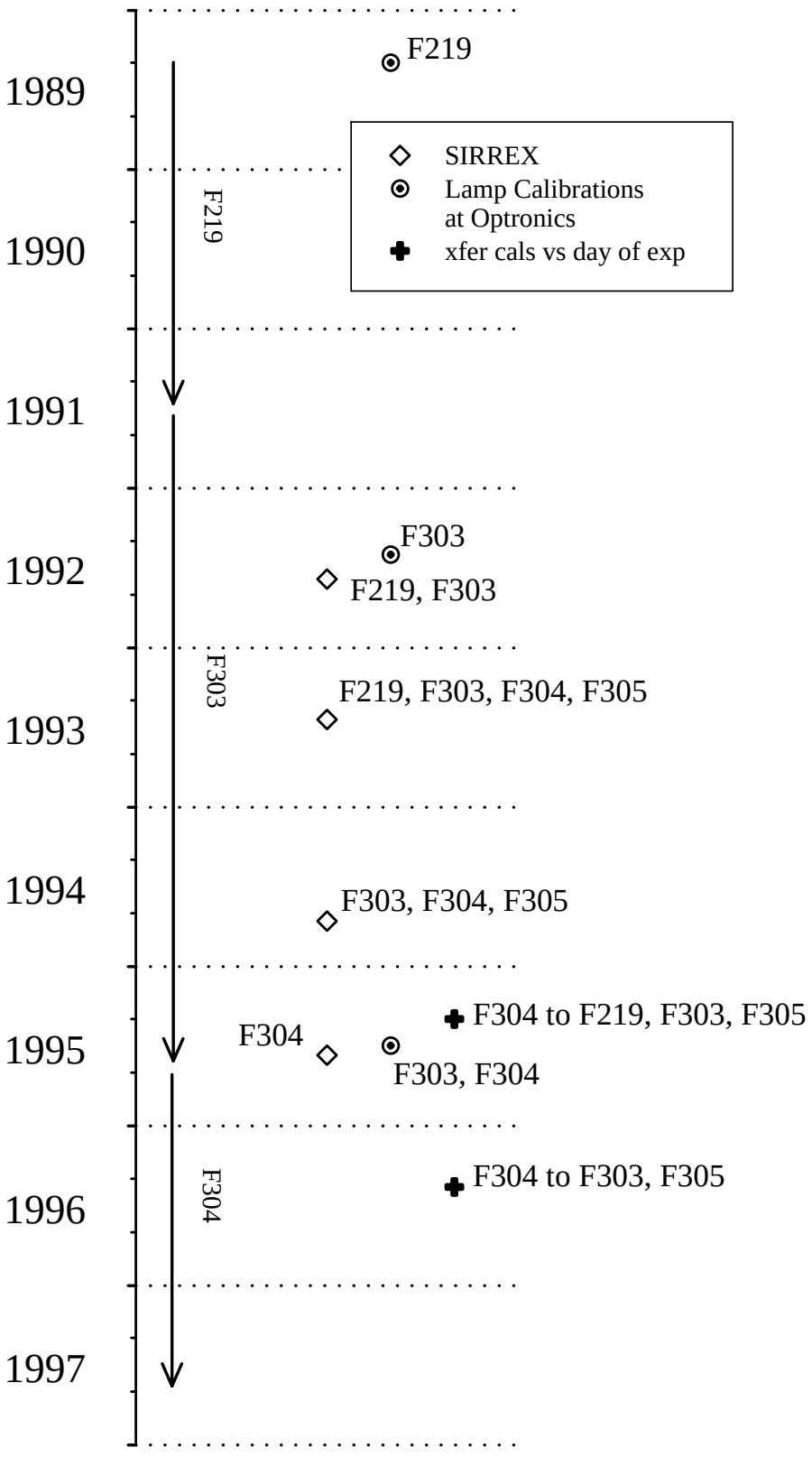

Fig. 17. A timeline of FEL lamp calibrations at Optronic Laboratories, transfer calibrations at UCSB, and SIRREX experiments.

Table 8. Wavelength centers and bandwidths measured at full-width at half-maximum (FWHM) power (in parentheses). All values are in nanometers and the upwelled spectral radiance is denoted as $E_u(z,\lambda)$. The channels marked with [94] were added in 1994. If a detector has been replaced, the wavelength given is the one most recently measured. The column headings denote the MER model and serial number, and the collector type.

	2040 S/N 8728				*2041 S/N 8729*		*2041 S/N 8734*		*2040 S/N 8714*			
λ	$E_d(z,\lambda)$		$L_u(z,\lambda)$		$E_d(0^+,\lambda)$		$E_d(0^+,\lambda)$		$E_d(z,\lambda)$		$E_u(z,\lambda)$	
[nm]	*Center*	*FWHM*	*Center*	*FWHM*	*Center*	*FWHM*	*Center*	*FWHM*	*Center*	*FWHM*	*Center*	*FWHM*
340							340.3	8.4				
380							378.4	10.0				
410	410.2	9.6	411.2	9.4	410.4	9.5	410.4	10.4	410.3	11.4	410.8	11.4
441	441.6	10.8	441.7	10.7	441.7	10.9	442.2	10.4	441.5	11.1	442.0	12.1
465	465.4	10.0	465.8	9.7			464.0	9.5				
488	488.0	9.9	486.7	9.6	487.8	10.1	488.5	11.4	483.6	10.7	487.9	10.8
510	510.2 [94]	9.3	511.9 [94]	8.2					507.4	11.1	507.5	11.4
520	518.6	11.5	519.4	11.4	519.5	10.3	518.5	10.0	520.1	8.5	518.0	8.3
540							537.8	9.5				
555	555.2 [94]	9.8	555.7 [94]	9.8								
565	564.8	11.1	565.5	10.9	564.6	11.7	563.4	10.8	563.4	10.8	563.3	9.5
587	587.1	10.4	586.0	9.9			585.4	10.2	587.0	9.6	586.5	10.5
625	623.4 [94]	10.7	624.8 [94]	10.7			622.6	10.6	624.0	12.1	624.2	12.0
665	664.4	9.5	664.8	9.4	662.9	11.2	663.0	9.7	662.4	9.3		
683	680.3 [94]	9.0	681.1	10.0			680.8	13.9				

F303, which has been used extensively for calibrations at UCSB, was examined at all three SIRREXs; F304 and F305 were both tested at SIRREX-2 and -3. In addition, a BSI Profiling Reflectance Radiometer (PRR) with the same type of photodiodes as the MERs, which was calibrated with lamp F303, was used for one of the training sessions at SIRREX-4 at NIST in May 1995.

In addition to the SIRREX comparisons, one other comparison between lamps was performed at UCSB. Before F304 replaced F303 as the lamp used for routine calibrations, the 1995 Optronic Laboratories calibration for lamp F304 was transferred onto F303, F219, and F305 using a third MER-2040 instrument (S/N 8733) with 13 irradiance channels between 340–683 nm. As mentioned above, F219, F304, and F305 were used only during the SIRREXs and had not aged between 1992 and 1995. The transfer from F304 to F303 and F305 was repeated in May 1996.

4.2.2 Radiometers

At the UCSB optical calibration facility, there are calibration histories for five BSI spectroradiometers [serial numbers (S/N) 8728, 8729, 8733, 8734, and 8714] spanning up to seven years (Fig. 18). The MER-2040 series of spectroradiometers is composed of discrete, sealed photodiodes, each with triple cavity interference filters giving a nominal full-width at half-maximum bandwidth of 10 nm. The wavelength centers range throughout the visible and ultraviolet-A (UVA) spectrum from 340–683 nm. The radiance detectors are identical 3-cavity filtered photodiodes mounted in a Gershun tube array. The half-angle field of view is 10.2° in air and 13.7° in water. Instrument 8714 is known as the Bio-Optical Profiling System II (BOPSII) and was described in Smith et al. (1997).

Radiometers 8728 (MER-2040) and 8729/8734 (MER-2041) are used routinely in the BBOP at the Bermuda Atlantic Time Series (BATS) station and have been calibrated three or four times per year since July 1992 (Table 8 and Fig. 18). The BBOP profiling instrument (S/N 8728) was designed originally with eight downwelling irradiance channels (410–665 nm) and nine upwelling radiance channels (410–683 nm). In January 1994, it was modified to meet the SeaWiFS protocols (Mueller and Austin 1995) and the number of channels was increased to 12 each of downwelling and upwelling channels (410–683 nm), plus upwelling natural fluorescence. The gains of all channels were also adjusted at this time. The original deck sensor (S/N 8729) has six downwelled channels (410–665 nm) and the optics have not been modified. In August 1994, it was replaced by S/N 8734, which has 13 downwelled channels (340–683 nm).

Radiometer 8733 (MER-2040) was used intensively in the field from 1992–1993 during the Tropical Ocean Global Atmosphere (TOGA) Coupled Ocean Atmosphere Response Experiment (COARE) and is now used occasionally on BBOP. It has been calibrated approximately once per year. Instrument 8733 has 13 each of downwelled and upwelled irradiance channels between 340–683 nm. Radiometer 8714, the BOPSII (MER-2040), has been used for profiling on all of the Palmer Area LTER and Ice Colors

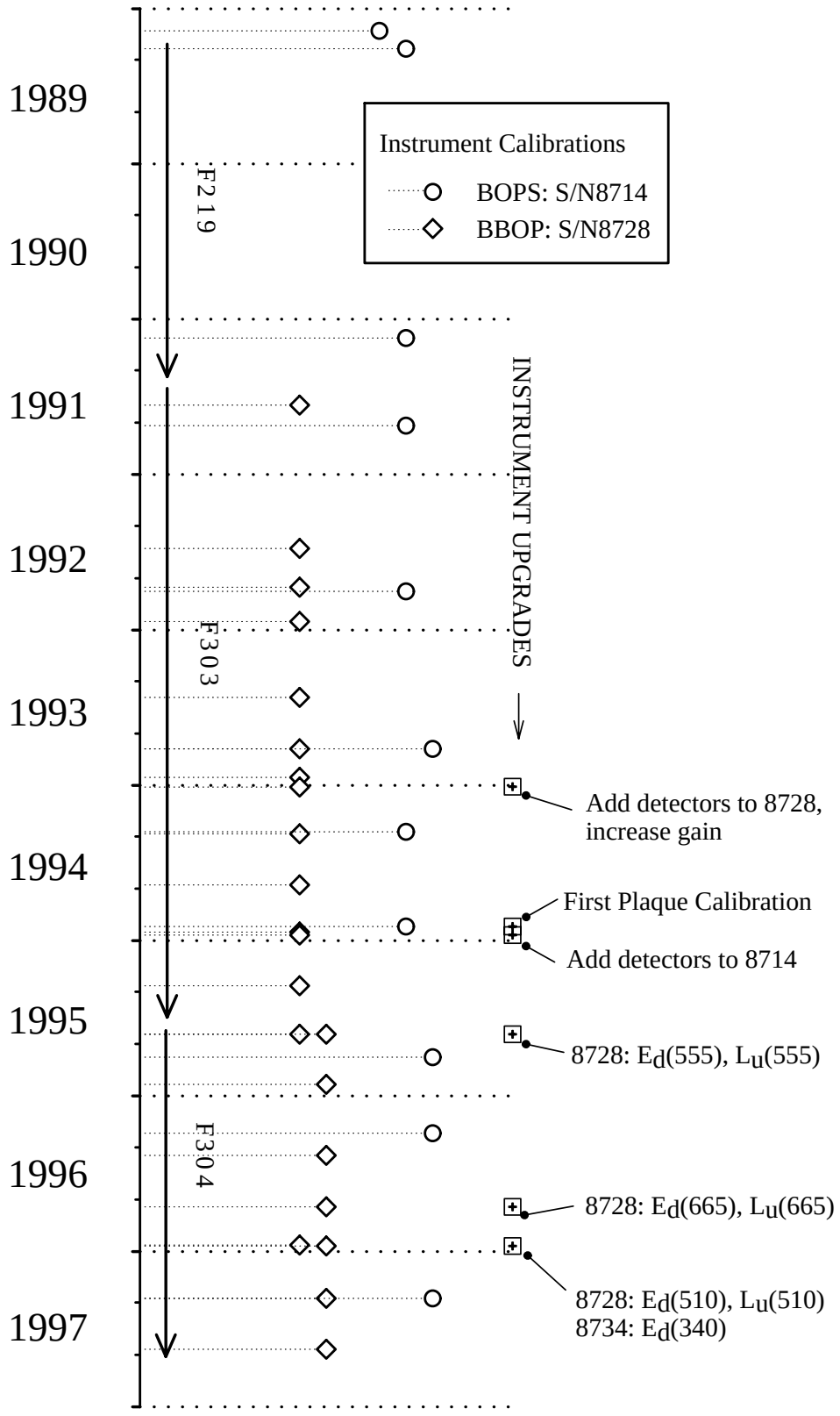

Fig. 18. A timeline of calibrations and upgrades for BBOP (S/N 8728, 8729, and 8734) and BOPSII (S/N 8714) radiometers.

Table 9. Comparison of lamp irradiances between 400 and 700 nm obtained from SIRREX experiments, Optronics, and the transfer of lamp F304 to F305. The data values are the ratios of lamp output measured during the SIRREX experiments to those provided by Optronics or to the transfer calibration. The standard deviation is indicated by σ.

	SIRREX-1		*SIRREX-2*		*SIRREX-3*	
Lamp	*Mean*	σ	*Mean*	σ	*Mean*	σ
F303-92	1.0087	0.0083	1.0178	0.0087	1.0332	0.0084
F303-95	0.9710	0.0104	0.9788	0.0037	0.9932	0.0028
F304-95			0.9916	0.0045	0.9919	0.0029
F305†			0.9895	0.0041	0.9905	0.0027
F219-89	1.0332	0.0079	1.0414	0.0107		
F219†	0.9854	0.0096	0.9937	0.0038		

† Transfer calibration from F304.

cruises in Antarctic waters, as well as many open ocean projects, and has been calibrated once or twice yearly since February 1989 (Fig. 18). This instrument had 8 channels of downwelled irradiance (increased to 13 for 410–665 nm in November 1994), and 8 channels of upwelled irradiance (410–624 nm, Table 9). Both 8728 and 8714 had individual detectors replaced.

This report is primarily concerned with the BBOP instruments, because they contribute data to the SeaWiFS Calibration and Validation Program. Data from the BOPSII and TOGA–COARE instruments (S/N 8714 and 8733) are used primarily to corroborate the conclusions, because their calibration histories are at least as long as that of the BBOP instrument and their calibrations involve the same lamps.

The wavelength properties of each detector were measured using a double-grating monochrometer. An uncalibrated FEL lamp and condensing lens were used as the illumination source for the entrance slit, and the output spot was centered on the radiometer's cosine collector or on an individual radiance detector. The wavelength producing the maximum signal was determined, followed by the wavelengths on each side of the peak producing 50% of the maximum signal. The reported wavelength for a detector is the average of the two half-maximum wavelengths; its bandwidth is the difference between these two wavelengths (Table 8). The wavelength response of the monochrometer was calibrated by observing the visible spectral lines of a mercury pen lamp. Repeat determinations for any detector have agreed to within 0.5 nm.

4.3 RESULTS

Because this report is concerned with accuracy, as well as radiometer stability, significant attention has been given to the calibrations of the lamps. The following discussion will illustrate:

a) Calibration lamp output must be examined closely;
2) The two profiling instruments (BBOP S/N 8728, and BOPSII S/N 8714) appear to be stable over several years; and
3) Long-term averages of calibration coefficients should be calculated whenever possible.

4.3.1 Lamps

FEL lamp F303 was used continuously for all calibrations from 1992–1995 for a total of approximately 50 h. Optronic Laboratories specifies that lamp irradiances are accurate and stable to within approximately 1% for 50 h or 1 year of use when the supplied current is maintained to within 0.1%. The two manufacturers' calibrations in 1992 and 1995 for F303 indicated that its output had changed by up to 5% and that it should not be used for further radiometer calibrations. The most extreme changes were noticed at wavelengths less than 500 nm†. Currently, F303 is used only for monitoring the performance of its replacement, F304. Given the possible change in the performance of the primary lamp, the response histories of two radiometers were examined with both lamp calibrations for evidence supporting the validity of one or both calibrations.

Because there is no long interruption between the calibrations of BBOP instruments (S/N 8728 and 8729/8734 are calibrated every 3–4 months), the slopes of radiometer 8728, calibrated with lamp F303 between January 1994 and August 1995, were calculated using both the 1992 and 1995 Optronic Laboratories irradiance calibrations for this lamp. To compare the relative changes over time, each slope was normalized to that determined on 9 August 1995, the date on which lamp F304 replaced F303. The normalized slopes calculated with both lamp calibrations were examined for drift or step changes, which might indicate when the calibration lamp's output had changed. While using a single FEL lamp and calibration, most channels on the BBOP profiling radiometer (S/N 8728) showed a constant calibration response over time (Fig. 19). When a different FEL lamp or a different calibration of the same lamp was used, however, there were significant changes of

† The raw data are available at the following universal resource locator (URL) address `http://www.icess.ucsb.edu/bbop`.

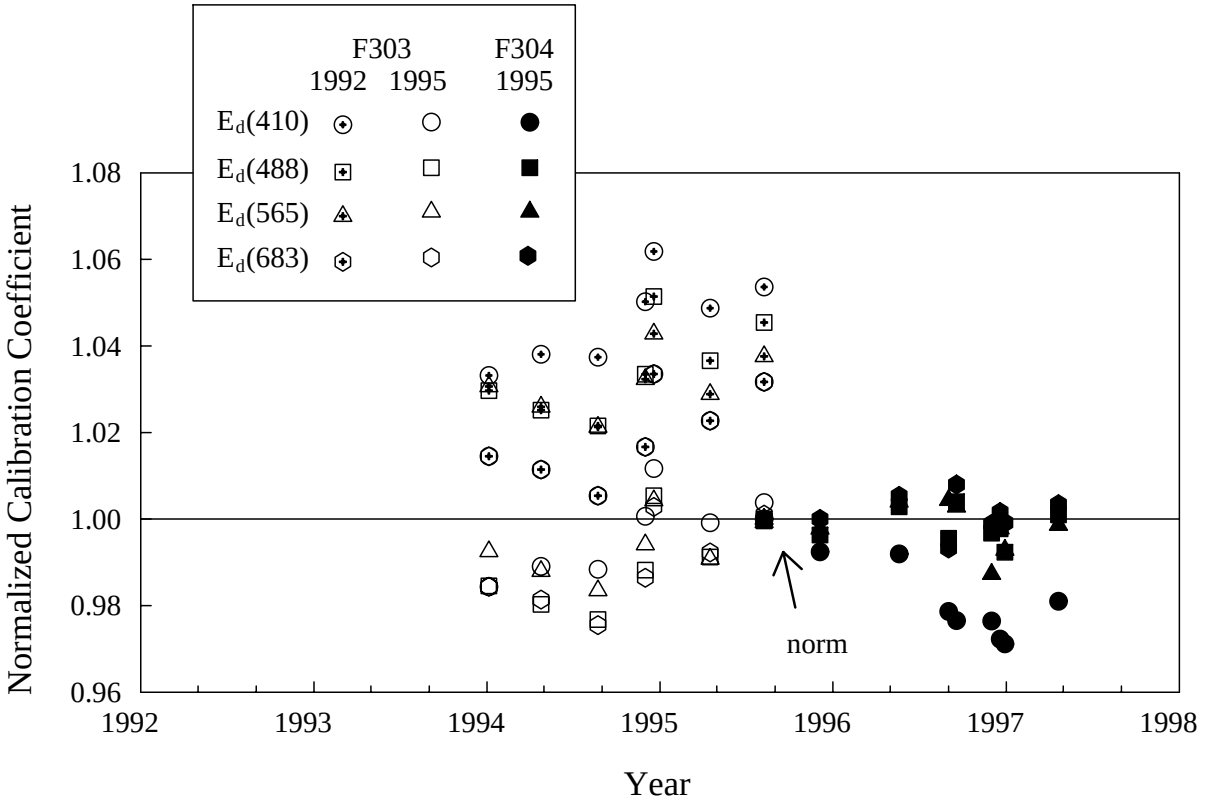

Fig. 19. The normalized calibration coefficients for four downwelling irradiance channels (radiometer 8728) using Optronic Laboratories calibrations of lamp F303 in 1992 and 1995. Data were normalized to the F304 values measured on 9 August 1995, the first date for which lamp F304 was used.

2–6% in the coefficients for most of the channels. Agreement was best between lamps or calibrations employing the July 1995 Optronic Laboratories calibration for lamps F303 and F304. In fact, the agreement was excellent when the 1995 Optronic Laboratories calibration was used for all radiometer calibrations with lamp F303 back to 1992 (below).

The response of the BOPSII radiometer (S/N 8714) to new lamps, or different calibrations of a lamp, was similar to that of radiometer 8728. There were marked steps in the slopes for each irradiance channel when lamps were replaced and their original calibrations were applied (data not shown). The calibration coefficients obtained for the BOPSII instrument using F219 with the manufacturer's lamp calibration compared poorly to later data. When the coefficients for instrument 8714 were recalculated using the 1995 transfer calibration from lamp F304 to F219, there was better agreement between early (pre-1992) and later calibrations. Similar to the BBOP instruments, when the July 1995 Optronic Laboratories calibration of F303 was used for all radiometer calibrations from 1992–1995, the agreement was much better (see below); in fact, 19 out of 21 channels varied less than 1%.

The requirement that radiometer calibrations be accurate, as well as stable, and the problems of reconciling different lamp irradiances led to a more in-depth analysis of the lamp calibrations. Simply computing coefficients using the current lamp irradiances provided by Optronic Laboratories apparently was not possible. It was implausible that the responses of two different radiometers had drifted with the same rate and magnitude as did the output of lamp F303.

4.3.2 SIRREX Data

The data from the three SIRREX activities were examined to determine whether or not they supported the two differing Optronic Laboratories calibrations for lamp F303. There are caveats accompanying each SIRREX data set, which must be taken into account when interpreting SIRREX data. During SIRREX-1 (July 1992), the required uncertainty of 1% was *not* achieved when transferring the NIST scale of spectral irradiance from the Goddard Space Flight Center (GSFC) standard lamp (F267) to the other lamps (Johnson et al. 1996). The data are, however, included here for completeness, and this goal was achieved during SIRREX-2 and -3. During SIRREX-3, a recent NIST calibration of the standard lamps (GSFC lamps F268 and F269) became available and indicated that the output of lamp F269 had drifted by approximately 1.5% sometime during the previous year, likely as early as SIRREX-2

(Mueller et al. 1996). This necessitated a recalculation of the SIRREX-2 data sets, and increased their combined uncertainty. The SIRREX-3 results should be the most reliable because many of the procedural problems experienced during the first two experiments were rectified and the standard lamps were calibrated by NIST only one month previously.

Each lamp's irradiance, at wavelengths used during the SIRREXs, was computed using the recommended Lagrangian interpolation procedure†. When the SIRREX-2 and -3 data for lamps F304 and F305 were first compared, it appeared the SIRREX-2 data were an average of 1.6% lower than those from SIRREX-3 between 400–1,000 nm, which supports the drift observed in the SIRREX standard lamps described by Mueller et al. (1996). To correct for this drift, the average ratios of SIRREX-2 to SIRREX-3 data were computed for both lamps F304 and F305 between 400 and 1,000 nm and this factor applied to the SIRREX-2 data for all lamps and all wavelengths. The ratio between SIRREX-2 and -3 can be computed only for lamps F304 and F305 because they had not been used between these two experiments. Each calibrated lamp's output was compared to the irradiance measured at each SIRREX experiment (Fig. 20 and Table 9). To examine the performance of lamps for which there was no current manufacturer's calibration, lamp irradiances were computed from the transfer calibrations (performed at UCSB) from F304 to F219 and F305. These were confined to wavelengths between 380 and 665 nm.

Lamp F303: In general, there was best agreement between each SIRREX experiment and the closest Optronic Laboratories calibration for lamp F303 (Fig. 20a). The color shift between 1992 and 1995 suggested by the Optronic Laboratories calibrations, however, was not confirmed at either SIRREX-2 or SIRREX-3. The SIRREX-2 (1993) data for F303 between 400 and 700 nm did not agree well with either the original 1992 data or the 1995 data (1.6 versus 2.1%, Table 9). There is good agreement above 400 nm between the SIRREX-3 (1994) and the 1995 Optronic Laboratories calibration of lamp F303 (0.7%, Table 9). It should be noted that during SIRREX-3, F303 was calibrated against the standard lamp F268, which was recently calibrated by NIST, rather than F269 which was observed to shift in irradiance during the experiment (Mueller et al. 1996). A change in the output of F303 could not be inferred from the SIRREX results.

Lamps F304 and F305: The Optronic Laboratories calibration of lamp F304 (1995) and the derived calibration of F305 compared well with both the SIRREX-2 and the SIRREX-3 data for these lamps, 0.8 and 1.0%, respectively (Fig. 20b and Table 9).

Lamp F219: There was very poor agreement between the original Optronic Laboratories F219 calibration and the earliest SIRREX data (SIRREX-1), but these dates were three years apart. The agreement was better between the derived F219 calibrations and SIRREX-2 in the visible region (Table 9).

In general, the SIRREX data supported the same conclusions as the radiometer comparisons: namely, that F303 (1995 calibration) and F304 agree and that the 1995 transfer calibration of F304 to F305 and F219 was reliable (data shown below). The SIRREX data do not support well the 1992 Optronic Laboratories calibration of lamp F303.

Because the 1995 Optronic Laboratories F304 calibration seems to be the touchstone for the other lamp calibrations, one additional comparison was examined to confirm its absolute values. A BSI PRR (S/N 9626) with the same type of photodiodes as the MERs was used for one of the training sessions at SIRREX-4 (May 1995) at NIST. Although the setup was not optimal, readings were taken with two FEL lamps, F423 and F422 (owned and calibrated by NIST). Using the F304 Optronic Laboratories calibrations to compute irradiances for the two NIST lamps, the agreement was within 1% for all but one value at 665 nm, where the disagreement was most likely due to reflected stray light from the dark color of the baffling on the calibration bench (Table 10). This instrument had been calibrated in March, May, and August 1995 at UCSB, and in May 1995 at BSI, and these calibrations also agreed within 1% at all wavelengths (data not shown).

The Optronic Laboratories F304 and F303 calibrations in July 1995 were in good agreement with the data from two SIRREX experiments in 1993 and 1994, as well as with data from two NIST calibrated lamps in 1995. Based on the radiometer responses, it appears that the irradiance of F303 had not changed since 1992. The excellent consistency between the early radiometer calibrations calculated with the 1995 Optronic Laboratories calibration of lamp F303 and those done with F304, since July 1995, support the hypothesis that the 1992 Optronic Laboratories calibration for lamp F303 was not accurate and should not be used. Rather, it appeared that the 1995 Optronic Laboratories F303 calibration should be used for all radiometer calibrations with this lamp. For all subsequent discussions, the 1995 Optronic Laboratories irradiances for lamps F303 and F304 will be used for the BBOP radiometers' calibrations from 1992 to mid-1995 (F303) and from mid-1995 to the present (F304).

4.3.3 Irradiance History

Once it was established which lamps and calibrations were most reliable, all of the calibrations of two UCSB profiling radiometers (S/N 8728 and 8714) could be examined in detail. Because of their different use and calibration timelines, the irradiance histories of these two radiometers will be discussed separately.

† This was from an internal Optronic Laboratories report titled "Report of Calibration of One Standard of Spectral Irradiance OL FEL-C, S/N: F-304," Project No. 903-479, 28 July 1995.

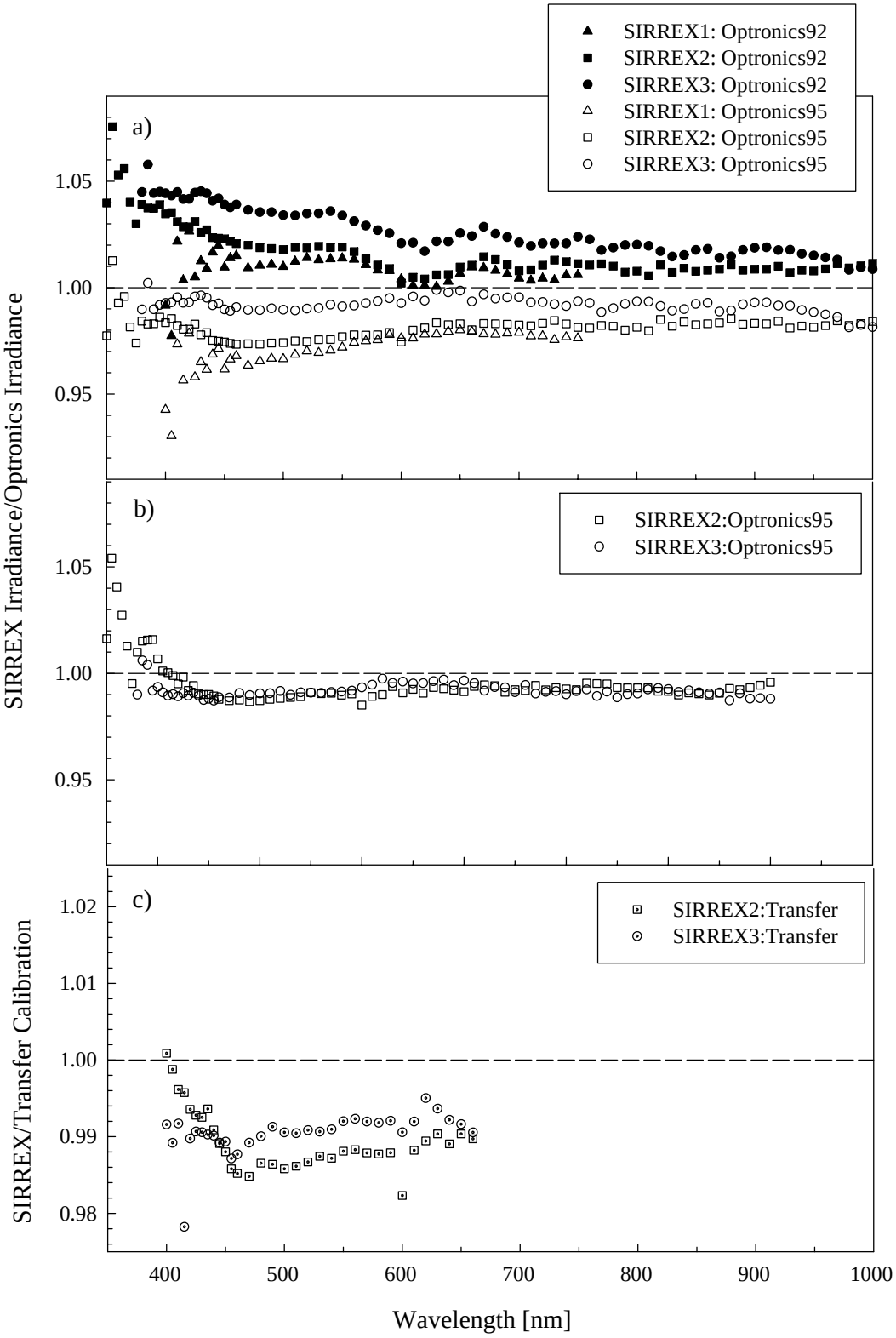

Fig. 20. Ratios of SIRREX results to Optronic Laboratories irradiances for three lamps used at the ICESS Calibration Facility: **a)** Lamp F303, ratios of three SIRREX irradiances to Optronic Laboratories calibrations from two dates, in 1992 and 1995; **b)** Lamp F304, ratios of two SIRREX irradiances to Optronic Laboratories calibration from 1995; **c)** Results from SIRREX-2 and -3 compared to the transfer calibration of F304 to F305, note scale change.

Table 10. Comparison of computed irradiances for lamps F422 and F423 measured during SIRREX-4 [$\hat{E}(\lambda)$] using PRR S/N 9626 [$\hat{E}'(\lambda)$] as the transfer radiometer. The percent differences (PD) from the actual irradiances are also given.

	F422 Irradiance			*F423 Irradiance*		
λ [nm]	$\hat{E}(\lambda)$	$\hat{E}'(\lambda)$	*PD* [%]	$\hat{E}(\lambda)$	$\hat{E}'(\lambda)$	*PD* [%]
412	2.6004	2.5827	−0.69	2.7239	2.7132	−0.40
443	3.9873	3.9513	−0.91	4.1652	4.1490	−0.39
490	6.5817	6.5255	−0.86	6.8502	6.8224	−0.41
510	7.8034	7.7309	−0.94	8.1107	8.0559	−0.68
555	10.6600	10.5983	−0.58	11.0500	11.0274	−0.21
665	17.0185	16.7927	−1.34	17.5592	17.4974	−0.35

4.3.3.1 BBOP Radiometers

To compare the differences among irradiance calibrations over the entire project, each detector's coefficient was normalized to that from the first calibration in July 1992. The gains of underwater instrument 8728 were adjusted in early 1994 and so later data were renormalized to the first calibration after this date. From 1992–1996, most of the channels of the profiling radiometer (S/N 8728) were very stable with no appreciable trends (Fig. 21a). The scatter of all channels, however, increased from January 1994 to December 1996, up to about 2%. The differences between slopes calculated on any two consecutive dates were small, about 0.2%. On two dates (9 August 1994 and 19 December 1996), calibrations were performed using both lamps F303 and F304 and the calibration coefficients were nearly identical. Those detectors, which did not remain stable to within 2% during four years, had shown marked deterioration (up to 5% in three months) and have been replaced (Fig. 22 and Sect. 4.4). There was a slight drift downwards in some of the blue channels, indicating that these detectors may have begun to deteriorate.

The original BBOP surface sensor (S/N 8729) was very stable from 1992–1994, but drifted towards increasing sensitivity during 1994–1995 (Fig. 21b). The last calibration before instrument 8729 was taken out of service agreed well with the calibration performed in early 1997, about two years later. Except for the most recent calibration (1997), lamp F303 was used for all calibrations of instrument 8729. There were no repairs or physical events that would explain the drift. Its replacement (S/N 8734) also showed a similar drift upward during 1995–1996, but has been stable since mid-1996 (Fig. 21c). In May 1996, a smudge of O-ring grease was cleaned from under the Teflon®† cosine collector, which was likely to have been the cause of the drift. Calibrations after this event were renormalized to the May 1996 values; since then, the instrument 8734 calibrations have been very stable (Fig. 21c). The two UV channels, $E_d(340)$ and $E_d(380)$, have shown marked deterioration and have been replaced (data not shown).

† Teflon is a registered trademark of E.I. du Pont de Nemours, Wilmington, Delaware.

4.3.3.2 BOPSII Radiometer

The calibration history of the BOPSII profiling radiometer (S/N 8714) began in February 1989 using lamp F219 (Fig. 17). In October 1992, lamp F303 replaced F219, which was in turn replaced by F304 in October 1995. For calculations with lamp F219, the transfer calibration from F304 to F219 was used. The 1995 Optronic Laboratories calibration for lamp F303 was used for all calibrations performed with that lamp. The data were treated similarly to that for the BBOP radiometer. Slopes were normalized to the January 1994 value. Most downwelling irradiance detectors showed similar variations to those in instrument 8728 (Fig. 23). During seven years, most calibration slopes for each channel were within 2%; in fact, 19 out of 21 channels varied less than 1%. Two detectors, $E_d(510)$ and $E_d(520)$, however, still showed large, unexplained drifts from 1989–1992.

4.3.4 Radiance History

The radiance calibration history is longer for the integrating sphere than for the plaque, however, the reflectance of this sphere has never been satisfactorily characterized and an arbitrary reflectance value was used in the slope calculations. From mid-1994 through 1996, the radiance channels of instrument 8728 were calibrated with both the sphere and the plaque, so the plaque calibrations could be transferred onto the earlier sphere calibrations.

Plaque radiance values were computed from the lamp irradiance corrected for the inverse square law, the manufacturer's determination of the plaque's reflectivity (provided at the time of purchase), and the assumed Lambertian distribution. Calibration coefficients for instrument 8728 were normalized to those from August 1994, the first date on which plaque calibrations were performed (Fig. 24a). As with the irradiance history, most of the radiance channels showed very little change. On instrument 8728, 10 out of 12 channels varied less than 1% from the normalized value during 10 calibrations (the range for all channels was 0.26–1.55%). Figure 24a also shows a slight decrease in the blue channels during 1995 and 1996, although the overall decrease is still less than 2%.

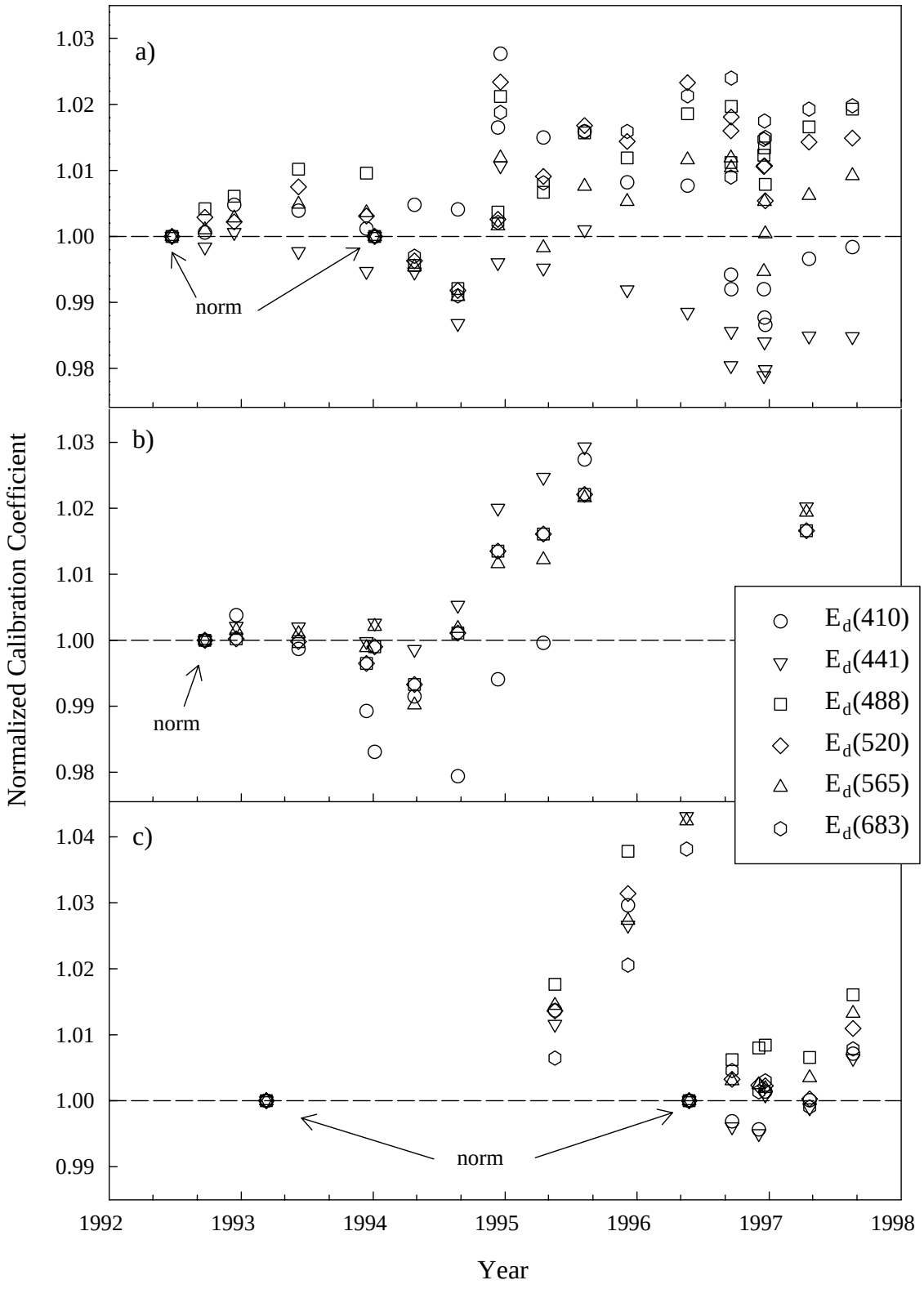

Fig. 21. The normalized calibration coefficients for selected downwelling irradiance channels on three BSI MER-2040 and -2041 radiometers used during BBOP computed using the 1995 Optronic Laboratories calibrations of F303 and F304: **a)** underwater instrument (S/N 8728), **b)** surface sensor (S/N 8729), and **c)** surface sensor (S/N 8734).

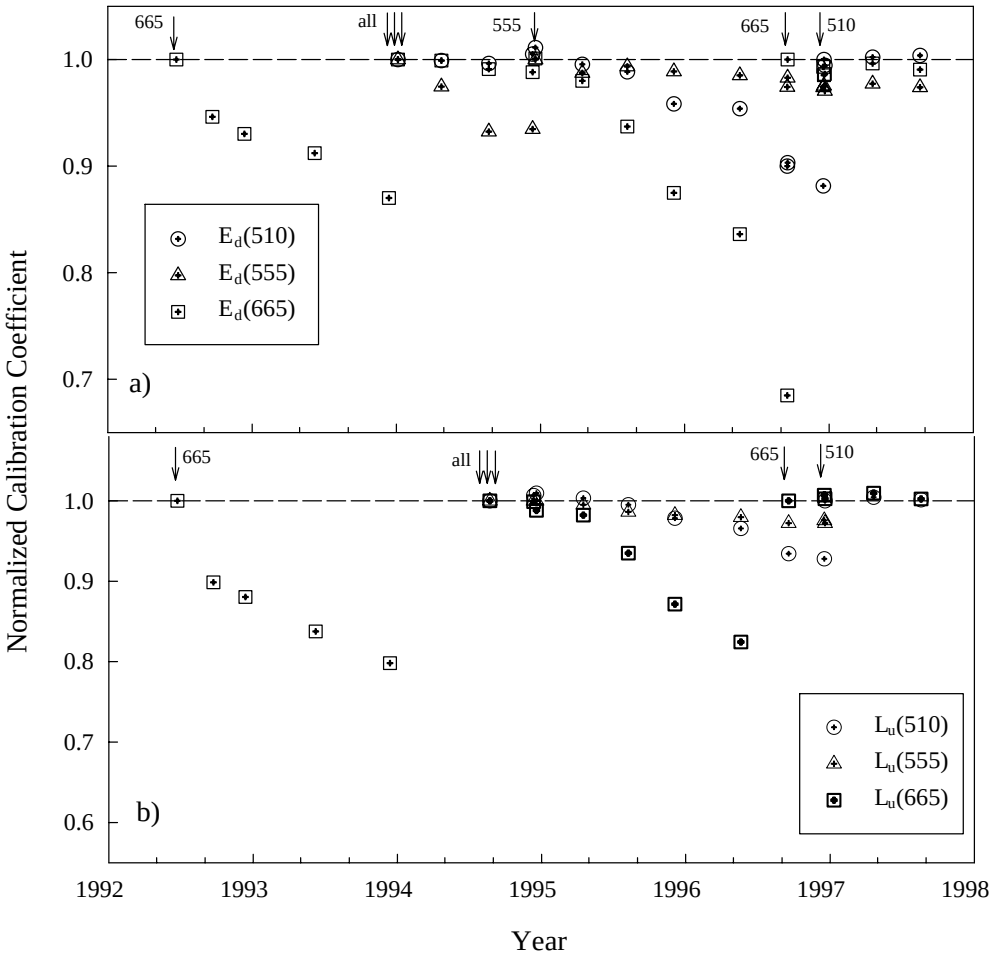

Fig. 22. Deteriorating detectors on the BBOP radiometers (S/N 8728 and 8734) from 1992–1997. The arrows indicate when detectors were replaced.

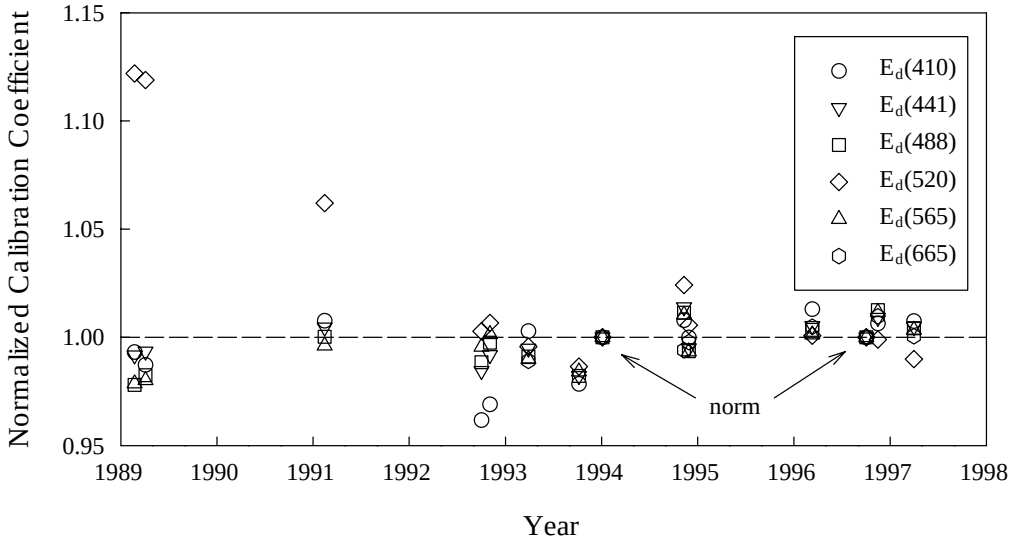

Fig. 23. The normalized calibration coefficients for selected downwelling irradiance channels on the BOPSII profiling radiometer (S/N 8714) calculated with the transfer calibration of F304 to F219 and the 1995 Optronic Laboratories calibrations of lamps F303 and F304.

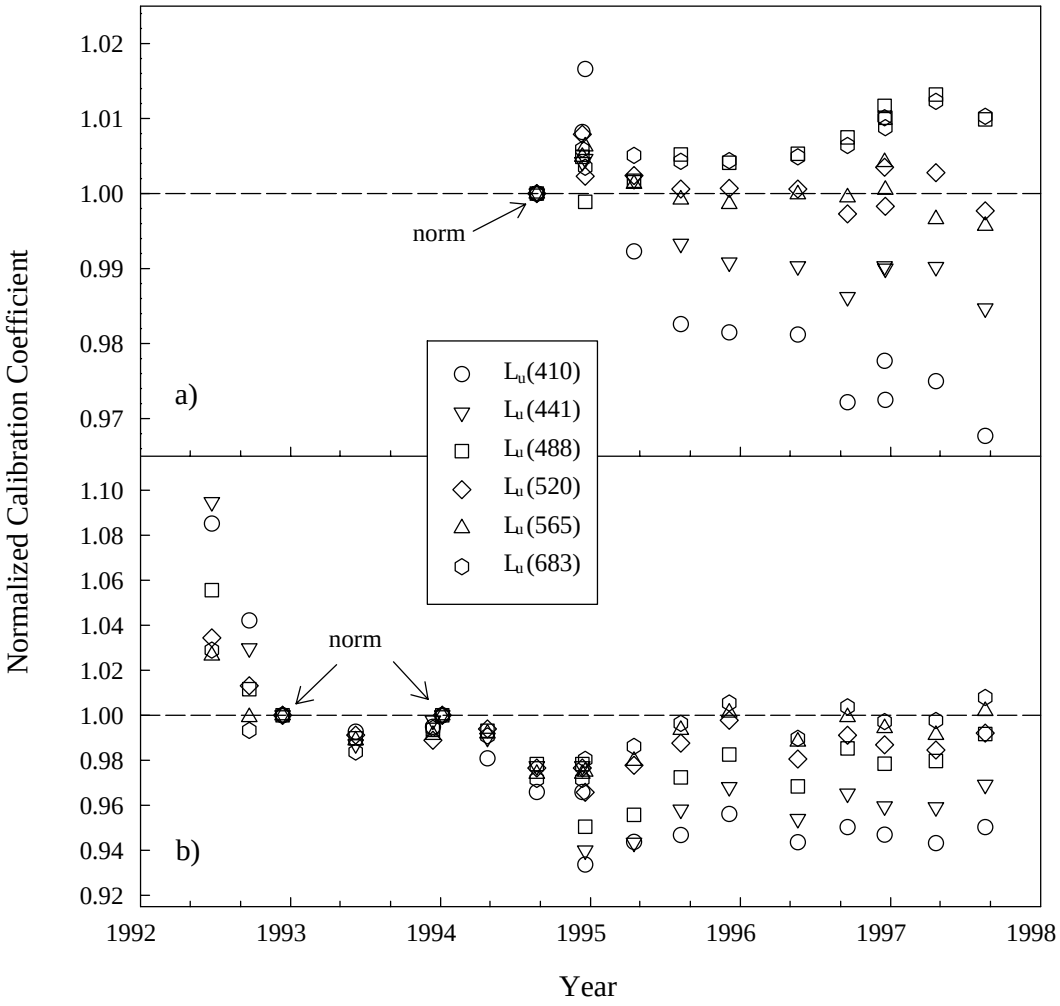

Fig. 24. The normalized calibration coefficients for selected radiance channels on the BBOP radiometer (S/N 8728) from 1992–1997: **a)** reflectance plaque, and **b)** integrating sphere.

Sphere coefficients were normalized twice, because of the gain change in January 1994. Coefficients from calibrations before the gain change were normalized to the December 1992 calibration, and those from later dates to the August 1994 data—the same date as plaque normalizations (Fig. 24b). Over the long term, calibrations with the sphere were more variable than those with the plaque. From August 1994 to September 1996, the same 10 channels discussed above had an average coefficient of variation (CV) of 1.4% when calibrated with the sphere. The plaque and sphere were illuminated by the same lamp, so the greater variation in the sphere calibrations may have been due to changes in the back loading of the sphere when the instrument was positioned close to the exit aperture, or to changes in the reflectivity of the sphere coating. These possibilities were examined before the plaque calibrations were transferred onto the earlier sphere calibrations.

Because the latter plaque data are very stable, two plaque calibrations were used to examine possible shifts in sphere reflectance. For two dates, 17 May 1995 and 18 September 1996, it was assumed that the nominal plaque reflectances were correct. These were used to compute the sphere reflectances that would yield the same slopes (in units of $\mathrm{V\,mW^{-1}\,cm\,nm\,sr}$) for the measured sphere voltages as were measured with the plaque (Fig. 25). The difference between the nominal and calculated sphere reflectances was clearly spectral and ranged from 0.34–0.83% in May 1995, and from 0.24–0.68% in September 1996. The differences between the 1995 and 1996 calculations were generally less than 0.2%. Although the differences between the two computed reflectances were greatest in the blue region, the changes were not large enough to suggest that the reflectivity of the sphere had changed during this time. When the two estimated sphere reflectances were used to calculate calibration slopes, their differences were magnified to approximately 2% (Table 11). Because the differences between the two computed sphere reflectances were small and within the reproducibility of the sphere calibrations, and any differences would be magnified if a single estimate of sphere reflectance was used, the average ratio of plaque-to-sphere coefficients was computed for

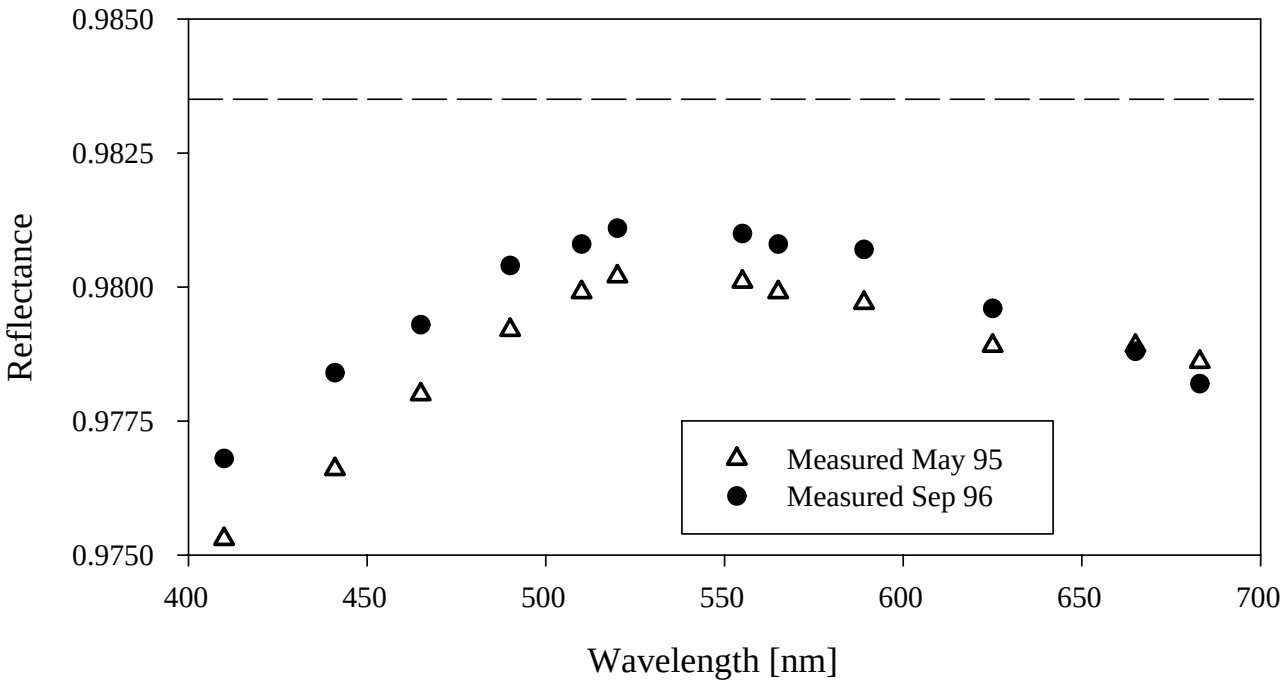

Fig. 25. Computed reflectance of the ICESS integrating sphere on two dates, 17 May 1995 and 18 September 1996. The dashed line shows the manufacturer's nominal reflectance.

each channel. These factors were applied to the average calibration slopes measured with the sphere in 1992 and 1993.

Table 11. Radiance calibration slopes for radiometer 8728 measured on 18 September 1996 computed from sphere reflectances estimated on two dates, May 1995 and September 1996. The units are in $\mathrm{V}\,\mu\mathrm{W}^{-1}\,\mathrm{cm}^2\,\mathrm{nm}\,\mathrm{sr}$.

λ [nm]	*May 95*	*Sept. 96*	*PD* [%]
410	0.90070	0.87252	3.13
441	0.93630	0.90027	3.85
465	0.86910	0.84426	2.86
490	0.88819	0.86418	2.70
510	0.85202	0.83449	2.06
520	0.87318	0.85510	2.07
555	1.03165	1.01033	2.07
565	0.90756	0.88888	2.06
589	0.86213	0.84250	2.28
625	0.90776	0.89353	1.57
665	1.08689	1.08205	0.45
683	0.99982	0.98244	1.74

This examination of the calibration histories of these radiometers demonstrated that most of the detectors were stable over the course of these instruments' 6–8 year histories. Furthermore, the stability of the calibration coefficients also implies stability of the amplifiers, analog-to-digital converters and optical windows of the MER instruments, as well as, reproducibility of calibration lamp geometry and the lamp power supply. A change in any of these components would have been evident in the calibration coefficients. Their absolute calibrations, however, are tied to just one lamp calibration by Optronic Laboratories (F304 in May 1995), which itself, is guaranteed to about 1%. The variety and number of comparisons of lamp F304's irradiance to other lamps lend confidence to these values.

4.4 LONG-TERM AVERAGES

Long-term averages of calibration slopes can be computed with confidence, because the radiometers used with BBOP appear to be very stable. These long-term averages should be used whenever possible and recomputed after major upgrades. Calibration coefficients for deteriorating channels should be interpolated. For these purposes, *stability* has been defined by a CV less than 1%. When the CV exceeded these limits, the calibration data were examined closely for trends or shifts and, in most cases, a physical reason for the change was evident which justified computing a new long-term average.

Tables 12–14 summarize the slopes that will be used for most channels on the three BBOP radiometers. For the profiling radiometer (Table 12), there are two main time periods: 1992–1993 during which there were a total of 15 channels, and 1994–1996 after the upgrade to 12 down- and 13 upwelling channels. In most cases, one slope can be used for each channel for each time period. At the end of 1994, both 555 nm detectors were replaced and the slopes of several other channels were affected as well: $E_d(488)$,

Table 12. The average calibration slope (ACS) values used for MER-2040 (S/N 8728) from 1992–1996. The CV and the number of observations (n) are also given. For most channels, only two slopes are necessary: before and after the gain change in January 1994. The top half of the table gives the average calibration slopes for the downwelled irradiance channels, $E_d(\lambda)$, in units of $\mathrm{V}\,\mu\mathrm{W}^{-1}\,\mathrm{cm}^2\,\mathrm{nm}$. For the channels affected by the repairs in January 1995 [$E_d(410)$, $E_d(488)$ and $E_d(520)$], it was necessary to compute separate averages for 1994 and 1995–1996. Before plaque calibrations were available, the average slopes for the upwelled radiance channels, $L_u(\lambda)$ (in units of $\mathrm{V}\,\mu\mathrm{W}^{-1}\,\mathrm{cm}^2\,\mathrm{nm}\,\mathrm{sr}$) were determined using the mean slope from the sphere calibrations and the plaque-to-sphere ratios (given in the bottom half of the table). Their CVs were calculated from the uncorrected sphere calibrations.

Measurement	*1992–1993*			*1994–1996*			*1994*			*1995–1996*		
Channel	*ACS*	*CV*	n	*ACS*	*CV*	n	*ACS*	*CV*	n	*ACS*	*CV*	n
$E_d(410)$	0.04796	0.21	5				0.03256	0.70	7	0.03211	0.90	3
$E_d(441)$	0.04568	0.23	5	0.03517	0.94	15						
$E_d(465)$	0.04855	0.14	5	0.03248	0.68	15						
$E_d(488)$	0.05436	0.42	5				0.03395	0.51	4	0.03450	0.46	11
$E_d(510)$	[1]						0.03411	0.37	6	[2]		
$E_d(520)$	0.04894	0.27	5				0.03314	0.47	4	0.03370	0.56	11
$E_d(555)$	[1]						[2]			0.03633	0.97	11
$E_d(565)$	0.05456	0.20	5	0.03409	0.67	15						
$E_d(587)$	0.05556	0.16	5	0.03548	0.80	15						
$E_d(625)$	[1]						0.03626	0.52	4	0.03684	0.48	11
$E_d(665)$	[2]						0.03449	0.59	4	[2]		
$E_d(683)$	[1]						0.03498	0.48	4	0.03563	0.56	11
$L_u(410)$	0.3482	0.38	3	0.8917	1.47	11						
$L_u(441)$	0.2800	0.69	3	0.9111	0.65	11						
$L_u(465)$	0.3071	0.42	3	0.8301	0.38	11						
$L_u(488)$	0.2804	0.52	3	0.8561	0.43	11						
$L_u(510)$	[1]						0.8843	0.41	4	[2]		
$L_u(520)$	0.2523	0.59	3	0.8560	0.30	11						
$L_u(555)$	[1]						0.8921	0.01	2	1.0198	0.96	8
$L_u(565)$	0.2476	0.59	3	0.8898	0.26	11						
$L_u(587)$	0.2440	1.04	3	0.8505	0.40	11						
$L_u(625)$	[1]			0.8967	0.29	11						
$L_u(665)$	[2]						0.8814	0.87	4	[2]		
$L_u(683)$	0.2379	0.83	3	0.9819	0.28	11						

[1] Not applicable.

[2] Indicates that a detector was deteriorating, e.g., $E_d(665)$, and no average could be computed for that time period.

Table 13. The ACS values used for MER-2041 (S/N 8729) from 1992 to August 1995, in units of $\mathrm{V}\,\mu\mathrm{W}^{-1}\,\mathrm{cm}^2$ nm.

Measurement	*Sept. 1992–Aug. 1994*			*Aug. 1994–1995*		
Channel	*ACS*	*CV*	n	*ACS*	*CV*	n
$E_d(410)$	0.02564	.91	7	0.02566	.68	3
$E_d(441)$	0.02587	.28	7	0.02635	.42	3
$E_d(488)$	0.02934	.22	7	0.03002	.45	3
$E_d(520)$	0.03037	.28	7	0.03094	.44	3
$E_d(565)$	0.03163	.42	7	0.03213	.55	3
$E_d(665)$	0.03492	.55	7	0.03539	.49	3

$E_d(520)$, $E_d(625)$, and $E_d(683)$. For these channels, new long-term averages were computed for 1995–1996. Several detectors—$E_d(510)$, $E_d(555)$, $E_d(665)$, $L_u(510)$, and $L_u(665)$—deteriorated (Fig. 22), and it was not possible to calculate their average slopes for many months. For these channels, the deterioration was assumed to be linear and a slope was calculated for each cruise using a least-squares regression. During 1996 and 1997, all of these aging detectors were replaced and new long-term averages must be determined.

Table 14. The ACS values used for MER-2041 (S/N 8734) from August 1995–1997 (in units of V $\mu W^{-1}\,cm^2\,nm$). No average could be computed for the time period of May 1995–1996 because of the drift of the instrument's response. For the $E_d(340)$ channel, the mean is for the time period of December 1996–August 1997.

	May 1996–Aug. 1997		
Channel	*ACS*	*CV*	*n*
$E_d(340)$	0.01496	2.12	3
$E_d(380)$	0.00538	0.31	6
$E_d(410)$	0.02477	0.40	6
$E_d(441)$	0.02888	0.41	6
$E_d(465)$	0.02049	0.38	6
$E_d(488)$	0.01534	0.51	6
$E_d(520)$	0.01617	0.40	6
$E_d(540)$	0.01278	0.41	6
$E_d(565)$	0.01108	0.47	6
$E_d(587)$	0.01257	0.36	6
$E_d(625)$	0.01411	0.36	6
$E_d(665)$	0.01581	0.36	6
$E_d(683)$	0.01499	0.32	6

The calibration coefficients of the two surface sensors (S/N 8729 and S/N 8734) appear to have drifted since 1992 (Figs. 21b–c, Sect. 4.3.2.1). For these, long-term averages will be used only for time periods when the responses for these instruments were stable. For instrument 8729, the overall drift (1992–1995) was about 2% (Fig. 21b), but the CV of the average slopes can be reduced to less than 1% by dividing the data into two time periods and calculating means for each (Table 13). There was no obvious physical reason for this drift. Radiometer 8734 drifted about 3–4% from May 1995 to May 1996, because of the grease accumulating under the cosine collector (Fig. 21c). Because the CVs during its first year of use were well over 1%, it was assumed that the drift was linear and the calibration slopes were interpolated as for deteriorating detectors. For calibrations after May 1996, the slopes were very steady and long-term averages can be used (Table 14).

For most detectors, the average slope calculated for years 1994–1996 (instrument 8728) or for 1995–1996 (instruments 8729 and 8734) will also be applicable to future data. The methods used here to examine past stability will accommodate the addition of new calibration data as it is available; it will be possible to closely track any changes in the performance of these instruments and adjust the calibration coefficients accordingly.

4.5 OTHER ISSUES

Although calibration lamp behavior was the first consideration when examining differences between calibrations, several other factors are involved in determining the final calibration coefficents. These may affect all of the coefficients calculated for a particular instrument (e.g., the effect of immersion on the cosine collector), or, like the lamp calibrations, may change over time (e.g., aging of the reflectance plaque).

4.5.1 Immersion Effects

The effect of immersion in water on acrylic cosine collectors is to decrease the irradiance responsivity of the radiometer compared to that measured in air. It has been determined experimentally that the immersion effects of different cosine collectors of the same design and material may differ by as much as 10% (Mueller 1995b). This makes questionable the practice of applying one immersion coefficient, which is based on material and design specifications, to all collectors in a class. The immersion coefficients for the BOPSII and BBOP profiling instruments were measured at SDSU CHORS during 1994 and 1995, respectively (Mueller 1995b, and Mueller 1996).

The final immersion coefficients for instrument 8728 were predicted from the linear regression (441–625 nm) or were the average of two measurements of immersion (for 410, 665, and 683 nm). The final immersion coefficients for instrument 8714 were predicted from the linear regression. Nominal immersion coefficients (provided by the manufacturer) and those determined at CHORS for these two instruments are presented in Table 15 and Fig. 26. Differences from the nominal values ranged from 3.5–10%. A single, nominal immersion coefficient cannot be applied to all instruments and possibly, several measurements of the immersion effect must be performed on a single instrument to determine an accurate coefficient. Uncertainties of 10% in accuracy or reproducibility are unacceptable for vicarious calibration. The measured immersion coefficients reported in Table 15 have been used for all calculations of calibration slope during BBOP. It is likely that when the immersion coefficients for the BBOP instrument have been more clearly defined by additional immersion tests that these calibration slopes will be recalculated.

4.5.2 Possible Plaque Aging

Figure 24a showed a slight decrease in the slopes of the blue channels on instrument 8728 during 1996, although the decrease was small—less than 2%. It is possible that the plaque is yellowing or becoming soiled, or that the

Table 15. Immersion coefficients ($1/F_i$) for radiometers used in this study (from Mueller 1995b and Mueller 1996). The nominal values were provided by the manufacturer (BSI) at the initial calibration of instrument 8728. The column headings denote the MER model and serial number, and the collector type, either E_d or E_u (upwelled irradiance).

λ [nm] *(Nominal)*	*Nominal Immersion*	*2040 (S/N 8728)* E_d	*2040 (S/N 8714)* E_d	E_u
410	0.705	0.7856	0.71311	0.71592
441	0.694	0.7637	0.71911	0.72351
465	0.691	0.7688		
488	0.691	0.7736	0.72796	0.73498
510	0.694	0.7785		0.73998
520	0.695	0.7803	0.73578	0.74275
555	0.705	0.7885		
565	0.708	0.7907	0.74528	0.75464
587	0.715	0.7958	0.75050	0.76090
625	0.726	0.8042	0.75915	0.77129
665	0.736	0.7642		
683	0.739	0.7870		

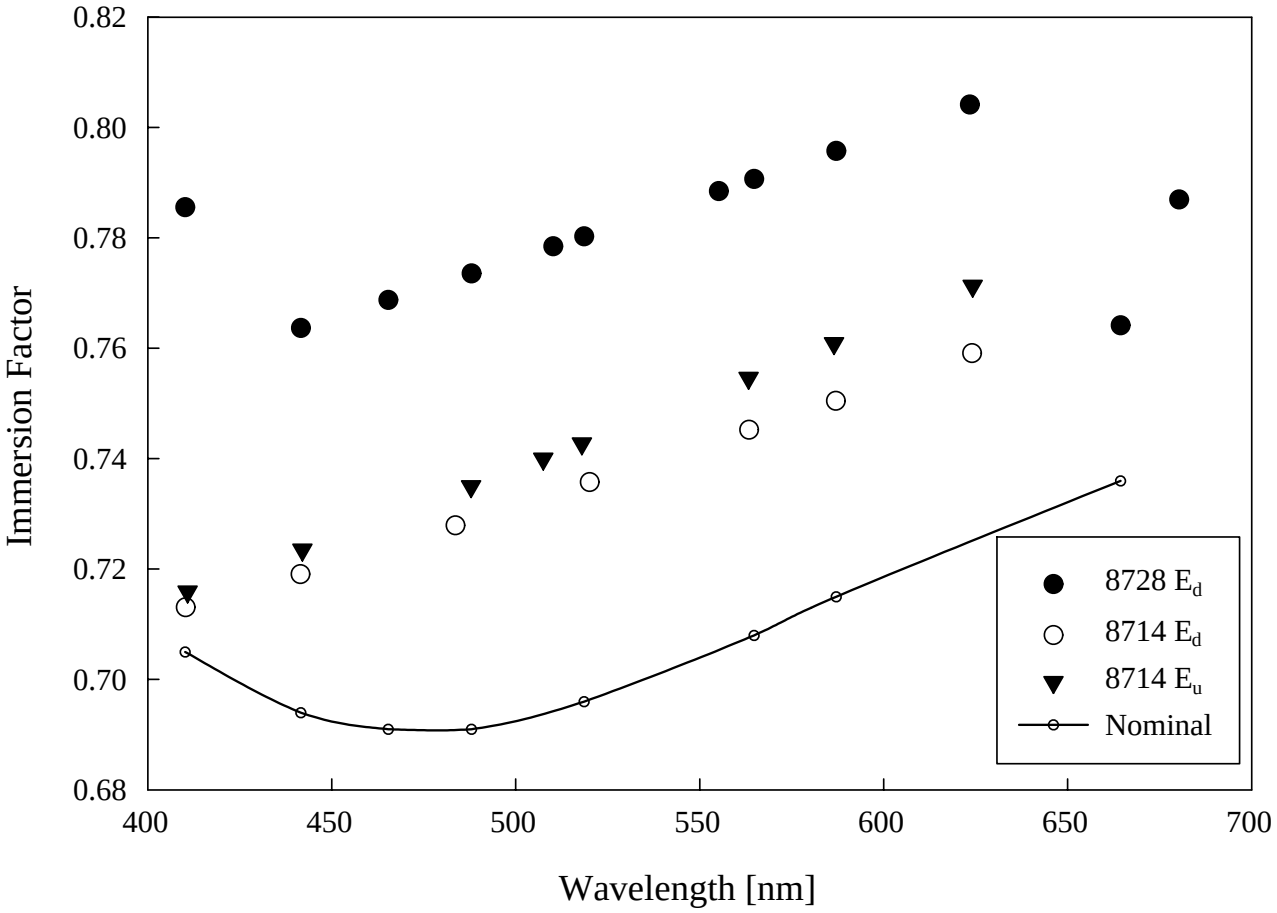

Fig. 26. The nominal and measured immersion coefficients for three irradiance heads on two radiometers.

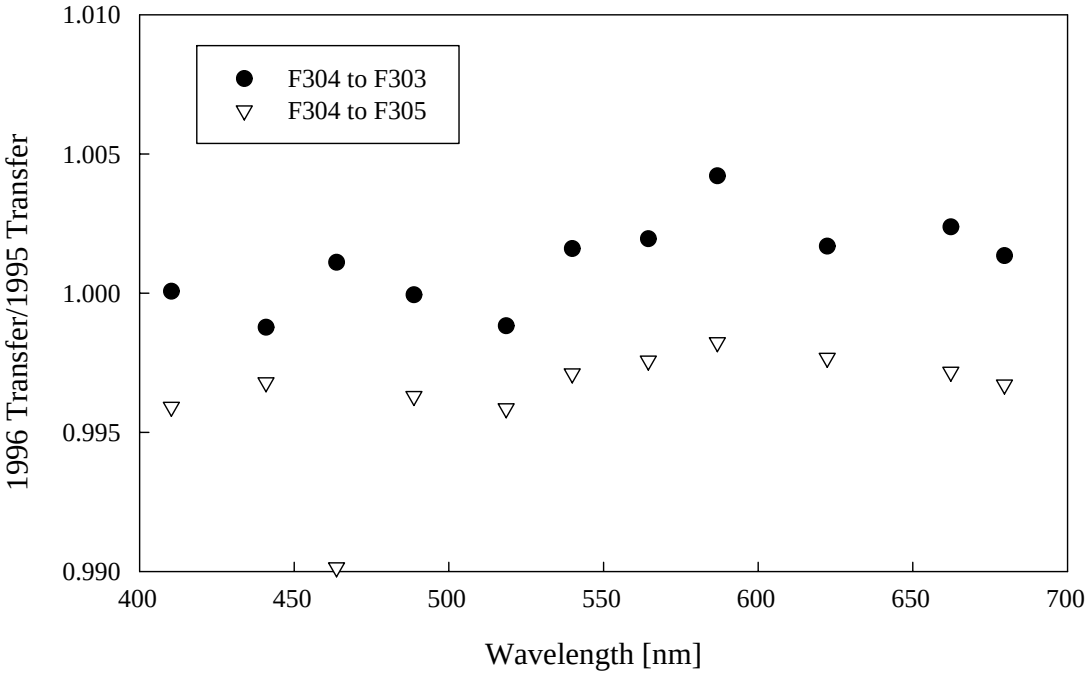

Fig. 27. The ratio of transfer calibrations performed in May 1996 to those from May 1995 from lamp F304, to lamps F303 and F305.

two blue detectors, $L_u(410)$ and $L_u(441)$, are deteriorating. Because calibrations of other recently purchased instruments are being monitored at ICESS, this question will be clarified. In addition, the plaque is scheduled to be recalibrated by the manufacturer in the near future.

4.5.3 Quality Control Measures

These results precipitated refinements in calibration methods and record keeping at ICESS. First, to avoid possible confusion when standard lamps are replaced, lamps dedicated to each project were purchased so that the consistency of calibrations can be monitored easily for many years. Second, annual in-house cross-checks between lamps were initiated in 1995.

The transfer calibration performed from lamp F304 to F305, and F303 in May 1995 was repeated in May 1996 (Fig. 27). With one exception, lamp F305 at 465 nm, the differences between the two transfers one year apart were less than 0.5%, implying that the output of these three lamps had not changed during the year following the 1995 lamp calibration at Optronic Laboratories. The agreement was particularly good between lamps F303 and F304. In fact, this 465 nm detector [S/N 8733, $E_d(465)$] was recently replaced after it was determined to be unstable. Lamp F303 was retired from routine calibrations in 1995 and now serves as a standard to which any other lamp's performance can be compared. Transfer calibrations such as these will be continued annually to closely monitor performance of lamps between routine calibrations at the manufacturer and future SIRREX workshops.

4.6 CONCLUSIONS

The variations of calibration slopes for most channels of radiometer 8728 were less than 1% between 1992 and 1997. Because the radiometers used for BBOP appear to be very stable, there can be excellent confidence in the long-term averages of calibration slopes and consequently, in the AOPs produced from profile data. These long-term averages should be used whenever possible.

When the 1995 calibrations of lamps F303 and F304 were used to calculate slopes, there was an almost seamless transition when F304 replaced F303 as the primary lamp for radiometer calibrations. The methods used here to examine past stability, accommodate the addition of new calibration data as they become available, enabling close monitoring of changes in instrument performance, and the necessary adjustment of calibration coefficients.

These results show that there can be confidence in the calibration of the MER-2040 series radiometers at the 1% level. It appears, however, that the calibration responses of these instruments may have been more stable than the irradiance of the lamps used as calibration standards. Ultimately, the absolute calibrations of the radiometers discussed here are tied to one lamp calibration by Optronic Laboratories at the midpoint of this time series, which itself, is guaranteed to about 1%. That calibration has been compared with as many others as possible, and as a result, there can be confidence in its accuracy. It is essential that comparisons such as these continue to ensure the high quality of radiometer data.

Glossary

ALOHA	A Long-term Oligotrophic Habitat Assessment [the Hawaii Ocean Time-series (HOT) deep-water station located about 100 km north of Oahu, Hawaii].
ACS	Average Calibration Slope
AI9901	Atlantic–Indian Ocean Cruise, 1999
AMT	Atlantic Meridional Transect
AOP	Apparent Optical Properties
BATS	Bermuda Atlantic Time Series
BBOP	Bermuda BioOptics Project
Ber95	Bering Sea Cruise, 1995
Ber96	Bering Sea Cruise, 1996
BOPSII	Bio-Optical Profiling System II (second generation)
BSI	Biospherical Instruments, Inc.
CalCOFI	California Cooperative Oceanic Fisheries Investigation
CARIACO	Carbon Retention in a Colored Ocean
CB-MAB	Chesapeake Bay–Middle Atlantic Bight
CDOM	Colored Dissolved Organic Matter
CHORS	Center for Hydro-Optics and Remote Sensing
COARE	Coupled Ocean Atmosphere Response Experiment
CoASTS	Coastal Atmosphere and Sea Time Series
CoBOP	Coastal Benthic Optical Properties (Bahamas)
CSC	Coastal Service Center, (NOAA, SC)
CV	Coefficient of Variation
CVT	Calibration and Validation Team
CZCS	Coastal Zone Color Scanner
DARR	Data Analysis Round-Robin (workshop)
EcoHAB	Ecology of Harmful Algal Blooms
EqPac	Equatorial Pacific
FEL	Not an acronym, but a type of irradiance lamp designator.
FL-Cuba	Florida–Cuba cruise.
FWHM	Full-Width at Half-Maximum
GOM	Gulf of Maine
GoA97	Gulf of Alaska Cruise, 1997
GSFC	Goddard Space Flight Center
HOT	Hawaii Ocean Time-series
HPLC	High Performance Liquid Chromatography
ICESS	Institute for Computational Earth System Science
IDL	Interactive Data Language
JES9906	Japan East Sea Cruise, 1999-06
JGOFS	Joint Global Ocean Flux Study
Lab96	Labrador Sea Cruise, 1996
Lab97	Labrador Sea Cruise, 1997
Lab98	Labrador Sea Cruise, 1998
LTER	Long Term Ecological Research
MCP	Modified Cubic Polynomial
MBARI	Monterey Bay Aquarium Research Institute
MBR	Maximum Band Ratio
MER	Marine Environmental Radiometer
MERIS	Medium Resolution Imaging Spectrometer
MF0796	R/V Miller Freeman Cruise, 1996-07
MOCE	Marine Optical Characterization Experiment
MODIS	Moderate Resolution Imaging Spectroradiometer
NABE	North Atlantic Bloom Experiment
NASA	National Aeronautics and Space Administration
NEGOM	Northeast Gulf of Mexico
NIST	National Institute for Standards and Technology
NOAA	National Oceanic and Atmospheric Administration
OC2	Ocean Chlorophyll 2 algorithm
OC2v2	OC2 version 2.
OC4	Ocean Chlorophyll 4 algorithm
OC4v2	OC4 version 2.
OC4v4	OC4 version 4.
OCTS	Ocean Color and Temperature Scanner
ORINOCO	Orinoco River Plume
PD	Percent Difference
PRR	Profiling Reflectance Radiometer
RED9503	Red Tide Cruise, 1995-03
Res94	Resolute Cruise, 1994
Res95-2	Resolute Cruise, 1995
Res96	Resolute Cruise, 1996
Res98	Resolute Cruise, 1998
RMS	Root Mean Square
ROAVERRS	Research on Ocean–Atmosphere Variability and Ecosystem Response in the Ross Sea
SDSU	San Diego State University
SeaBAM	SeaWiFS Bio-optical Algorithm Mini-workshop
SeaWiFS	Sea-viewing Wide Field-of-view Sensor
SIMBIOS	Sensor Intercomparison and Merger for Biological and Interdisciplinary Oceanic Studies
SIRREX	SeaWiFS Intercalibration Round-Robin Experiment
SIRREX-1	The first SIRREX, July 1992.
SIRREX-2	The second SIRREX, June 1993.
SIRREX-3	The third SIRREX, September 1994.
SIRREX-4	The fourth SIRREX, May 1995.
SMAB	Southern Mid-Atlantic Bight
S/N	Serial number
SNR	Signal-to-Noise Ratio
SPO	SeaWiFS Project Office
TOGA	Tropical Ocean Global Atmosphere
TOTO	Tongue of the Ocean study (Bahamas)
UCSB	University of California, Santa Barbara
URL	Universal Resource Locator
UVA	Ultraviolet-A
WOCE	World Ocean Circulation Experiment

Symbols

a	Absorption coefficient.
A	Coefficient.
a_w	Absorption coefficient for pure water.
b	Intercept.
B	Coefficient.
b_b	Backscattering coefficient.
b_w	Backscattering coefficient for pure water.
C_a	Chlorophyll a concentration.
$\tilde{C}_a$	*In situ* chlorophyll a concentration.

$\hat{E}(\lambda)$ Irradiance measured during SIRREX-4.
$\hat{E}'(\lambda)$ Irradiance measured using a PRR as the transfer radiometer.
$E_d(\lambda)$ Downwelled spectral irradiance.
$E_u(\lambda)$ Upwelled spectral irradiance.

f Function.
F_i Immersion coefficient.

$K(490)$ Diffuse attenuation coefficient at 490 nm.
$K_w(\lambda)$ Diffuse attenuation coefficient for pure water.

$L_u(z,\lambda)$ Upwelled spectral radiance.
$L_W(\lambda)$ Spectral water-leaving radiance.
$L_W(\lambda_1)$ Water-leaving radiance for wavelength λ_1.
$L_W(\lambda_2)$ Water-leaving radiance for wavelength λ_2.

m Slope.

n Number of observations.
N Number of data sets.
N_F Number of fluorometric chlorophyll a sets.
N_H Number of HPLC chlorophyll a sets.

R^2 Squared correlation coefficient.
R_2 $\log_{10}(R_{555}^{490})$.
R_{2S} $\log_{10}(R_{555}^{490})$, see R_{3C}, where the argument of the logarithm is a shorthand representation for the maximum of the three values. In an expression such as R_{2S}, the numerical part of the subscript refers to the number of bands used, and the letter denotes a code for the specific satellite sensors [S is SeaWiFS, M is the Moderate Resolution Imaging Spectroradiometer (MODIS), O is the Ocean Color and Temperature Scanner (OCTS), E is the Medium Resolution Imaging Spectrometer (MERIS), and C is CZCS].
R_{3C} $\log_{10}(R_{550}^{443} > R_{550}^{520})$,
R_{4E} $\log_{10}(R_{560}^{443} > R_{560}^{490} > R_{560}^{510})$, see R_{3C}.
R_{4O} $\log_{10}(R_{565}^{443} > R_{565}^{490} > R_{565}^{520})$, see R_{3C}.
R_{4S} $\log_{10}(R_{555}^{443} > R_{555}^{490} > R_{555}^{510})$, see R_{3C}.
R_B^A R_{rs} ratio constructed from band A divided by band B.
R_{rs} Remote sensing reflectance.
$\tilde{R}_{rs}$ *In situ* remote sensing reflectance.
$\hat{R}_{rs}$ Interpolated remote sensing reflectance.
$R_{\lambda_j}^{\lambda_i}$ A compact notation for the $R_{rs}(\lambda_i)/R_{rs}(\lambda_j)$ band ratio.

x The abscissa.

y The ordinate.

z Depth.

γ_a $\log(C_a)$.

λ Wavelength.

σ Standard deviation.

References

Austin, R.W., and Petzold, T., 1981: The determination of the diffuse attenuation coefficient of sea water using the Coastal Zone Color Scanner. *Oceanography from Space,* J.F.R. Gower, Ed., Plenum Press, 239–256.

Evans, R.H., and H.R. Gordon, 1994: Coastal zone color scanner "system calibration": A retrospective examination, *J. Geophys. Res.,* **99,** 7,293–7,307.

Firestone, E.R., and S.B. Hooker, 1998: SeaWiFS Prelaunch Technical Report Series Final Cumulative Index. *NASA Tech. Memo. 1998–104566, Vol. 43,* S.B. Hooker and E.R. Firestone, Eds., NASA Goddard Space Flight Center, Greenbelt, Maryland, 4–8.

Gordon, H.R., and W.R. McCluney, 1975: Estimation of the depth of sunlight penetration in the sea for remote sensing. *Appl. Opt.,* **14,** 413–416.

——, and K. Ding, 1992: Self-shading of in-water optical instruments, *Limnol. Oceanogr.,* **37,** 491–500.

——, and M. Wang, 1994: Retrieval of water-leaving radiance and aerosol optical thickness over the oceans with SeaWiFS: A preliminary algorithm, *Appl. Opt.,* **33,** 443–452.

Gregg, W.W., and R.H. Woodward, 1998: Improvements in high frequency ocean color observations: Combining data from SeaWiFS and MODIS, *IEEE Trans. Geosci. Remote Sens.,* **36,** 1,350–1,353.

Johnson, B.C., S.S. Bruce, E.A. Early, J.M. Houston, T.R. O'Brian, A. Thompson, S.B. Hooker, and J.L. Mueller, 1996: The Fourth SeaWiFS Intercalibration Round-Robin Experiment (SIRREX-4), May 1995. *NASA Tech. Memo. 104566, Vol. 37,* S.B. Hooker and E.R. Firestone, Eds., NASA Goddard Space Flight Center, Greenbelt, Maryland, 65 pp.

Kahru, M., and B.G. Mitchell, 1998a: Spectral reflectance and absorption of a massive red tide off Southern California. *J. Geophys. Res.,* **103,** 21,601–21,609.

——, and ——, 1998b: Evaluation of instrument self-shading and environmental errors on ocean color algorithms. *Proc. Ocean Optics XIV,* Kona, Hawaii, S. Ackleson and J. Campbell, Eds., [Available on CD-ROM.]

Maritorena, S., and J.E. O'Reilly, 2000: OC2v2: "Update on the initial operational SeaWiFS chlorophyll a algorithm." In: O'Reilly, J.E., and 24 Coauthors, 2000: SeaWiFS Postlaunch Calibration and Validation Analyses, Part 3. *NASA Tech. Memo. 2000–206892, Vol. 11,* S.B. Hooker and E.R. Firestone, Eds., NASA Goddard Space Flight Center, Greenbelt, Maryland, 3–8.

McClain, C.R., 2000: "SeaWiFS postlaunch calibration and validation overview." In: McClain, C.R., E.J. Ainsworth, R.A. Barnes, R.E. Eplee, Jr., F.S. Patt, W.D. Robinson, M. Wang, and S.W. Bailey, SeaWiFS Postlaunch Calibration and Validation Analyses, Part 1. *NASA Tech. Memo. 2000–206892, Vol. 9,* S.B. Hooker and E.R. Firestone, Eds., NASA Goddard Space Flight Center, Greenbelt, Maryland, 4–12.

——, and G.S. Fargion, 1999: SIMBIOS Project 1999 Annual Report, *NASA Tech. Memo. 1999–209486,* NASA Goddard Space Flight Center, Greenbelt, Maryland, 128 pp.

Morel, A., 1974: "Optical properties of pure water and pure seawater." In: *Optical Aspects of Oceanography,* N.G. Jerlov and E. Steemann Nielsen, Eds., Academic Press, San Diego, California, 1–24.

——, and S. Maritorena, 2000: Bio-optical properties of oceanic waters: a reappraisal. *J. Geophys. Res.,* (submitted).

Mueller, J.L., 1993: The First SeaWiFS Intercalibration Round-Robin Experiment, SIRREX-1, July 1992. *NASA Tech. Memo. 104566, Vol. 14,* S.B. Hooker and E.R. Firestone, Eds., NASA Goddard Space Flight Center, Greenbelt, Maryland, 60 pp.

——, 1995a: "An integral method for analyzing irradiance and radiance attenuation profiles." In: Siegel, D.A., M.C. O'Brien, J.C. Sorensen, D.A. Konnoff, E.A. Brody, J.L. Mueller, C.O. Davis, W.J. Rhea, and S.B. Hooker, 1995: Results of the SeaWiFS Data Analysis Round-Robin (DARR-94), July 1994. *NASA Tech. Memo. 104566, Vol. 26,* S.B. Hooker and E.R. Firestone, Eds., NASA Goddard Space Flight Center, Greenbelt, Maryland, 44–52.

——, 1995b: "Comparison of irradiance immersion coefficients for several Marine Environmental Radiometers (MERs)." In: Mueller, J.L., R.S. Fraser, S.F. Biggar, K.J. Thome, P.N. Slater, A.W. Holmes, R.A. Barnes, C.T. Weir, D.A. Siegel, D.W. Menzies, A.F. Michaels and G. Podesta, 1995: Case Studies for SeaWiFS Calibration and Validation, Part 3. *NASA Tech. Memo. 104566, Vol. 27,* S.B. Hooker, E.R. Firestone, and J.G. Acker, Eds., NASA Goddard Space Flight Center, Greenbelt, Maryland, 3–15.

——, 1996: MER-2040 SN 8728: Irradiance Immersion Factors, *CHORS Tech. Memo. 004–96,* Center for Hydro-Optics and Remote Sensing, San Diego State University, San Diego, California, 3 pp.

——, B.C. Johnson, C.L. Cromer, J.W. Cooper, J.T. McLean, S.B. Hooker, and T.L. Westphal, 1994: The Second SeaWiFS Intercalibration Round-Robin Experiment, SIRREX-2, June 1993. *NASA Tech. Memo. 104566, Vol. 16,* S.B. Hooker and E.R. Firestone, Eds., NASA Goddard Space Flight Center, Greenbelt, Maryland, 121 pp.

——, and R.W. Austin, 1995: Ocean Optics Protocols for SeaWiFS Validation, Revision 1. *NASA Tech. Memo. 104566, Vol. 25,* S.B. Hooker, E.R. Firestone, and J.G. Acker, Eds., NASA Goddard Space Flight Center, Greenbelt, Maryland, 67 pp.

——, B.C. Johnson, C.F. Cromer, S.B. Hooker, J.T. McLean, and S.F. Biggar, 1996: The Third SeaWiFS Intercalibration Round-Robin Experiment (SIR- REX-3), 19–30 September 1994. *NASA Tech. Memo. 104566, Vol. 34,* S.B. Hooker, E.R. Firestone, and J.G. Acker, Eds., NASA Goddard Space Flight Center, Greenbelt, Maryland, 78 pp.

——, and C.C. Trees, 1997: "Revised SeaWiFS prelaunch algorithm for the diffuse attenuation coefficient $K(490)$." In: Yeh, E-n., R.A. Barnes, M. Darzi, L. Kumar, E.A. Early, B.C. Johnson, and J.L. Mueller, 1997: Case Studies for SeaWiFS Calibration and Validation, Part 4. *NASA Tech. Memo. 104566, Vol. 41,* S.B. Hooker and E.R. Firestone, Eds., NASA Goddard Space Flight Center, Greenbelt, Maryland, 18–21.

O'Reilly, J.E., S. Maritorena, B.G. Mitchell, D.A. Siegel, K.L. Carder, S.A. Garver, M. Kahru, and C. McClain, 1998: Ocean color chlorophyll algorithms for SeaWiFS, *J. Geophys. Res.,* **103,** 24,937–24,953.

Pope, R.M., and E.S. Fry, 1997: Absorption spectrum (380–700 nm) of pure water, II. Integrating cavity measurements, *Appl. Opt.,* **36,** 8,710–8,723.

Siegel, D.A., M.C. O'Brien, J.C. Sorensen, D.A. Konnoff, E.A. Brody, J.L. Mueller, C.O. Davis, W.J. Rhea, and S.B. Hooker, 1995: Results of the SeaWiFS Data Analysis Round-Robin (DARR-94), July 1994. *NASA Tech. Memo. 104566, Vol. 26,* S.B. Hooker and E.R. Firestone, Eds., NASA Goddard Space Flight Center, Greenbelt, Maryland, 58 pp.

Smith, R.C., and K.S. Baker, 1981: Optical properties of the clearest natural waters (200–800 nm). *Appl. Opt.,* **20,** 177–184.

——, D.A. Menzies, and C.R. Booth, 1997: Oceanographic Bio-Optical Profiling System II, Ocean Optics XIII, S.G. Ackelson and R. Frouin, Eds., *Proc. SPIE,* **2963,** 777–789.

Wang, M., 2000: "The SeaWiFS atmospheric correction algorithm updates." In: McClain, C.R., E.J. Ainsworth, R.A. Barnes, R.E. Eplee, Jr., F.S. Patt, W.D. Robinson, M. Wang, and S.W. Bailey, SeaWiFS Postlaunch Calibration and Validation Analyses, Part 1. *NASA Tech. Memo. 2000–206892, Vol. 9,* S.B. Hooker and E.R. Firestone, Eds., NASA Goddard Space Flight Center, Greenbelt, Maryland, 57–63.

Zibordi, G., and G.M. Ferrari, 1995: Instrument self-shading in underwater optical measurements: experimental data, *Appl. Opt.,* **34,** 2,750–2,754.

——, J.P. Doyle, and S.B. Hooker, 1999: Offshore tower shading effects on in-water optical measurements. *J. Atmos. Ocean. Technol.,* **16,** 1,767–1,779.

The SeaWiFS Postlaunch Technical Report Series

Vol. 1

Johnson, B.C., J.B. Fowler, and C.L. Cromer, 1998: The SeaWiFS Transfer Radiometer (SXR). *NASA Tech. Memo. 1998–206892, Vol. 1,* S.B. Hooker and E.R. Firestone, Eds., NASA Goddard Space Flight Center, Greenbelt, Maryland, 58 pp.

Vol. 2

Aiken, J., D.G. Cummings, S.W. Gibb, N.W. Rees, R. Woodd-Walker, E.M.S. Woodward, J. Woolfenden, S.B. Hooker, J-F. Berthon, C.D. Dempsey, D.J. Suggett, P. Wood, C. Donlon, N. González-Benítez, I. Huskin, M. Quevedo, R. Barciela-Fernandez, C. de Vargas, and C. McKee, 1998: AMT-5 Cruise Report. *NASA Tech. Memo. 1998–206892, Vol. 2,* S.B. Hooker and E.R. Firestone, Eds., NASA Goddard Space Flight Center, Greenbelt, Maryland, 113 pp.

Vol. 3

Hooker, S.B., G. Zibordi, G. Lazin, and S. McLean, 1999: The SeaBOARR-98 Field Campaign. *NASA Tech. Memo. 1999–206892, Vol. 3,* S.B. Hooker and E.R. Firestone, Eds., NASA Goddard Space Flight Center, Greenbelt, Maryland, 40 pp.

Vol. 4

Johnson, B.C., E.A. Early, R.E. Eplee, Jr., R.A. Barnes, and R.T. Caffrey, 1999: The 1997 Prelaunch Radiometric Calibration of SeaWiFS. *NASA Tech. Memo. 1999–206892, Vol. 4,* S.B. Hooker and E.R. Firestone, Eds., NASA Goddard Space Flight Center, Greenbelt, Maryland, 51 pp.

Vol. 5

Barnes, R.A., R.E. Eplee, Jr., S.F. Biggar, K.J. Thome, E.F. Zalewski, P.N. Slater, and A.W. Holmes 1999: The SeaWiFS Solar Radiation-Based Calibration and the Transfer-to-Orbit Experiment. *NASA Tech. Memo. 1999–206892, Vol. 5,* S.B. Hooker and E.R. Firestone, Eds., NASA Goddard Space Flight Center, 28 pp.

Vol. 6

Firestone, E.R., and S.B. Hooker, 2000: SeaWiFS Postlaunch Technical Report Series Cumulative Index: Volumes 1–5. *NASA Tech. Memo. 2000–206892, Vol. 6,* S.B. Hooker and E.R. Firestone, Eds., NASA Goddard Space Flight Center, Greenbelt, Maryland, 14 pp.

Vol. 7

Johnson, B.C., H.W. Yoon, S.S. Bruce, P-S. Shaw, A. Thompson, S.B. Hooker, R.E. Eplee, Jr., R.A. Barnes, S. Maritorena, and J.L. Mueller, 1999: The Fifth SeaWiFS Intercalibration Round-Robin Experiment (SIRREX-5), July 1996. *NASA Tech. Memo. 1999–206892, Vol. 7,* S.B. Hooker and E.R. Firestone, Eds., NASA Goddard Space Flight Center, 75 pp.

Vol. 8

Hooker, S.B., and G. Lazin, 2000: The SeaBOARR-99 Field Campaign. *NASA Tech. Memo. 2000–206892, Vol. 8,* S.B. Hooker and E.R. Firestone, Eds., NASA Goddard Space Flight Center, 46 pp.

Vol. 9

McClain, C.R., E.J. Ainsworth, R.A. Barnes, R.E. Eplee, Jr., F.S. Patt, W.D. Robinson, M. Wang, and S.W. Bailey, 2000: SeaWiFS Postlaunch Calibration and Validation Analyses, Part 1. *NASA Tech. Memo. 2000–206892, Vol. 9,* S.B. Hooker and E.R. Firestone, Eds., NASA Goddard Space Flight Center, 82 pp.

Vol. 10

McClain, C.R., R.A. Barnes, R.E. Eplee, Jr., B.A. Franz, N.C. Hsu, F.S. Patt, C.M. Pietras, W.D. Robinson, B.D. Schieber, G.M. Schmidt, M. Wang, S.W. Bailey, and P.J. Werdell, 2000: SeaWiFS Postlaunch Calibration and Validation Analyses, Part 2. *NASA Tech. Memo. 2000–206892, Vol. 10,* S.B. Hooker and E.R. Firestone, Eds., NASA Goddard Space Flight Center, 57 pp.

Vol. 11

O'Reilly, J.E., and 24 Coauthors, 2000: SeaWiFS Postlaunch Calibration and Validation Analyses, Part 3. *NASA Tech. Memo. 2000–206892, Vol. 11,* S.B. Hooker and E.R. Firestone, Eds., NASA Goddard Space Flight Center, 49 pp.